FOUR-DIMENSIONAL CHARACTERIZATION OF TREE CANOPY WETTING DURING PRECIPITATION EVENTS

DORIS K. SIU

A THESIS SUBMITTED TO THE FACULTY OF GRADUATE STUDIES
IN PARTIAL FULFILMENT OF THE REQUIREMENTS
FOR THE DEGREE OF
MASTER OF SCIENCE

GRADUATE PROGRAM IN GEOGRAPHY
YORK UNIVERSITY
TORONTO, ONTARIO

September 2013

© Doris K. Siu, 2013

ABSTRACT

This study develops a four-dimensional (4D) Geographic Information System (GIS) model to track the movement of water through a tree canopy during a precipitation event. The goal is to understand how the wetting process of a tree canopy is correlated to spatial, temporal and environmental factors. Precipitation data at a one-minute temporal resolution was collected for a six-month period (June to November 2009) in which 20 leaf wetness sensors were installed within the canopy of a Japanese Lilac Tree on York University's Keele campus in Toronto, Ontario, Canada. Water movement varied depending on sensor position, rain category, and season. Drizzle events significantly differed compared to other rain categories and the wetness along the upper edge was significantly different from other regions of the tree canopy. These results demonstrate that the internal complexities of the tree canopy govern the heterogeneous nature of canopy wetting and drying phases.

DEDICATION

This thesis is dedicated to my son, Lucas, for without his love and support it would not have been possible. Lucas has taught me that even the largest task could be accomplished if it is done one step at a time. Thank you sweetheart in always believing in Mommy.

ACKNOWLEDGEMENTS

Special thanks to the distinguished faculty members who served on my committee: Dr. Tarmo K. Remmel, Dr. Richard L. Bello, and Dr. Martin J. Bunch. As my advisor, Dr. Remmel provided detailed guidance and encouragement throughout the course of preparing for and conducting this research. But more importantly, Dr. Remmel always believed in me and this I am truly thankful for: his belief that it was, indeed, possible to finish, kept me going whenever progress came to a standstill. Sincere appreciation is extended to my second reader, Dr. Bello, for providing me with invaluable advice for data analysis.

My thanks go to the National Science and Engineering Research Council (NSERC) and the Ontario Ministry of Training, Colleges, and Universities for awarding me with the Canadian Graduate Scholarship (CGS) and Ontario Graduate Scholarship (OGS) respectively. This financial support provided equipment and funding for the completion of this thesis.

Research scientist, Dr. Douglas R. Cobos, at Decagon Devices generously contributed his operational expertise on the leaf wetness sensor (a key component in my research) during the design phase of this project. Additionally, I am heartily thankful to colleagues Connie Ko, Patrick Mojdehi, and Yikalo Araya for their assistant in the field. My thanks also go to Milissa Elliott, James MacKay, and Vicki Simkovic for sharing their knowledge on botany. I am extremely grateful for the assistance provided by JingRu (Jerry) Zheng; his expertise in data visualization was an integral building block in my research. I also offer my enduring gratitude to my two best friends, Averil Herman and Seung Hee Yun, who have both been very supportive throughout my long journey and never once doubted my abilities to successfully complete this degree.

I would also like to thank my husband, parents, and in-laws for their pride in this accomplishment. It is with great honour to share with all of them this milestone. I would like to express my thanks to my husband, Joran Siu, who shared with me his knowledge in computer programming. But more importantly, Joran has been extremely supportive throughout this long journey: it was not about having all the answers, but just being there when I needed him the most. To my parents, thank you for nourishing my love for reading when I was young and for keeping me motivated to stay in school. Also, I am grateful for the time my mother-in-law, Priscilla Siu, spent to take care of my son, Lucas Siu, in times when I really needed some quiet.

Most of all, my biggest thank you goes to Lucas, whose loving smile gave me the necessary strength to push towards the finish line. It is amazing how a hug can go a long way.

I would like to express my gratitude to everyone acknowledged. Thank you to everyone for enabling the production of this thesis.

TABLE OF CONTENTS

LIST OF TABLES

LIST OF FIGURES

1. INTRODUCTION

1.1 Hydrology, the Water Cycle, and Precipitation

Hydrology is the study of the interactions of water on Earth, including its occurrence, distribution, circulation, and chemical and physical properties (Trenberth 1992; Ward and Robinson 2000). Water, the subject matter of hydrology, moves within the closed system of Earth. Thus, other than evaporation and precipitation, all water on Earth (including saltwater and freshwater) is part of the hydrosphere (Muzylo et al. 2012; Laird et al. 2011). Although water covers 71% of the area of Earth, the ratio of saltwater to freshwater is 40 to 1, and only 0.3% of the net global freshwater is mobile (Eakins and Sharman 2010; Environment Canada 2011). It is this mobile freshwater that supports our global water supply and contributes actively to the hydrological (water) cycle. Therefore, most of the freshwater on Earth is not accessible to human use – either located in deep underground aquifers as groundwater or frozen in the icecaps of Antarctica and Greenland (Oke 1987; Ward and Robinson 2000; Campbell and Reece 2005).

The mobile water on Earth moves continually through the water cycle (Figure 1) via processes including condensation, precipitation, evaporation and transpiration (evapotranspiration), infiltration, subsurface flow, and runoff (Crockford and Richardson 2000). The water cycle, thus, describes the aforementioned processes, which drives the movement of water throughout the hydrosphere between the atmosphere, soil water, surficial water (e.g., oceans and lakes), groundwater, and vegetation (e.g., trees). The evaporation of water into the atmosphere requires energy that comes from the sun; the sun's heat is trapped in the Earth's atmosphere, leading to cyclic positive temperature changes. This heat is then released when water vapour condenses to precipitation (rain or snow). When precipitation forms, it travels through the atmosphere and undergoes infiltration, evaporation, or interception (e.g., by vegetation). Thus, the water cycle continues this exchange of water throughout the hydrosphere via the following transfer processes: 1) evaporation from surficial bodies of water and/or transpiration from vegetation (e.g., in both cases, water moves back into the atmosphere and does not reach the ground surface), 2) percolation into the ground (groundwater movement where the direction is defined by Darcy's Law), and/or 3) streamflow and surface runoff (water runs overland into nearby streams and lakes) (Todd et al. 2006; Buttle and Lafleur 2007).

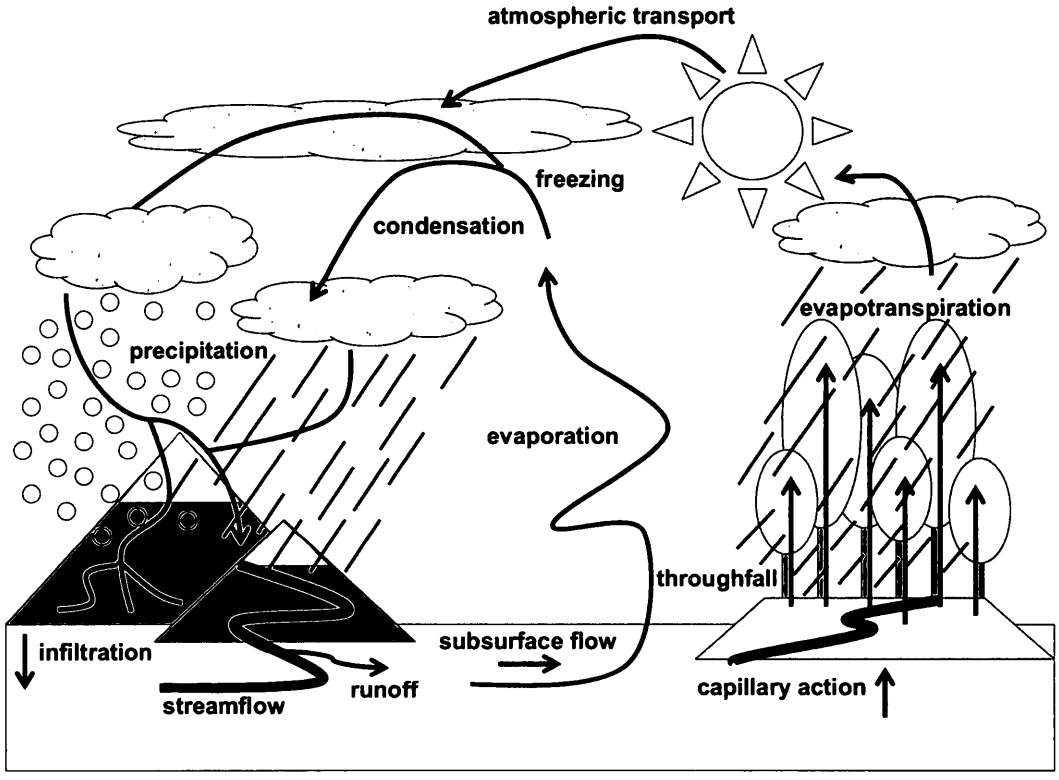

Figure 1. A schematic illustrating the continuous movement of water in a process called the hydrological or water cycle.

A water balance study quantifies and assesses the hydrological cycle for a particular region or catchment by measuring certain components of the water cycle, such as rainfall and streamflow. The water balance of a forest, for instance, is the balance between the inputs of water (e.g., precipitation and upstream drainage) and the outputs of water (e.g., evaporation and drainage downstream) (Oke 1987; Crockford and Richardson 2000). Hydrological budgets of landscapes are often studied on the spatial scale of watersheds (drainage basin), or the area of terrain from which water flows into a stream, river, or lake (Winkler et al. 2010). Streamflow represents the balance of water that remains after all losses back to the atmosphere and storage opportunities within a watershed have been satisfied (Spittlehouse and Winkler 2002). Forest vegetation directly affects the amount of: 1) water available for streamflow, 2) groundwater recharge through the interception of rain and snow, and 3) evapotranspiration of intercepted water by leaves (Hopp and McDonnell 2011; Konrad et al. 2011; Muzylo et al. 2012; Vose et al. 2011; Buttle and Farnsworth 2012). Understanding how streamflow is generated is vital in evaluating the effects of forest disturbance (e.g., fire, logging) on hydrologic response and in identifying the best management practices in a watershed. Therefore, altering forest vegetation

can have an important influence on water balances at the stand, site, and watershed scale. Studying the interactions between water and trees at a micro-scale (e.g., at a finer spatial and temporal resolution) presents the opportunity to quantify water usage by trees and thereby contribute to the optimization of water use.

Much effort in water resource management is directed at optimizing water use for the sustainability of this natural resource. Global net freshwater withdrawal rates have tripled over the last 50 years (from 48 billion $m^3 \cdot a^{-1}$ to 152 billion $m^3 \cdot a^{-1}$); the water withdrawal rate for Canadians, for example, has increased by 87.5% (from 24 billion $m^3 \cdot a^{-1}$ to 45 billion $m^3 \cdot a^{-1}$) over the same 50-year period (UNEP 2011). In Canada, water conservation has been implemented to manage this natural resource; the 1987 Federal Water Policy and 1990 Green Plan sets out a national strategy for water management with Canadian population continuing to rise (Environment Canada 1987; Ministry of the Environment 2011). Highlighted in the water policy strategies was the importance of acknowledging the consumptive use of water by the forests (Environment Canada 1987). Unfortunately, the federal government did not meet the expectations outlined in the 1987 Federal Water Policy; in the absence of national-level leadership, many provincial governments have independently created their own water management policies. The provincial water policies recognized that water is best managed on a watershed basis and forests have a great influence on watersheds (Anderson et al. 2010). A healthy forest supports a healthy watershed, which in turn provides water for aquatic ecosystems that support recreational and economic activities, irrigation for agricultural use, and potable water for drinking. Trees also intercept and transpire incoming precipitation, which can reduce water yield and the timing or magnitude of seasonal flows. The hydrological benefits of forests, therefore, can be described as "costs"; understanding the nature of water use by trees can help with water management.

Water resource managers have begun emphasizing forest hydrology to study global water supply patterns (Bergkamp et al. 2003; Bruijnzeel 2004; Calder 2005; Calder 2007; Van Dijk and Keenan 2007). Forested catchments supply almost two-thirds (62%) of the global water supply for domestic, agricultural, and industrial needs in both upstream and downstream areas (Sutanto et al. 2012; Zingari and Achouri 2010). Additionally, climate change is altering the role in which forests regulate water flow, and thus influence the availability of water resources that contribute to the global water supply (Bergkamp et al. 2003; Miralles et al. 2010). Much research in the past 50 years has focused on quantifying the amount of water used by trees (Bosch and Hewlett 1982; McCulloch and Robinson 1993). A healthy 30 m tall tree has about 200,000 leaves; in a day, a tree this size can take approximately 378.5 L of water from the soil and release it back into the air as oxygen and water vapor (Bosch and Hewlett 1982; Lam and

Quattrochi 1992; Calder 1997; Laird et al. 2011). This estimate, however, assumes that all plants evapotranspire the same, which is not the case (Pan et al. 2003). Unfortunately, there is no simple answer to the question of how much water forests (or trees) use and research continues to improve our ability to predict and quantify such water usage (Lam and Quattrochi 1992; Perks et al. 1996; Smelser and Baltes 2001; Laird et al. 2011; Muzylo et al. 2012; Freeborn et al. 2012).

1.2 Rainfall Partitioning and Hydrological Processes

For any given precipitation event, the precipitation duration is the interval of time elapsed between the beginning (start of wetting period) and the ending of a rainfall event (end of wetting period and thus start of drying period) (AMS 2000; Barry and Chorley 2003; Ahrens 2007). Data on precipitation, unlike the other components of the hydrological cycle, is more readily available for more sites and for longer periods. Precipitation is the product of condensation of atmospheric water vapour that is deposited (from clouds) onto the surface of the Earth, commonly in the form of rain, snow, or ice pellets (Ahrens 2007; Environment Canada 2011). The amount of precipitation is usually expressed in millimeters of liquid water or centimeters of liquid water depth (in the case of snow, snow water equivalent (SWE) can be used to express the amount of water in a snowpack) (Schmidt and Gluns 1991; Schmidt and Troendle 1992; Ward and Robinson 2000). Of interest for this study is liquid precipitation, which principally comprises rainfall and drizzle.

Rainfall is precipitation in the form of liquid water drops with diameters approximately 0.5 mm or greater (AMS 2000; Barry and Chorley 2003). Drizzle however, comprises drops that are less than 0.5 mm in diameter; drizzle events are also lighter in intensity and the drops, albeit smaller in size, are much more numerous (AMS 2000). Any given rainfall event can be distinguished based on the quantity of raindrops per unit of time (intensity) and the presence of temporal gaps over hourly periods of time (character).

For purposes of observation, the intensity of rainfall at any given time and place may be classified as light (rate of fall between a trace to 2.5 $mm \cdot h^{-1}$), moderate (rate of fall between 2.6 $mm \cdot h^{-1}$ to 7.6 $mm \cdot h^{-1}$), and heavy (rate of fall over 7.6 $mm \cdot h^{-1}$) (AMS 2000; Environment Canada 2011). With regard to character, raindrops fall in two distinct patterns: continuous (no temporal gaps for at least one hour) and intermittent (several temporal gaps throughout rainstorm, at least one gap during the hour) (AMS 2000; Environment Canada 2011). The temporal gaps that define the character of rainstorms are distinguished by the quantity of rainfall over an hourly period; the presence of rainfall defines the beginning of the rain event and the absence of rainfall after a one-hour period defines the end of the rain event (Williams 1997; AMS 2000). Although

the duration of a rainstorm is important to consider, it is the intensity and character that defines the type of rainstorm event, as classified in Table 1 below.

Table 1. Chart outlining different rainfall types, ordered from least to most intense rainstorms.

Type	Intensity	Character
Drizzle	Light	Intermittent
Light rain showers	Light	Continuous
Rain showers	Moderate	Intermittent
Moderate rain showers	Moderate	Continuous
Heavy rain showers	Heavy	Continuous
Thunderstorms	Heavy	Intermittent

Rainstorm events over vegetated landscapes, such as forests, present the potential for interception, which is a form of water retention within the tree canopy (in the case of vegetation); interception prevents water from reaching the ground directly and thus does not contribute to direct runoff (Todd et al. 2006; Buttle and Lafleur 2007). Rainfall partitioning in forests is a function of rainfall characteristics, meteorological conditions, vegetation structure, and the interaction between these factors (Xiao et al. 2000; Staelens et al. 2008). The amount of precipitation intercepted by a tree canopy varies with tree species, leaf type, leaf and stem density, age, health, and canopy architecture (Symonds 1973; Xiao et al. 2000; Campbell and Reece 2005; Winkler et al. 2010; Ruudji et al. 2012). Furthermore, wind (speed and direction), radiation, air temperature, and rain characteristics (i.e., duration, intensity, character) may contribute to the variability in interception rates (Voigt 1960; Spittlehouse and Winkler 2002; Staelens et al. 2008; Buttle and Farnsworth 2012).

The transport of intercepted rainfall (Figure 2) can be partitioned as throughfall, stemflow, or leaf flow (Lankreijer et al. 1993; Winkler et al. 2010; Buttle and Farnsworth 2012). Throughfall is any precipitation passing through the canopy (e.g., precipitation entering the tree canopy through canopy gaps), stemflow is the flow of water down branches or the trunk, and leaf flow (leaf drip) is precipitation that drops from leaves. Notably, experiments conducted by Buttle and Lafleur (2007) inferred that interception research mainly focuses on the collection of throughfall and stemflow measurements. However, foliage largely determines interception loss where the presence of leaves decreases the amount of throughfall and stemflow. Leaves favour water collection, but also prevent branches from becoming wet and conducting water down the trunk. Clearly, leaves influence the moisture dynamics within a tree canopy and quantifying only

throughfall and stemflow in interception modeling does not adequately capture the moisture heterogeneity that exists within the tree canopy.

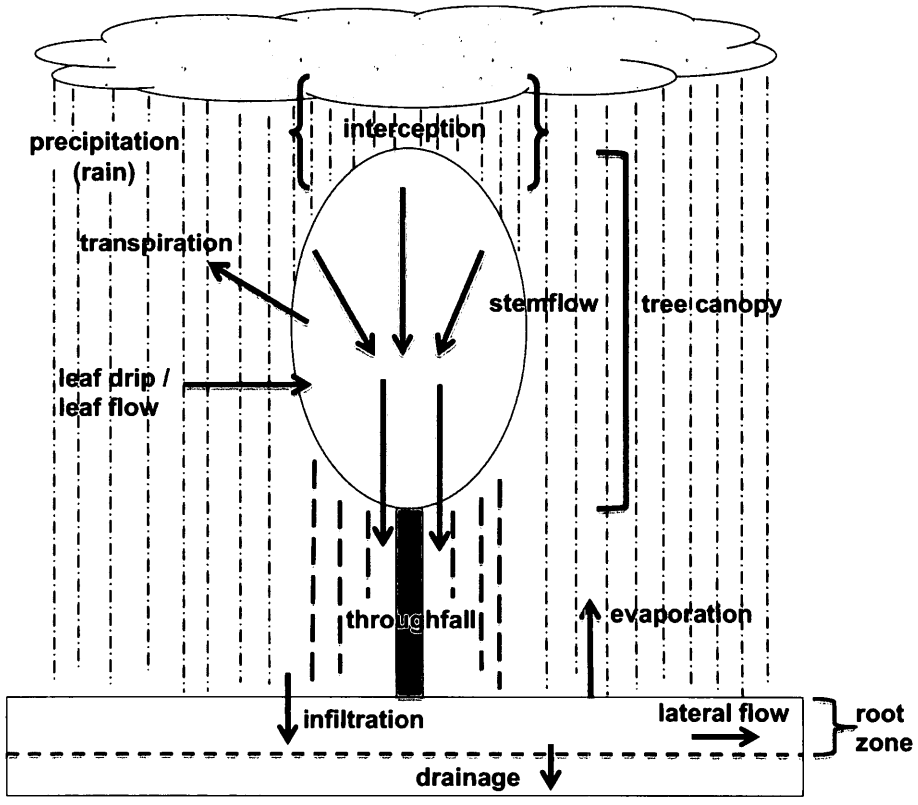

Figure 2. The pathway water travels once it's intercepted by vegetation varies depending on canopy architecture, rainfall intensity or duration, wind, and temperature. Water is commonly transported as throughfall, stemflow, or leaf flow once intercepted by the tree canopy.

Accurate estimates of throughfall and leaf flow are required for quantifying groundwater recharge in a forest and ultimately the hydrology of the surrounding area. Tree canopies intercept up to 35% of the gross annual precipitation, making it an important component of the water balance (Hatfield and Prueger 2011; Ruudji et al. 2012). To understand the wetting and drying phases within a tree canopy during and following precipitation events, the following processes are defined below.

Evaporation and transpiration are two different mechanisms through which removal of water from the surface of the Earth into the atmosphere takes place (Pidwirny 2006). These two mechanisms are similar since they both result in the loss of water that is released into the atmosphere (Freeman 1920). However, evaporation and transpiration are also different;

evaporation takes place from the surface of water bodies when liquid water converts to water vapour while transpiration is the process of loss of water from plants through pores called stomata within leaves (Freeman 1920). When the stomata close, the air trapped by in the stomata becomes nearly saturated with water vapour. Conversely, when the stomata opens, this high humidity air is exchanged with lower humidity air outside the leaf, due to the leaf-to-air water vapour concentration gradient, causing a net loss of water from the plant (Mooney et al. 1983). This transfer of water to the atmosphere through plants is called transpiration.

In hydrology, the total loss of water through both evaporation and transpiration are collectively termed evapotranspiration (Lawrence et al. 2003; Hamlet et al. 2007). This process is analogous to a plant sweating where plants secrete water through the plant stomata and transport water from the leaves into the atmosphere. Environmental conditions (e.g., radiation, air temperature, humidity, wind speed) and plant characteristics (e.g., height, roughness, ground cover) influence evapotranspiration. Evapotranspiration is expressed as a rate (depth of water over time) that is either evaporated from surface waters and soils or transpired from plants. Both evaporation and transpiration rates are partially controlled by the vapour pressure deficit (VPD). VPD is the difference between the amount of moisture in the air and how much moisture the air can hold when it is saturated (Addington et al. 2004).

During a rain event, the tree canopy resembles a sponge because it can store the intercepted water temporarily under two circumstances: 1) until moisture is evapotranspired from the tree canopy, or 2) until the tree canopy reaches its maximum storage capacity (when all leaves within the tree canopy are completely wet) allowing for additional moisture to escape the tree canopy via primarily leaf flow (Lankreijer et al. 1993; Xiao et al. 2000; Buttle and Lafleur 2007; Kume et al. 2008). The leaves and branches of a tree form, what is termed a tree crown; it is the tree crown that intercepts precipitation during a rainstorm event. When it rains, most of the raindrops hit a leaf or branch surface and either adheres to or is absorbed into the surface. This water content remains there as "temporary storage" before being released by evaporation into the atmosphere or falling as drops to the ground (Lewis 2002; Xiao and McPherson 2003). The brief retention of rainwater by the tree canopy is called rainfall interception (Cappiella et al. 2005).

During a rainstorm event, the ability for the tree canopy to collect and retain falling precipitation varies throughout the storm, which reflects the changing state of interception storage for trees (Buttle and Lafleur 2007; Staelens et al. 2008; Takahashi et al. 2010). At first, when the entire tree (all the leaves, twigs, and stems) is dry, the available storage is at a maximum; therefore, once the canopy is wet, precipitation reaches the ground at a much slower rate since water is being absorbed by the canopy. As the leaves become wetter, the weight of water on them eventually overcomes the surface tension (coalescing drops) and further additions from

rainfall are almost entirely offset by the water droplets falling from the lower edges of the leaves (e.g., water drips off leaves since the canopy can no longer hold more water). Since interception losses are high during the beginning of a storm, the frequency of wetting and re-wetting is likely of greater importance than the actual amount of rainfall because the relative importance of interception losses tends to decrease as the amount of rainfall increases (Lankreijer et al. 1993; Xiao et al. 2000; Siles et al. 2010; Muzylo et al. 2012). Water in the tree canopy that is not evaporated or absorbed will drip down to the ground as the canopy fills with water. Rainfall flowing from the trunk (stemflow) reduces the impact of the raindrops and prevents some of the ground and soil displacement that causes erosion (Staelens et al. 2008; Ruudji et al. 2012).

Individual trees intercept only a small percentage of the total rainfall, and, as a result, are not as effective at reducing and slowing the delivery of stormwater (Riekerk et al. 1995). Stormwater is the rainfall that accumulates on the ground during and immediately after a rainstorm. It flows over the surface towards natural waterways, thus contributing to streamflow, subsurface flow, and runoff. Since trees intercept rainfall, the presence of trees in a watershed can reduce the amount of runoff. However, a forest that comprises of multiple tree crowns is more effective at influencing the total annual surface runoff than an individual tree for a given area (Xiao and McPherson 2003). Studying the internal hydrological processes of tree canopies presents the possibility of quantifying water usage of an individual tree, in addition to improving groundwater recharge estimates of a forest.

1.3 Interception Modeling

Interception can be measured using interception models (e.g., Horton 1919; Leyton et al. 1967; Rutter et al. 1971; Gash 1979), which are process models designed to calculate the water balance of a forest canopy. Prior to the application of interception modeling, interception loss was calculated as the difference between gross rainfall and net rainfall using rain gauges (Voigt 1960). Although it is simpler to measure interception loss directly than to collect the climate and vegetation data necessary to model interception loss, modeling has a number of advantages. First, it provides a summary of the behaviour; second it enables the results of one field study to be extrapolated to other areas; and third it can provide insights into the process (Lankreijer et al. 1993).

Current interception models assume homogeneous wetting and drying phases across the entire tree canopy, and do not consider leaf flow. Since the quantity of intercepted water is a function of environmental conditions, clearly, the entire tree canopy does not wet and dry at the same rate (Voigt 1960; Lloyd et al. 1988; Lankreijer et al. 1993; Winkler et al. 2010). Also, the

presence of leaves significantly decreases the amount of throughfall and stemflow, resulting in leaf flow and evaporation to become the primary methods of water transport in the tree canopy during a precipitation event (Lankreijer et al. 1993). However, leaf flow and throughfall are difficult to separate; accordingly, the complexity in distinguishing between leaf flow and throughfall accounts for the rationale of measuring only one process (specifically throughfall) in interception models (Lankreijer et al. 1993).

Earlier interception models, like the Horton model (Horton 1919), are limited in applicably because these models could only be applied to forests that were similar to the location the model was derived (e.g., temperate regions for uniform plantations). Horton (1919) was the first to propose the idea that interception loss for rainstorms (which would saturate the vegetation canopy) is the summation of the evaporation loss of intercepted water during rainfall and the water held on the canopy at the end of the storm (which will subsequently be evaporated) (Herbst et al. 2008). A shortcoming of the Horton model is that it is very simplistic and does not account for temporal variations (in the duration, frequency, and magnitude of rainfall events) and inter-annual variations (in the fraction of intercepted rainfall at the site) (Lloyd et al. 1988). Therefore, empirical results could not be applied for similar vegetation covers at other sites due to simplified parameters. Still, the Horton model served as a basis for later interception models; models that followed Horton were then based on more fundamental physical reasoning, which minimized the aforementioned shortcomings (Lloyd et al. 1988).

The development of the Rutter model (Rutter et al. 1971) and Gash models (Gash 1979; Gash et al. 1995) replaced the use of simple percentage values seen in the Horton model. The Rutter model calculates the water balance for a wet canopy and computes a running balance of the amount of water on the canopy with evaporation being estimated from meteorological data (Rutter et al. 1971; Rutter et al. 1975; Rutter and Morton 1977). This model requires the following parameters: canopy storage capacity, the depth of water left on the canopy in conditions of zero evaporation, when rain and throughfall have ceased, the drainage rate, and free throughfall coefficient. The Gash model is a storm-based simplification of the Rutter model and is calibrated using hourly meteorological data allowing the model to run on daily rainfall values. Although the Rutter model requires the same variables to compute, the Gash model considers rainfall to occur in a series of discrete storms each of which comprises three periods: wetting, saturation, and drying (Gash 1979). These later interception models are more versatile since they applied rainfall and meteorological data into its calculations; however, the Rutter and Gash model assume that both rainfall and evaporation rates are constant during a rainstorm resulting in the time lag between rain events to be sufficient in drying the canopy surface (Lloyd 1990; Xiao et al. 2000). Although several applications of these models to interception losses in

natural forests yielded satisfactory agreement between predicted and field measurements, the Rutter and Gash model are unable to explain tree canopy heterogeneity (e.g., when only a small fraction of the canopy surface is dry due to the short time intervals between events) (Pearce and Rowe 1981; Gash et al. 1995; Llorens 1997).

More recently, the Gash model was revised to account for canopy architecture by computing interception separately for each season (Gash et al. 1995; Valente et al. 1997; Liu 2001). This revision (the Liu model) provides estimates of interception for different forest densities with greater confidence in the partitioning of rainfall (throughfall, stemflow, interception loss) for each rain event. However, the Horton model (Horton 1919), Rutter model (Rutter et al. 1971; Rutter et al. 1975), Gash models (Gash 1979; Gash et al. 1995), and Liu model (Liu 1997; Liu 2001) do not adequately capture the internal complexities of the tree canopy, specifically the variability in canopy surface wetting and drying during and following various rain events. Rainstorms are not homogeneous; drizzle tends to produce more interception loss than intense rainstorms with the same total rainfall, and the amount of intercepted water evaporated after a rain event is dependent on the time lag between successive rain events (Zinke 1967; Massman 1983; Mulder 1985; Whitehead and Kelliher 1991; Zeng et al. 2000). Although this study does not develop a new interception model, the application of finer spatial and temporal resolution for studying canopy moisture offers insight on the limitations of current interception modeling.

1.4 Project Objectives

This thesis presents a method to quantify canopy moisture on individual leaves for a tree canopy at a one-minute temporal resolution for individual storm events. A four-dimensional (4D) geographic information system (GIS), which includes the three-dimensional (3D) representation of the tree and the forth dimension of time, is utilized to visualize the spatial and temporal variability (heterogeneity) of moisture within the tree canopy. Despite the importance of canopy interception in processes such as storm-water management and flood control, very few studies have characterized interception systematically (i.e., rainfall partitioning) in order to understand how interception alters the timing and distribution of precipitation in a given area (American Forest 1996; Calder 1997; Xiao et al. 2000).

The redistribution of gross precipitation as a result of vegetation interception, or the partitioning of gross precipitation, is an important component in hydrological studies. Conceptually, canopy rainfall interception is the difference between gross precipitation (precipitation from above canopy) and net precipitation (precipitation from below canopy). Another approach is to consider canopy rainfall interception as the fraction of the precipitation

held by plant canopy surfaces, which is the case in this study. The intercepted water is stored on the canopy surface only temporarily, as ultimately it may fall to the ground around the tree bole as stemflow, or drip to the ground from leaves as leaf flow. However, the common procedure in interception modeling is based upon both throughfall and stemflow, but does not account for leaf flow (Horton 1919; Rutter et al. 1971; Rutter et al. 1979; Gash 1979; Gash et al. 1995; Liu 1997; Liu 2001).

This study demonstrates that leaf flow is the best metric for capturing canopy heterogeneity through the analysis of the instantaneous leaf surface wetness at a micro-scale during a rain event. The possibility of incorporating leaf flow into interception modeling to improve water storage estimates is alluded to. However, development of a new interception model is beyond the scope of this project. The instantaneous leaf surface wetness is measured using leaf wetness duration sensors; over the past 40 years, many attempts have been made to design a leaf wetness sensor (Van der Wal 1978; Sutton et al. 1984; Bedient and Huber 1992; Sutton et al. 2001) since understanding leaf wetness is critical for predicting, for instance, epidemics of fungal disease (e.g., plant health) and surface runoff (e.g., irrigation). Although technological advancements have greatly facilitated leaf wetness measurements, leaf wetness duration, by contrast, is very difficult to define because various portions of leaves and canopies wet and dry at different times. However, leaf wetness research has primarily focused on agricultural crops (e.g., Schuepp et al. 1990; Fuentes and Gillespie 1992) and other than fruit tree canopies (e.g., Henshall and Beresford 1997; Batzer and Gleason 2008), leaf wetness sensors have not been placed in tree canopies to quantity canopy moisture.

The purpose of this study is to characterize canopy moisture dynamics at the individual leaf scale in 4D in order to understand how a tree canopy is wetted during different types of rainfall events. The intent of this study is fivefold:

(1) To evaluate seasonal influences on instantaneous wetness (e.g., comparing summer versus fall months or presence of leaves versus absence of leaves);
(2) To assess instantaneous wetness at various positions within a tree canopy (e.g., comparing surface moisture differences for the top versus bottom of the canopy);
(3) To evaluate how the differences in precipitation type, specifically drizzle versus thunderstorms (low versus high intensity storms), affect the instantaneous wetness within the canopy;
(4) To assess the point at which the tree canopy saturates (e.g., comparing surface moisture wetness differences for consecutive time intervals in a given rainstorm); and

(5) To determine if wind influences instantaneous wetness within the canopy during various types of rainstorms.

The application of 4D GIS to visualize and characterize the moisture dynamics within a tree canopy presents the prospect of understanding wetting and drying phases at the individual tree scale. Although modeling one tree is subject to several uncertainties with regard to applicability, this innovative approach demonstrates the importance of considering spatial and temporal scale in interception measurements. Traditional interception models do not account for the spatial variability of rainfall (Zeng et al. 2000) and neglects leaf flow as a variable for analysis. Insight on the transport of water via leaf flow is provided by this study as measurements in instantaneous wetness within the tree canopy relates to leaf flow; thus, results from this study can potentially improve the accuracy in interception model estimates and predicting forest health (based on canopy moisture). Further, the contribution for a better understanding of water usage in vegetated areas is also highlighted in this research project. Observations at a very fine spatial and temporal resolution, which is presented through the collection of one-minute instantaneous leaf wetness during a given rain event, offers the ability to characterize wetness variability within the tree canopy for different rain types. This study, therefore, proposes an innovative method to quantify in 4D the spatial distribution of moisture within a tree canopy during and following a precipitation event. Research from this study also supports the motivation of water conservation and efficiency in forested environments.

2. METHODS

2.1 Study Site

A Japanese Lilac tree, *Syringa reticulata* (Blume), with a tree crown height of 6 m and width of 5.5 m, was selected for this study (Figure 3a). Characteristic features in the bark, flowers, and leaves were used to identify the tree species (Figure 4). This tree was located on York University's Keele campus, on the northwest corner of the York University Development Centre building on Albany Road, Toronto, Ontario, Canada (43° 46.741' N, 079° 29.979' W). This Japanese Lilac was isolated (i.e., not in a forest) to remove the effect of neighbouring trees in this study.

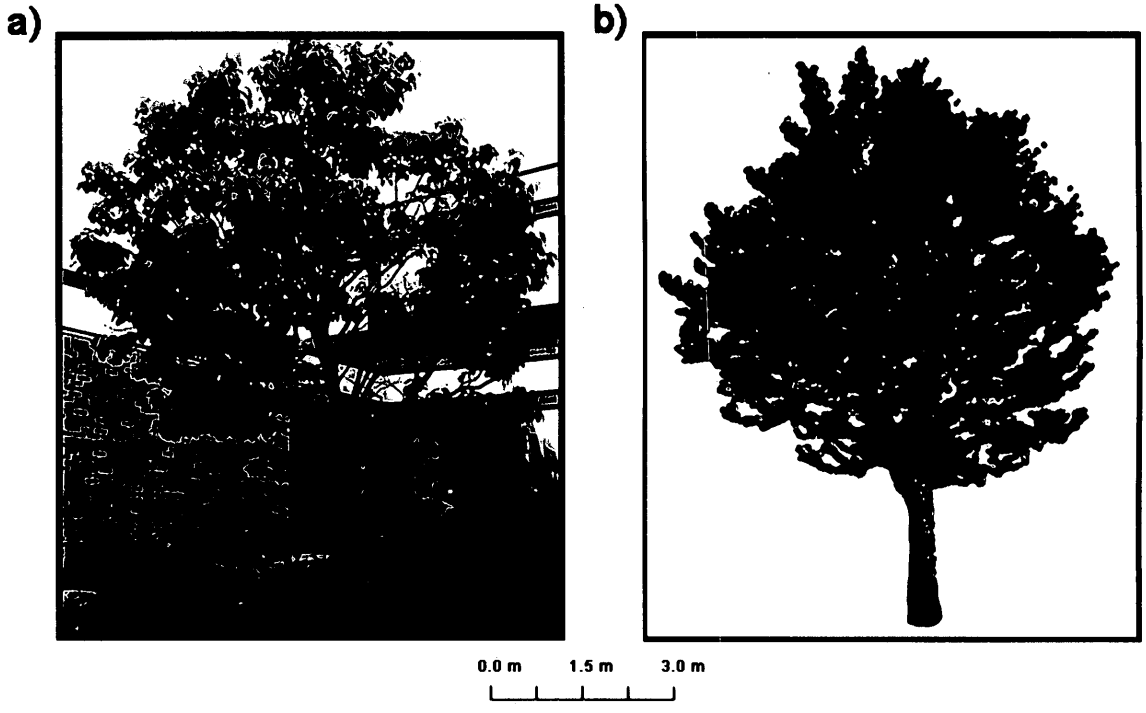

Figure 3. a) Japanese Lilac tree used in this study and b) 3D tree canopy model of Lilac tree (3D image extracted from terrestrial LiDAR point cloud containing 65,535 points with point density of 130 points/m^2).

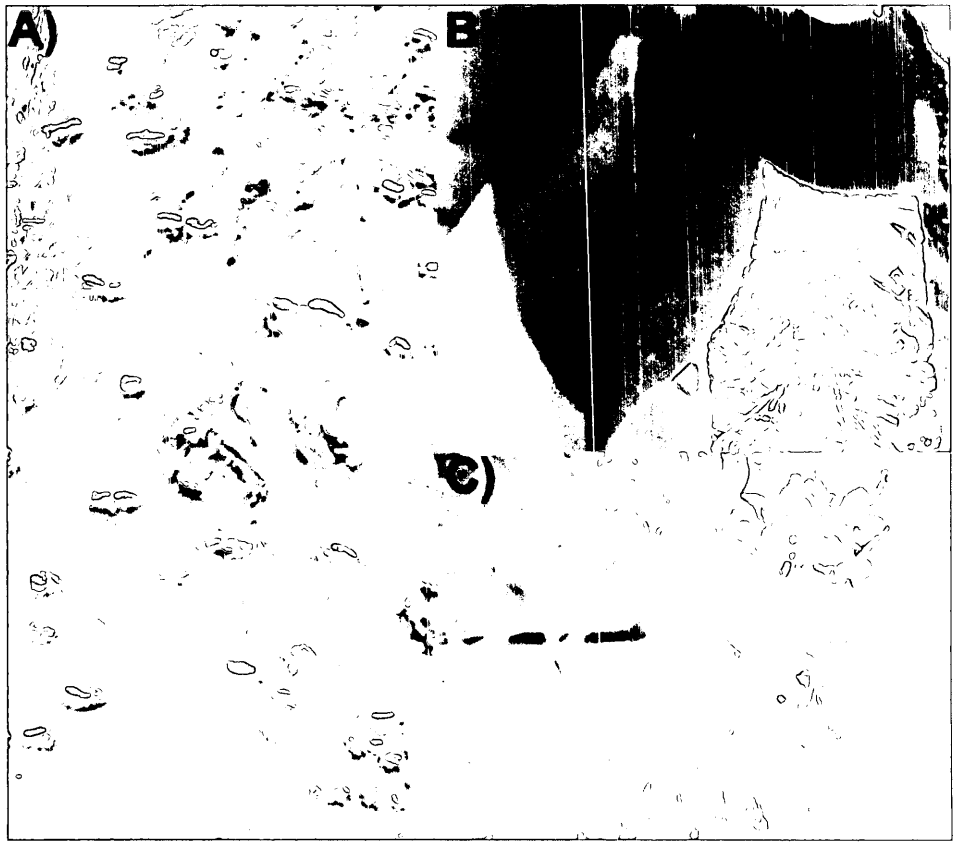

Figure 4. Japanese Lilac trees are characterized by (A) its dark gray-brown bark with prominent horizontal lenticels, (B) dark green smooth oval leaves, and (C) creamy white flowers that form in mid-spring.

Lilacs are small deciduous trees with stiff, spreading upright branches that form a vase-shaped crown (Kloefkorn 2011). The bark is dark gray-brown and is smooth, sometimes lustrous, with prominent horizontal lenticels; older trunks are gray and scaly (Figure 4a) (Dombroski and Gleason 2005; Kloefkorn 2011). Lilacs have one main stem (bole) with multiple stems spreading outwards, and its root system is shallow and dense.

Japanese Lilac leaves are dark green on the above surface and grayish-green on the below surface (Figure 4b). These leaves also have a simple structure (ovate), measuring 5 to 11.5 cm long and 2.5 to 7 cm wide. Furthermore, the leaves grow with one blade attached to a stalk and have no projections around the margins of the leaf (a consistent and smooth leaf edge) (Gerhold 2007; Kloefkorn 2011). Thus, these leaves are unlobed and the margins around the entire leaf are without teeth (smooth). The leaf surface is glabrous above (free of hair, smooth) and covered with veins below (resemble a network like rivers and its tributaries). In autumn, the

leaves often fall without changing colour. Lilacs typically have a low canopy with a typical clearance of 2 to 3 m from the ground.

Lilac buds are brown, medium-large in size (sessile with four pairs of scales), and opposite in arrangement. Flowers are yellow, white, or off-white (creamy white) (Figure 4c) and have a strong sweet fragrance. These plumes of flowers rise above the foliage from mid to late spring, but in the winter display fruit. The fruit is light tan to brown and are in cluster of capsules about 10 to 15 m long (Gerhold 2007).

A sample of soil (300 g) from the study site was collected to determine the pH and particle size. The soil pH was determined using a pH meter; a reading of 6.2 was recorded for the study site. A sieve analysis (gradation test) was performed to assess particle size distribution (Brady and Reil 2002; Hanlon 2009). The soil sample was placed into the top sieve of the mechanical shaker (a nested column of sieves, each with different sized screen openings that form the wired mesh cloth screen) and shook for one-hour. Since each lower sieve in the column has smaller openings than the one above, the particle size could be determined once the shaking was complete. After the soil was separated by particle size, each sample was weighed to determine its mass. The soil at the study site was classified as a clay loam; the quotient of the mass of each sample and the mass of the total soil sample produced the following percentages: 37% clay, 35% silt, and 28% sand. The texture of soil reflects the composition of mineral particles in the fine Earth fraction (< 2 mm diameter), specifically the content of sand, silt, and clay.

2.2 Instrumentation

Precipitation data for the Japanese Lilac tree canopy and meteorological data for the study site was collected for a six-month period from June to November in 2009; both data sets were measured on a one-minute temporal resolution. More specifically, the rainfall interception data was measured by installing 20 leaf wetness sensors (LWS) (Figure 5) within the tree canopy. These LWS are wired devices that are sensitive to moisture on its above surface; the LWS were attached to four dataloggers (five ports on each datalogger) (Figure 6) in order to retrieve the recorded moisture readings. Meterological data was measured using a weather station (Figure 11) that was installed 3 m from the trunk of the Lilac tree. Likewise, the sensors in the weather station (i.e., soil moisture sensors, pyranometer, humidity sensor, and rain gauge) were also attached to a datalogger in order to retrieve the recorded measurements. Further details the aforementioned instrumentation used in this study are outlined below.

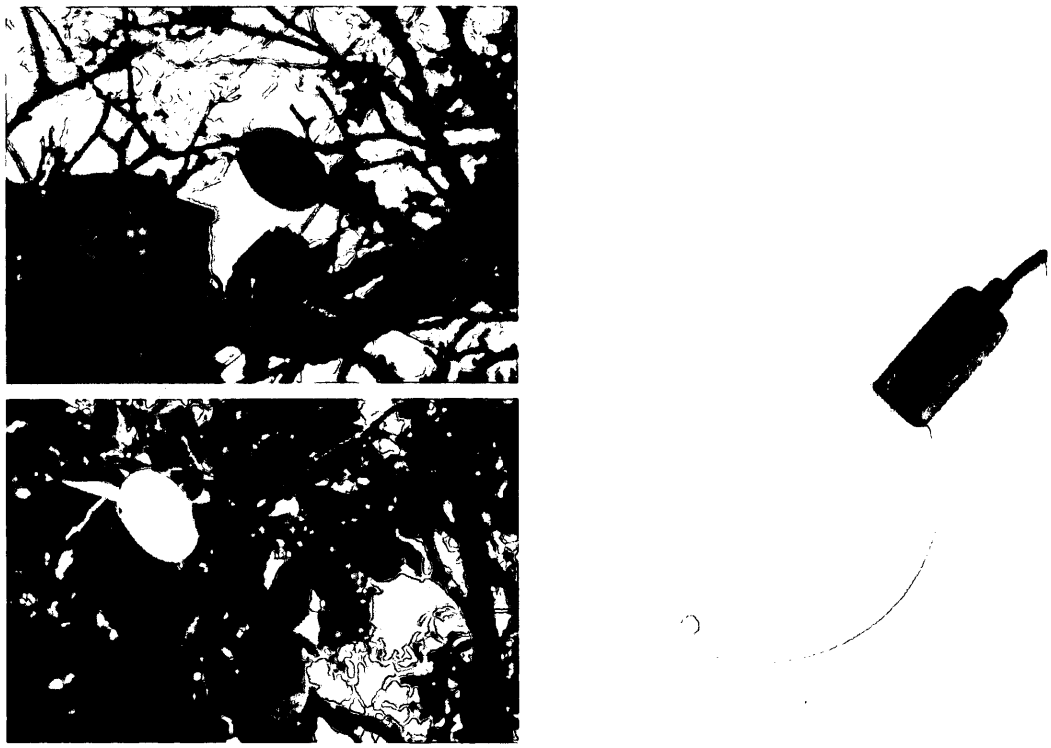

Figure 5. The Leaf Wetness Sensor (11.2 cm × 5.8 cm × 0.075 cm) used to detect and quantify moisture (as counts, which can be converted into mm of rainfall) on individual leaves in the tree canopy.

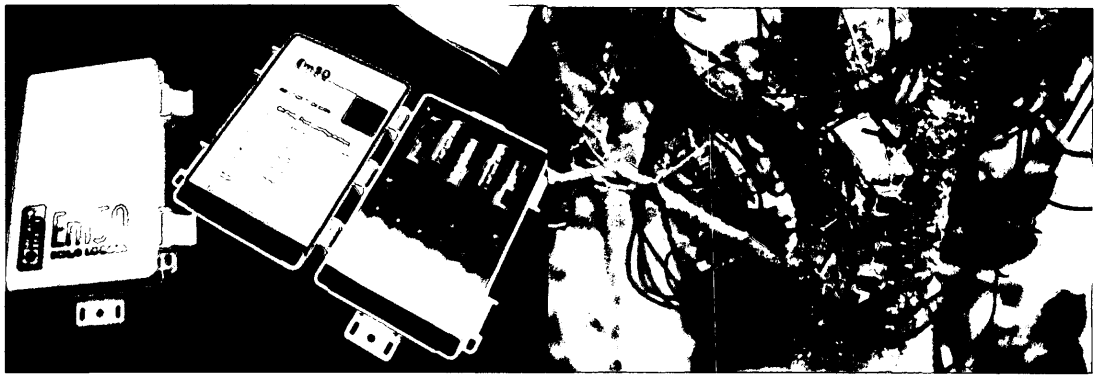

Figure 6. The data loggers used for storing sensor data for both the leaf wetness sensors and weather station.

The LWS is a dielectric leaf wetness sensor that approximates the thermodynamic properties of real leaves to mimic other leaves in a canopy for accurate measurements of leaf wetness amount and duration (Decagon Devices 2007). The LWS takes measurements of the dielectric constant for the sensor surface (top surface of the sensor); the value of this dielectric

constant is dependent on the moisture levels at the time of measurement. The dielectric constant (relative permittivity) of a material is a measure of the electric flux that is generated when an electric field or charge is placed across that substance. Different materials have different dielectric constants; water's dielectric constant is unique to air's dielectric constant.

The LWS is effectively a capacitor; copper traces under the surface form conducting electrodes, with the surface zone of the sensor acting as the dielectric material of the capacitor. Capacitance is proportional to the permittivity of the dielectric material. Furthermore, the time required to charge or discharge a capacitor, typically referenced as RC (resistor-capacitor) time constant, is directly proportional to the capacitance. As a result, the amount of surface moisture on the sensor can be detected by measuring the time constant for charging the LWS capacitor with a given input. The LWS used in this study generates a 5 MHz square wave as input, and electronics in the sensor converts the time constant measured in charging the capacitor into a millivolt output. This output (in counts) is directly proportional to the permittivity and hence, the amount of moisture on the surface. Given that the permittivity of air (1) contrasts with the permittivity of liquid water (80), the LWS is able to detect minute increases in moisture levels on the surface with high accuracy.

The LWS is made of fiberglass with a thickness of 0.65 mm to give the instrument a heat capacity that closely matches that of a real leaf, allowing the LWS to retain water for the same duration as a real leaf (Decagon Devices 2007). These sensors are wired and connected to a data logger in order for measurements to be logged at a one-minute time interval. The sensor's white color allows it to closely match the radiative properties of a real leaf. Healthy leaves absorb well in the near-infrared (NIR) region (700 - 1400 nm) of the electromagnetic spectrum and reflect most of the visible portion of the spectrum. The surface coating on the sensor matches this radiative property of a real leaf because the LWS selectively reflect much of the energy in the NIR region (Decagon Devices 2007). Although these sensors absorb radiation differently, spectroradiometer measurements indicate that they achieve a similar energy balance, allowing the sensor to achieve an evaporation rate very close to that of a real deciduous leaf in a temperate biome. This property was also confirmed by a comparison laboratory experiment using a spectroradiometer for the LWS spectral response versus the real leaf spectral response in April 2010.

The coating on the LWS is hydrophobic, meaning that it is similar to the leaves' tendency to repel water, which matches the wetness state of leaves with waxy cuticles, as in the case of a Japanese Lilac tree. Since hydrophobic materials are typically non-polarized, it does not attract water molecules, as a result, the sensor will only detect moisture when moisture is present (Decagon Devices 2007). Thus, the LWS will not give a false positive reading during periods of

high relative humidity. The accuracy of the readings depends more on the physical properties of the leaves that the researcher wishes to replicate than the sensor itself. Notably, in the case where the leaves on a tree do not resemble the shape of the sensor, then the accuracy could be poor. However, in the case of a Japanese Lilac tree, the leaf shape and size is analogous to the LWS used in this study (Figure 5).

In order to address the first research objective of this project (see §1.4), a total of 20 LWS were installed throughout the tree canopy (Table 2, Figure 7, and Figure 8). Table 2 outlines the spatial variability of the location of the LWS in the tree canopy. Planimetric (Figure 7) and profile (Figure 8) schematics are provided to convey the sensor distribution in the canopy in the following pages. The LWS was installed in the tree canopy in a position that was representative of the local orientation. For instance, if the leaves around the intended position of the LWS were oriented at a 20° angle, then the LWS was also positioned at that same angle.

Table 2. A list of the sensor locations for all 20 LWS in the Japanese Lilac tree canopy based on default numbers (range from 1 to 20).

Location Description	Sensor Number
Top of canopy (T)	4, 14
Upper edge of canopy (UE)	2, 3, 6, 7, 8, 9
Within canopy (W)	5, 10, 11, 12, 13, 16
Lower edge of canopy (LE)	1, 17, 19, 20
Bottom of canopy (B)	15, 18

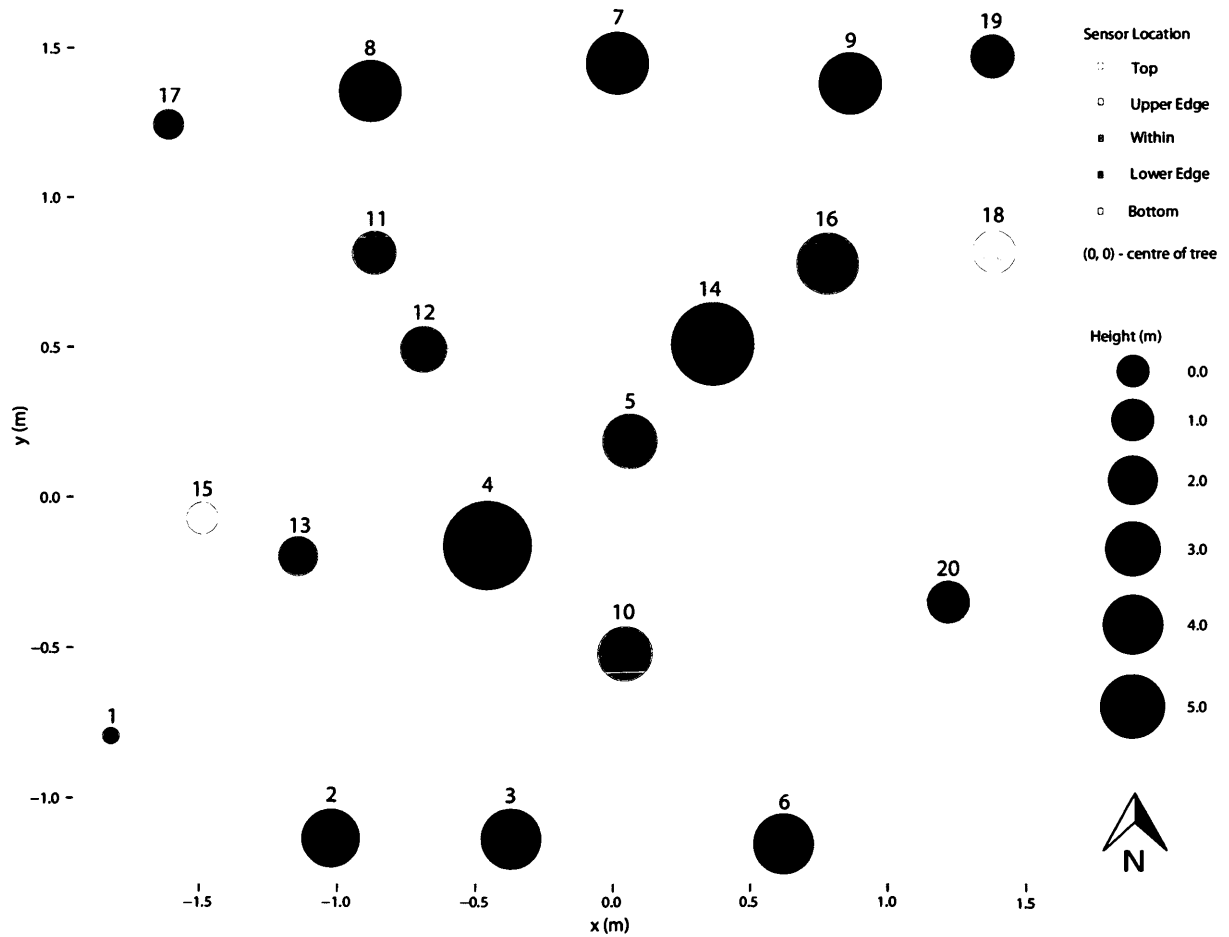

Figure 7. A planimetric view of the study site illustrating the location of the 20 leaf wetness sensors (represented by circles) as described in Table 2 where point (0, 0) is the centre of the tree.

Figure 8. A profile view of the study site illustrating the location of the 20 leaf wetness sensors (represented by circles) as described in Table 2 and coded in reference to the planimetric view illustrated in Figure 7.

A small laboratory investigation was conducted to test LWS sensitivity to water moisture. Six LWS were used in this investigation where three LWS were sprayed 5 mL of water (droplets) onto the sensor for one-minute, and the remaining three LWS were dipped into a beaker of 5 mL of water for one-minute. Results exemplified that despite the differences in the input method, the moisture readings were the same across sensors (LWS behaved similarly over the one-minute interval). Thus, this demonstrated the sensitivity of the LWS in capturing moisture dynamics under various rainstorm conditions (e.g., drizzle vs. rain shower), which addresses the second objective of this project (see §1.4).

Units of measure for the rain data retrieved from the LWS are in the units of counts, which quantifies the millivolt output of the sensor. The higher the count value, the more wet the sensor is. The sensor values can range from 425 to 1400 counts where values greater than 450 counts indicate that the sensor is wet (Decagon Devices 2007). Below is a diagram illustrating a sample of raw output from the LWS (Figure 9). Notice that the LWS raw output is recorded as count values; the units of counts can be converted into a more comparable unit, like mass of water per unit area (w in $mg \cdot cm^{-2}$). A small calibration laboratory controlled experiment was conducted to convert the count values into mass of water per unit area (Figure 10). This conversion equation was validated with Decagon's experimental data provided by Dr. Doug Cobos. Furthermore, the units of $mg \cdot cm^{-2}$ can be later converted into mm of rainfall (in order to compare with rain gauge data) using the relationship that the density of water is 1 $g \cdot cm^{-3}$ and thus 1 mg = 1 mL = 1 cm^3. The conversion equation is outlined below (Eq. 1 and 2), which uses constants obtained from Decagon Inc. (2007):

$$w\left(\frac{mg}{cm^2}\right) = 0.047 \times (RAW) - 20.895 \quad (1)$$

$$\mathrm{H_2O}(mm) = w\left(\frac{cm^3}{cm^2}\right) \times \frac{10mm}{1cm} \quad (2)$$

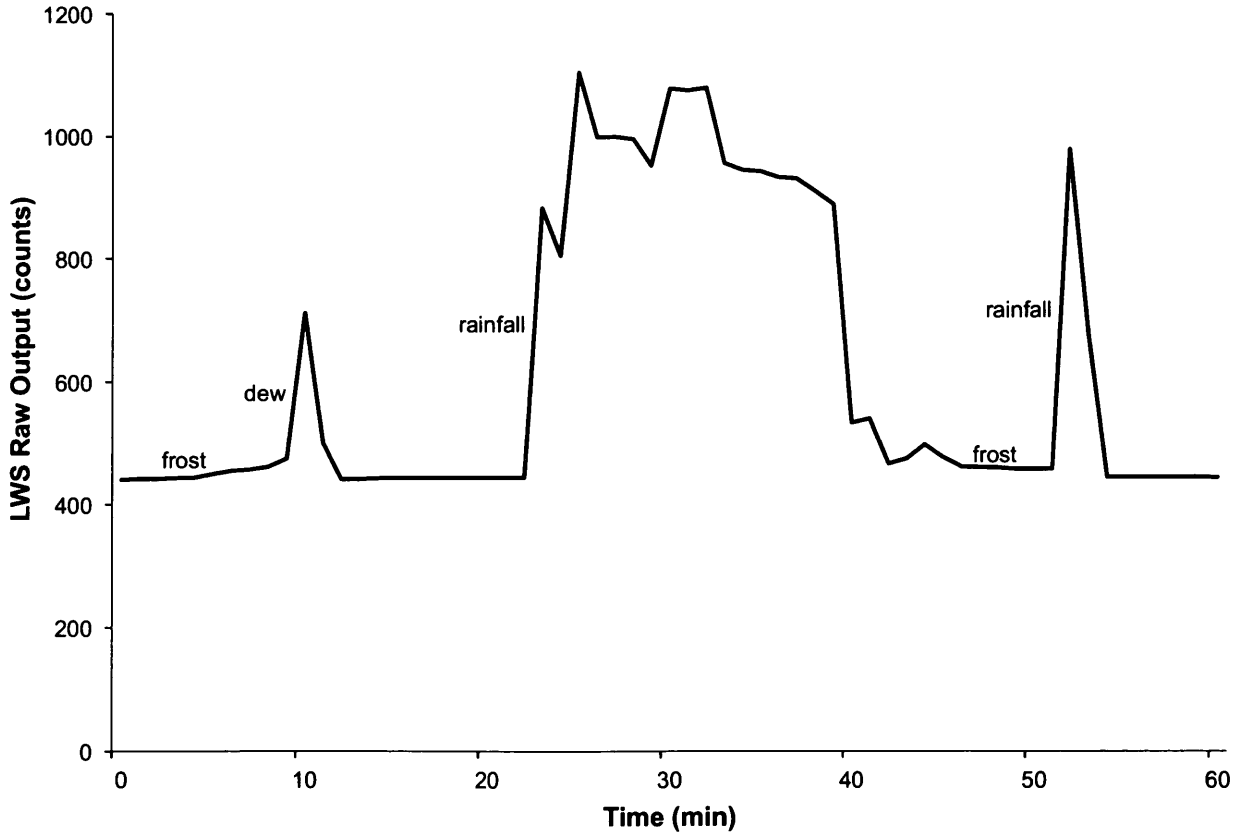

Figure 9. A sample of theoretical LWS raw data (in counts) recorded for every minute over a one-hour interval (data provided by Decagon Devices 2007). LWS readings above 450 indicate the presence of moisture; the patterns observed for frost, dew, and rainfall are representative of LWS readings for any given precipitation event. Because ice has a much lower dielectric constant than that of liquid water, the sensor output from frost will be much lower than that from a similar amount of rain or dew.

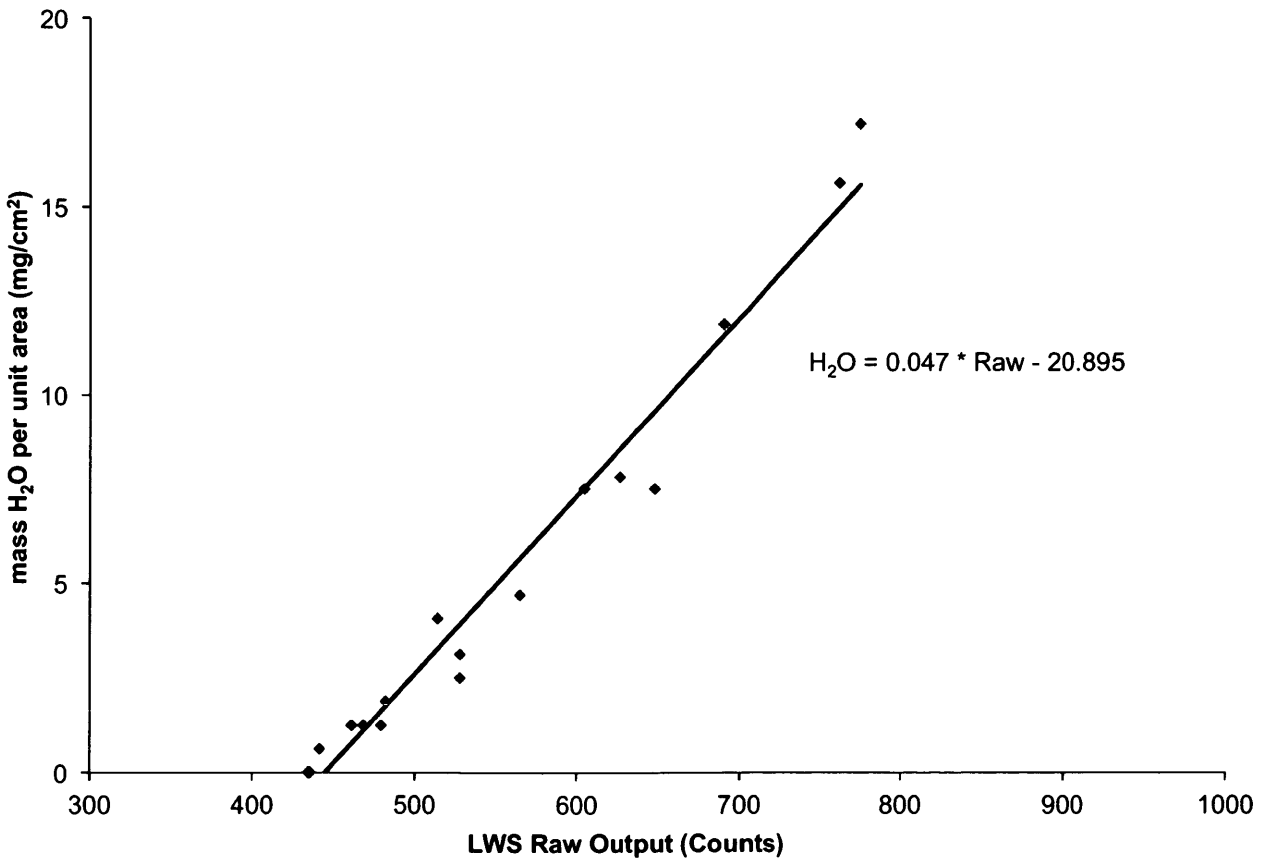

Figure 10. The relationship between LWS output (raw data) in counts and mass of water per unit area ($mg \cdot cm^{-2}$), with conversation equation provided above (data provided by Decagon Devices 2007).

A data logger is a device that reads various types of electrical signals and stores the data in internal memory that can later be downloaded to a computer. These devices record data and are housed in a weatherproof enclosure for outdoor use. The advantage of using data loggers is that they operate independently of a computer. The data loggers used for this study are multi-channel designs, capable of handling five inputs per logger (Figure 6). Powered by five AA alkaline batteries, the loggers were attached to the branches of the Japanese Lilac tree. Four of the five data loggers installed were connected to the 20 LWS, while the remaining data logger was connected to the instrumentation installed at the local weather station. Data was downloaded bi-weekly from the loggers via USB cable. The loggers recorded one sample every minute during the six-month study period for all sensor inputs (e.g., 20 leaf wetness sensors × 1440 minutes per day × 165 days in study period = 4,752,000 rows of data).

The small local weather station (WS) (Figure 11) was installed approximately 3 m from the Lilac tree to collect meteorological data to describe the tree's surrounding environment. This WS consists of two soil moisture sensors, a pyranometer to measure incoming solar radiation, a humidity sensor, and a tipping-bucket rain gauge to collect rain data (Figure 11). Information on wind speed and direction was obtained from a nearby WS (Figure 12) maintained by the Department of Earth and Space Science and Engineering (ESSE) at York University (43° 46.525' N, 079° 30.611' W).

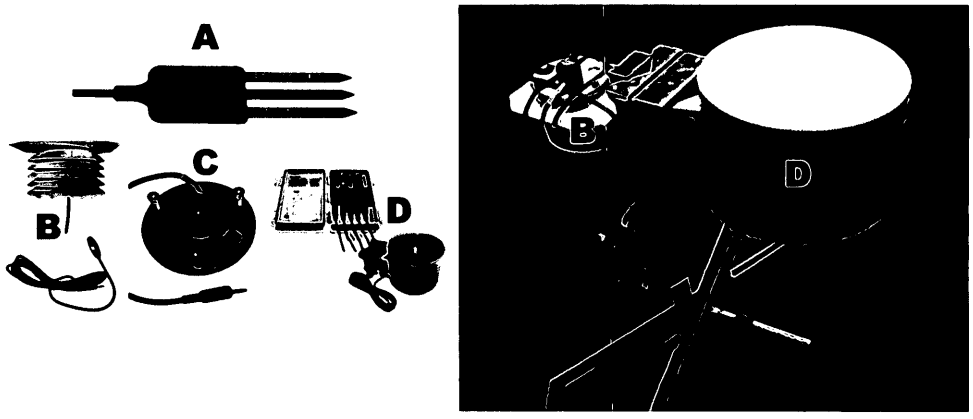

Figure 11. The local weather station installed approximately 3 m from the tree and consists of 2 soil moisture sensors (A), relative humidity/air temperature sensor (B), pyranometer (C), and tipping bucket rain gauge (D).

Soil moisture sensors (Figure 11a) use capacitance to measure the water content of soil. The two soil moisture sensors were installed on a 45° angle at a depth of 3 cm: one near the weather station and the other beneath the tree canopy. The probe on the soil moisture sensor

should be installed angled down at approximately 45° to the ground because it allows the probes to read soil moisture content in the most active portion of the root zone (Zotarelli et al. 2009). This device reports the volumetric water content of soil in percent.

A pyranometer (Figure 11b) is a device used to measure the solar radiation flux density (incoming solar radiation in $W \cdot m^{-2}$) from a field of view of 180° and does not require any power to operate. The solar radiation spectrum extends approximately from 300 to 2800 nm. The pyranometer used in this study is a glass dome, where the dome limits the spectral response from 300 to 2800 nm (cutting off the part above 2800 nm), while preserving the 180 degrees field of view. Inside the dome is a thermopile sensor, which absorbs the solar radiation. This radiation is converted to heat and the heat flows through the sensor to the pyranometer housing. The thermopile sensor generates a voltage output signal that is proportional to the solar radiation. Accurate measurements depend on cleanliness of the lens and installation at a horizontal (180°) angle. The domed top of the pyranometer is self-cleaning and comes with a leveling plate for proper installation. Equation 3 is used to convert the raw data to solar radiation units in $W \cdot m^{-2}$. The conversation equation provided below uses constants that were obtained from Decagon Inc. (2007).

$$\frac{W}{m^2} = (RAW)(\frac{1500}{4096})(5.0) \quad (3)$$

A humidity sensor (Figure 11c) measures the relative humidity in the air. This means that it measures both air temperature and moisture. Relative humidity expressed as a percentage, specifically, it is the ratio of actual moisture in the air to the highest amount of moisture the air can hold at that measured temperature. Thus, the warmer the air is, the more moisture the air can hold, meaning that the relative humidity changes with fluctuations in temperature. The humidity sensor used in this study relies on electrical capacitance (the ability of two nearby electrical conductors to create an electrical field between them). This device has sensors that are composed of two metal plates with a non-conductive polymer film between them. The film collects moisture from the air, and the moisture causes minute changes in the voltage between the two places. These changes in voltage are then converted into digital readings showing the amount of moisture in the air. A radiation shield was attached to the sensor to remove ambient interference, thus improving the accuracy on readings.

A tipping-bucket rain gauge (Figure 11d) consists of a funnel that collects and channels the precipitation into a small seesaw-like container. This device is used to collect rain data; once the threshold (precipitation equal to 0.2 mm) is met, the lever tips and water is dumped into a separate bucket beneath while sending an electrical signal that is recorded. This self-emptying electronic rain gauge has drain holes in the base of the bucket that allow water to drain out of the rain gauge. The recorder consists of a pen mounted on an arm attached to a geared wheel that moves once with each signal sent from the collector. The advantage of the tipping bucket rain gauge is that the intensity of the rain (light, medium, or heavy) can be determined by counting the number of "clicks" in a set period (usually one hour). Also, this device is used for measuring the total amount of precipitation at the study site. The ideal site for installation of the rain gauge is important for most accurate rainfall measurements. It is best to install in sheltered areas that block wind and eddy currents in the vicinity of the gauge. The general rule for installation follows that the height of nearby objects should not exceed about twice their distance from the gauge.

2.3 Data from Alternate Sources

Environment Canada's National Climate Data and Information Archive provides users with access to historical weather and climate data from local weather stations. Daily data was available from three nearby Environment Canada weather stations: North York (43° 46.815' N, 079° 28.100' W; 4.7 km from study site), Buttonville (43° 51.500' N, 079° 22.050' W; 18.0 km from study site), and Pearson (43° 40.415' N, 079° 37.000' W; 17.3 km from study site). Data collected at these weather stations include total amount of precipitation (mm), temperature (°C), wind speed ($m \cdot s^{-1}$), and wind direction (azimuth in degrees from true north). The purpose of obtaining weather station data from these three other weather stations is to determine if the rain events occurring at the study site are representative of the rain events occurring within the surrounding area.

Additionally, wind data (speed and direction) was obtained from York University's ESSE Meteorological Observation Station (EMOS weather station, 43° 46.545' N, 079° 30.665' W; 0.3 km from study site) (Figure 12). The EMOS weather station was initially installed in May 2002; the station is mounted on a 10 m tower, located beside the Tait MacKenzie building. This weather station serves as a real-time data collector of meteorological information for the York University campus, collecting data at a five-minute interval. The station collects data on wind speed, wind direction, temperature, humidity, precipitation amounts, soil temperature, and radiation.

Figure 12. The EMOS at York University, which stands 10 m tall and collects precipitation, atmospheric, and wind data (Figure from Taylor and Salmon 1993).

Of interest for this study is the wind data, since an anemometer (device used to collect wind data) was unavailable at the local weather station installed within the study site. Notably, the Japanese Lilac tree is located near the corner of a building the influence of local eddies circulating within the study site may have an effect on local atmospheric conditions (Figure 13). An eddy is a circulation that develops when the wind flows either adjacent to or over obstructions (e.g., buildings) (Held and Hoskins 1985). The size of the eddy is directly proportional to the size of the obstruction and the speed of the wind (Oke 1987; Zhai et al. 2004). When wind speeds exceed 10 $m \cdot s^{-1}$, the flow may be broken up into irregular eddies that may cause irregular variations in the wind (Green 1970; Held and Hoskins 1985; Zhai et al. 2004).

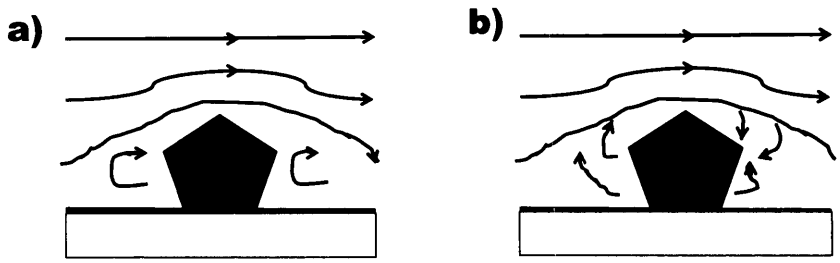

Figure 13. Eddy currents (small arrows) form when wind (larger arrows) flows over obstructions, such as a building (pentagon), in a) low wind speed (below 10 $m \cdot s^{-1}$) and b) high wind speed (above 10 $m \cdot s^{-1}$) conditions.

The anemometer for EMOS is located at the height of 10 m (highest point on the tower) and relays wind direction and speed data. Ideally, a tower should be installed in open terrain with no obstructions. Finding such a site is difficult at a university due to the presence of many buildings, but corrections can be made to the measured wind speeds. Using the distances and direction in degrees true to both the left and right extremities of the obstacle as seen from the tower, together with the obstacle heights, the software package ShelCor can help evaluate how much adjustment (correction factor) to the wind speed data is required (Taylor and Salmon 1993; Salmon and Taylor 2012). With regards to this study, it was assumed that the wind data retrieved from EMOS was consistent with the wind experienced at the study site and that the local eddies did not influence wind significantly.

2.4 GIS Database

GIS is used to collect, store, manage, and analyze spatial data; a function of GIS is the ability to query databases using a selection of attributes (e.g., rain type) or a selection of locations (e.g., LWS position) to find the relationships between different results (Le Duc 1992). To build the GIS database, the raw experimental data (LWS and WS data) was downloaded from the dataloggers and then preprocessed into a CSV output format compatible with the database definitions. Data in the GIS database contained raw data (e.g., LWS and WS data), positional data (e.g., x, y, z coordinates of relative position of LWS), wind data (e.g., wind speed and wind direction from York University's EMOS weather station), derived data (e.g., true north based azimuths for wind direction and mm values for LWS count), and historical data (e.g., data from alternate sources such as data from nearby Environment Canada weather stations). The database was structured into separate tables and indexed by date/time and sensor number (e.g.,

LWS). Data from alternate sources were collected at a different temporal scale (every 5 minutes) from the raw data (every minute), thus data was interpolated to allow for comparison (e.g., data for minute 1 was the same for minute 2 to 4). An outline of the variables stored in the GIS database is described in Table 3.

Table 3. A list of the variables stored in the GIS database, along with the units of measurement and the measurement interval for each variable.

Variable	Units	Measurement Interval (min)
LWS (raw)	counts	1
LWS	mm	1
RH	%	1
Temperature	°C	1
Radiation	$W \cdot m^{-2}$	1
Soil temperature	°C	1
Soil moisture	$m^3 \cdot m^{-3}$	1
Total precipitation	mm	1
Wind speed	$m \cdot s^{-1}$	5
Wind direction	azimuth	5

Given the focus of this project is to study rainfall data, the raw LWS data was analyzed to determine the beginning and the end of each rain event. The start of the rain event was defined as the time when the rain gauge readings initially recorded a rainfall (non-zero reading). Similarly, the end of a rain event was defined as the moment when the rain gauge readings returned to zero. Note that LWS readings may not be zero at the end of a rain event, as moisture levels may persist on leaves for an extended duration after rainfall has stopped. As such, the start of the wetting and the end of the drying phase in the tree canopy may not coincide with the start and end of the rain event respectively. Therefore, rainfall data was classified as data recorded during a rain event rather than based on the duration of the wetting and drying phases. This consideration is explained further in §2.7.

The following three cases demonstrate the difficulty in defining the wetting and drying phase for a tree canopy:

(1) Raindrops during a 20-minute drizzle event may not enter the tree canopy until minute five of the event.

(2) A 10-minute thunderstorm event saturated the entire tree canopy. After the thunderstorm, the tree canopy is still wet despite no additional inputs of intercepted rainfall.

(3) A series of four 30-minute isolated rain showers occur over a 12-hour period. Following each rain shower, the canopy does not completely dry before the next rain shower, therefore parts of the tree canopy are being re-wetted prior to completely drying.

A separate table was created to record the start and end date/time of each rain event, indexed in sequential order; this table was used as the rain event ID for each rain event that occurred during the study period. Other attributes related to a rain event, such as rain classification (e.g., drizzle, moderate rain shower, thunderstorm), were also recorded in this table.

The data from the various tables were combined and filtered into the desired format for subsequent analyses. The times and attributes in the rain event table were used to filter the raw and derived data in order to extract information about one particular or a subset of events (e.g., to retrieve rain data only for thunderstorms in August). The organization of the GIS database allows analysis to focus on specific data subsets via queries. Additionally, to facilitate ANOVA analyses on the relationship among multiple attributes to sensor wetness readings, the data in the database was combined to form the most suitable representation in tabular format. For example, Table 4 shows a snapshot of such an output representation, where each individual LWS sensor reading was correlated to other attributes based on the date/time stamp. This table contained 16 attributes (variables) and 349,180 observations (rows). There was a total of 7 attribute tables in the GIS that contained subsets of the stored data: LWS data, WS data, York University WS data, Environment Canada data, LWS positional data, rain event durations, and rain event classification.

2.5 Data Visualization

While databases are useful for storing and sorting geospatial data, data can also be interpreted via visualization. One approach for 3D visualization is the application of Light Detection and Ranging (LiDAR) systems. LiDAR is a laser range finding device that produces high-density measurements (point clouds) of where objects are in 3D space (Isenburg et al. 2006). Thus, this 3D remote sensing technology is used to develop 3D scenes. Laser pulses are emitted from the device, returning once the laser pulse hits a surface. A pulse of laser light is emitted at a precise time (t_1); the reflection of that pulse from the surface is detected and recorded at time (t_2). Using the constant velocity of light (approximately $c = 3.0 \times 10^8$ ms^{-1}), the time difference between the emission (t_1) and the reflection (t_2) can be converted into a slant range distance (line-of-sight distance). A typical LiDAR system contains a Global Navigation Satellite System (GNSS) to provide position information and a laser system to provide range (distance) information between the laser firing point and the ground point (Kilian et al. 1996; Bang et al. 2008). However, since the terrestrial LiDAR scanner used in this study did not have a Global Positioning System (GPS) receiver attached, the scan of the tree was based on relative positioning on the Cartesian plane coordinate system in 3D space. Thus, the LiDAR scan produced a point cloud, which is a description of a set of points (stored as a text file in comma delimited format), specified by a 3-tuple, [x, y, z] defined on a coordinate system. Each row of point cloud data files contains information for one point. In addition to the easting (x), northing (y), and elevation (z) columns in the point cloud data file, intensity (i) was also stored.

In the case of this study, the application of terrestrial LiDAR offers a 3D visualization of the Lilac tree canopy (Figure 3b). Since the purpose of using LIDAR technology is to obtain a 3D tree canopy model and to isolate the tree structure (branches and leaves) from the installed LWS (differentiated based on different intensity levels), terrestrial LIDAR was used due to its higher point density over a shorter range (Bang et al. 2008). The Optech ILRIS terrestrial laser scanner (Figure 14) was installed on a tripod (at a height of 1 m from the ground) and used to capture a 3D model of the Lilac tree. This terrestrial scanner is a fully portable, laser-based ranging and imaging system that is controlled via a wireless handheld Portable Device Assistant (PDA). The point density and scanning angles were set at default: 130 points/m^2, and horizontal and vertical scanning angle of 50° from nadir respectively. This device was positioned centred, facing the target (Lilac tree), at a distance of 30 m away from the target object. The minimum required distance the scanner can be positioned from the target is 30 m for the Optech terrestrial scanner; therefore, the East-facing side of the tree could not be scanned due to the presence of the

building. Three scans of the tree were taken (from the North, the South, and the West) at a 30 m distance from the tree using the recommended scanning angle of 50° from nadir to allow for a 20% overlap between scans (a requirement for point cloud registration) (Kilian et al. 1996; Bang et al. 2008). The purpose of taking multiple scans is primarily to eliminate potential scanner shadow zones (Isenburg et al. 2006). The method used for scanner registration was to stitch the scans together into one LiDAR point cloud based on three known positions in the scene (i.e., the bird nest in the tree, and the top and bottom corners of the building).

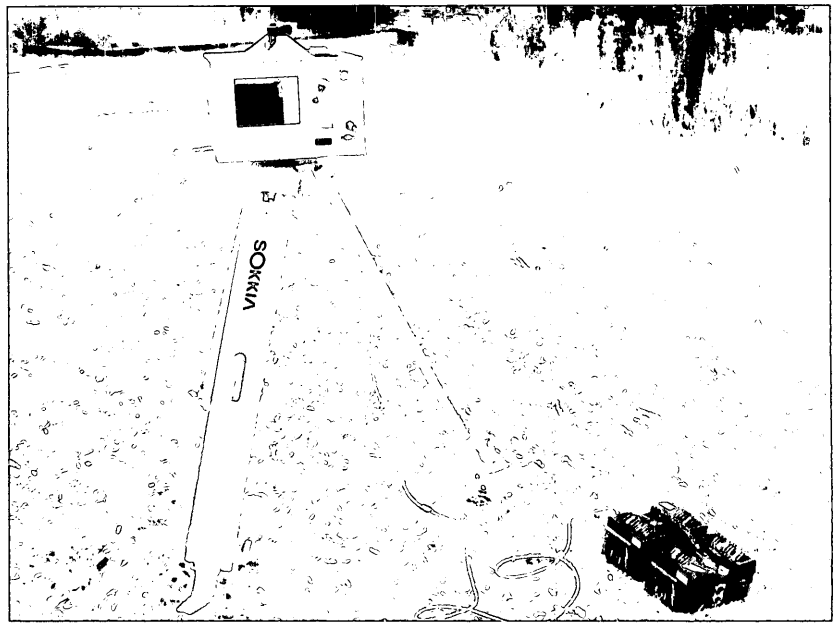

Figure 14. The Optech ILRIS terrestrial laser scanner installed on a tripod positioned 30 m from the target area and used to capture a 3D model of the Japanese Lilac tree.

Once the registered point cloud was obtained, the entire LiDAR scan was viewed in order to distinguish the objects in the scene (e.g., tree and building). Then, the tree was isolated from the building by comparing the intensity levels for the tree points with the building points (Figure 3b, 15a). Since different objects produce different levels of intensity, distinctive intensity levels made it possible to differentiate between the tree points and the building points within the 3D point cloud for the entire scene (e.g., Baltsavias 1999; Song et al. 2002; Ahokas et al. 2006; Brennan and Webster 2006). The same approach was used to distinguish between tree points and sensor points to create a skeletonized 3D branching structure of the tree (Figure 15b). Table 4 outlines the intensity ranges used to distinguish between different objects in the scene.

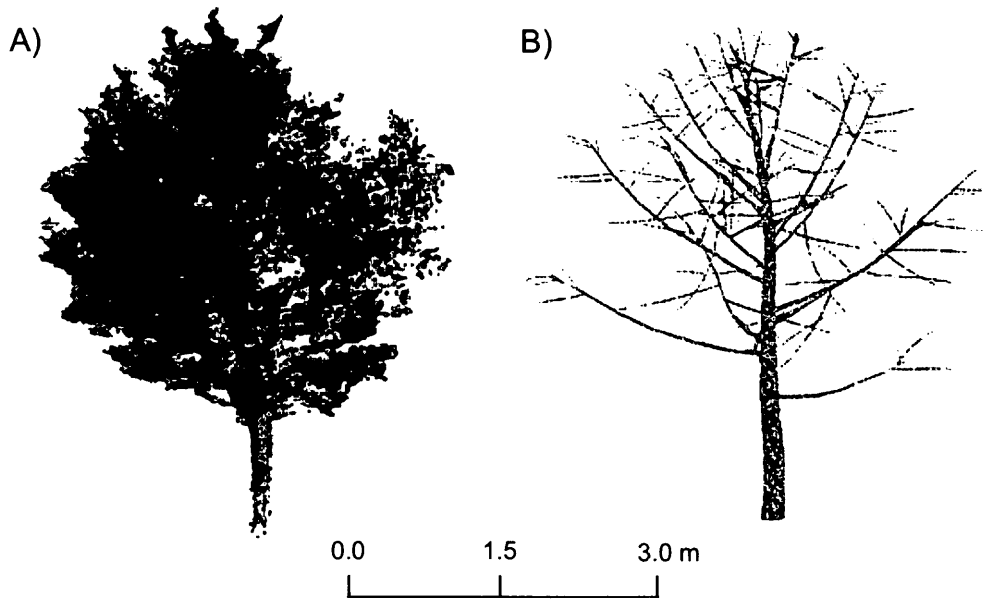

Figure 15. After isolating the tree from other objects in the scene (A), the tree points are differentiated from the LWS points in the point cloud using intensity. Then, a skeletonized 3D branching structure of the tree (B) was created.

Table 4. A list of the intensity ranges used to distinguish between different objects in the LiDAR point cloud scans.

Object	Intensity Range (%)
Asphalt	5 - 23
Branches on tree	22 - 28
Building	30 - 39
Grass	40 - 52
Leaves on tree	58 - 67
LWS sensors	70 - 77

Since the points that represented the 20 LWS sensors could be distinguished from the leaves in the tree canopy, it was possible to obtain the positional locations of the LWS. The [x, y, z] coordinate for the 20 LWS was translated based on relative positioning that corresponded to the centre of the tree defined as [0, 0, 0]. Data describing the 3D position of the 20 LWS was stored as a table in the GIS database.

In order to develop a 4D GIS model of the Lilac tree canopy during a precipitation event, the 3D tree canopy model requires an additional dimension of time (i.e., moisture readings collected for every minute of each rainstorm event). The point cloud retrieved from the terrestrial LIDAR scan was then used to build a 3D tree canopy model (i.e., a skeletonized branching structure of the tree) that resembles Figure 15b.

Then, the 3D tree point cloud data was exported into a software package containing integrated 3D modeling and animation tools (e.g., *Autodesk 3ds Max*). The visualization dimension to this project is seen in Figure 16. Notice how the tree point cloud now looks smooth and the sensors can be easily differentiated from the tree branches (Figure 16). Further, the sensor position (x, y, z relative coordinate positions) was plotted on a 3D grid to create another type of animation where the colour of the dot changed depending on wetness (binary colour change where a wet reading would result in the sensor point changing to a different colour) (Figure 17).

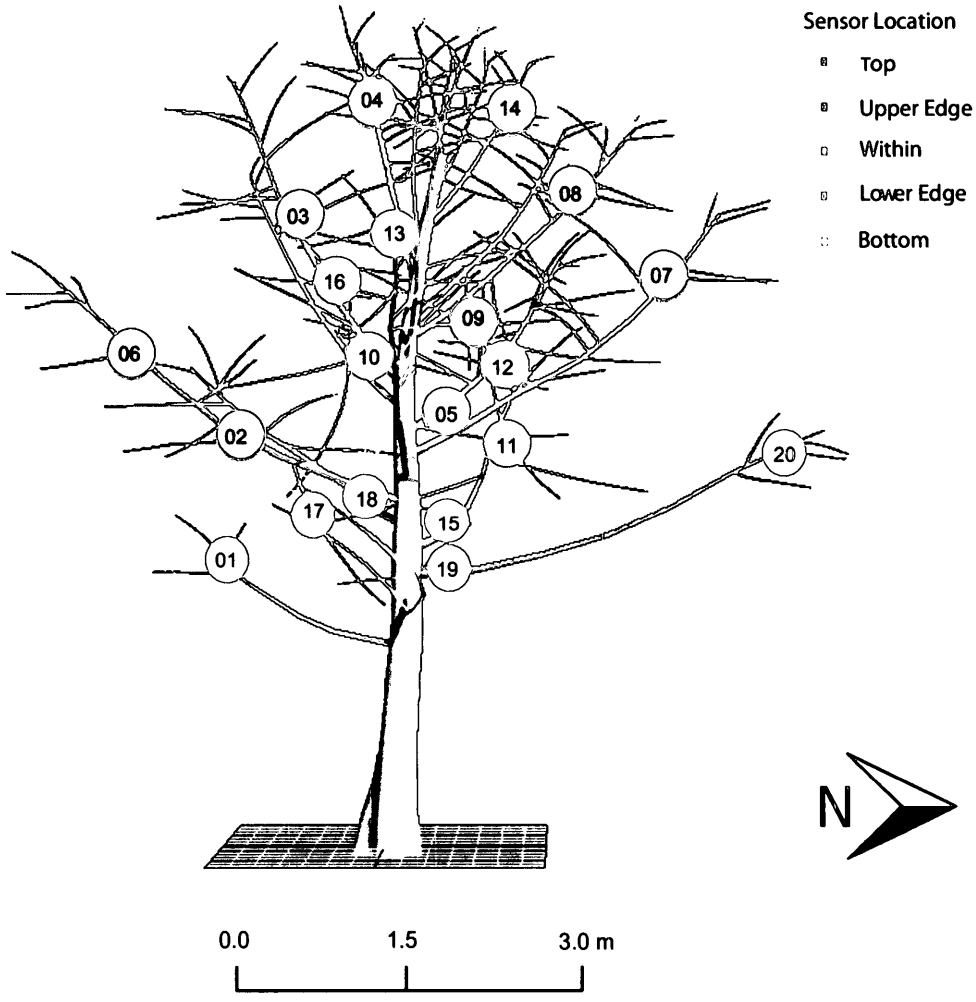

Figure 16. One frame from a rain event animation displaying the 3D visualization of the Japanese Lilac branching system; using the x, y, and z coordinates in relative space, the locations of the 20 LWS were added to this visualization.

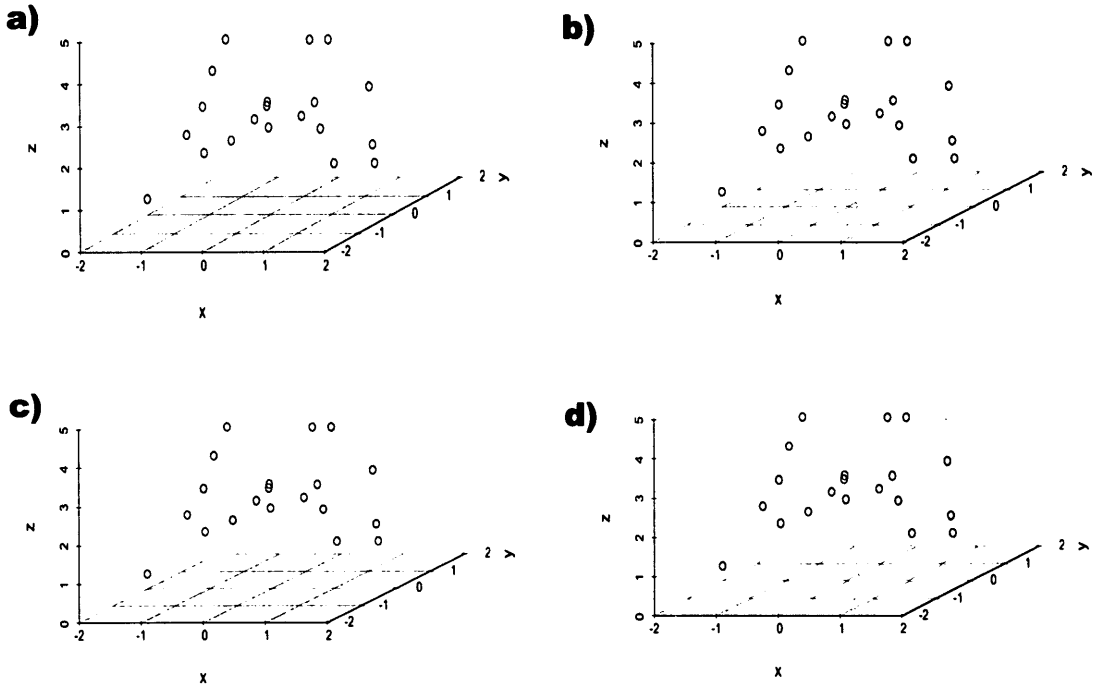

Figure 17. Four frames from a rain event animation displaying the 3D visualization of the 20 LWS sensors using the x, y, and z coordinates in relative space. A green dot indicates a dry reading and a blue dot indicates a wet reading: a) t = 0 minutes into rain event, b) t = 5 minutes into rain event, c) t = 10 minutes into rain event; d) t = 15 minutes into rain event.

Animations were created that reflect the frames illustrated in Figure 16 and 17, for all 79 rain events. This set of animations was viewed and patterns were observed for various sensor positions and rain types. For instance, all drizzle events were viewed to determine if the sequence of sensors that wetted displayed similar wetting patterns for the same rain type. Additionally, the trends observed for drizzle events, for example, were then compared to the trends observed in thunderstorms to determine if the patterns were unique to the rain type.

Viewing animations allows for characterization of canopy moisture dynamics and offers insight on the types of ANOVA tests to perform in order to statistically support the observed patterns. Thus, the ability to animate (rotate) a 3D point cloud (e.g., Figure 16, 17) is powerful since it provides visualization of the entire tree canopy structure (Raper 1989; Tversky et al. 2002). By incorporating moisture data for a given time interval during a rain event, the moisture dynamics within the tree canopy can be tracked throughout the event by observing the sequence of the sensors wetting for a given rain event. Figure 17 illustrates an example of four frames during a 15-minute rain event; this figure demonstrates how viewing an animation highlights the sequence in which sensors are wetted during a rain event. Notice how in the frame for t = 5

(Figure 17b), only six sensors (located along the upper edge of the canopy) have wetted while the frame for t = 15 (Figure 17d), almost all the sensors have wetted. Visualizing how the tree canopy wets under different rain conditions through animated images for different instances of time presents the opportunity to visualize the characterization of the flow of moisture. Thus, creating an animation is an alternate approach from graphical visualization and supports the recognition of patterns in the given data.

2.6 Hypotheses and ANOVA

Traditional interception models typically assume homogeneous conditions during a rainstorm event (see §1.3), in that the behaviour of moisture in the tree canopy is modeled as a binary case of wet or dry (Lankreijer et al. 1993). However, in reality, various portions of leaves and the canopy may be wet and/or dry at different times (Huber and Gillespie 1992). Due to variations in rainfall throughout and among rain events, the significance in wetting dynamics can be computed to demonstrate the heterogeneous nature of canopy wetting.

One-way Analysis of Variance (ANOVA) tests were used to determine if any of the moisture dynamic metrics were significantly different based on one or more sensor location or rain characteristics. The null hypotheses for the ANOVA tests stated that the means of the moisture dynamic metric (i.e., average moisture readings on LWS sensors) are equal across all factors being investigated (e.g., sensor location). For each test, the 95% confidence interval on the mean was computed ($\alpha = 0.05$). If the test is significant, the null hypothesis (H_0) is rejected and it is concluded that at least one of the means differ from the others (Bluman 2006). In situations of a significant result consisting of three or more means, a post hoc test is required to provide specific information on which means are significantly different from each other. A Tukey HSD (Honest Significant Difference) test was performed to assess each pairwise combination of the means to determine exactly which set of means differed from the other (Bluman 2006). In the following subsections, the description of the ANOVA tests performed and its statistical notation is outlined in further detail.

2.6.1 ANOVA Tests Based on Sensor Location

One-way ANOVA tests were computed to determine whether the mean LWS readings (in mm) differed based on sensor location. The sensor locations of the LWS in the tree canopy were factored into the following categories: top (*T*), upper edge (*UE*), within (*W*), lower edge (*LE*), and bottom (*B*). A general ANOVA test was first performed for all LWS readings across all events against the following H_0 and H_A hypothesis. A significant result will demonstrate that in general, at least one of the general sensor positions differs from the others in the mean LWS moisture readings.

1) H_0: $\mu_T = \mu_{UE} = \mu_W = \mu_{LE} = \mu_B$

H_A: At least one of the sensor positions differs from the others in mean moisture readings.

To refine whether certain dynamics impacted the variance of the mean LWS moisture readings for different sensor locations, further ANOVA tests were computed against a subset of the data. These data subsets were filtered to include only the relevant LWS readings. Dynamics include: season (e.g., summer vs. fall), canopy coverage (e.g., presence of leaves vs. no leaves), rain intensity (e.g., high intensity vs. low intensity), and rain character (e.g., intermittent vs. continuous). The following sets of hypotheses outline the statistical notation for the aforementioned dynamics.

Two separate ANOVA tests were applied against the following H_0 and H_A for summer data and fall data. Significant results can indicate that the variations in wetness readings for certain sensor locations are seasonal.

2) H_0: $\mu_{T\text{-season}} = \mu_{UE\text{-season}} = \mu_{W\text{-season}} = \mu_{LE\text{-season}} = \mu_{B\text{-season}}$
where season is either summer or fall. Summer data includes data from June to September 21st. Fall data includes data from September 22nd to November.

H_A: At least one of the sensor positions differs from the others in mean moisture readings during the summer or fall season.

Two separate ANOVA tests were applied against the following H_0 and H_A for periods with the presence of leaves (ON) and the absence of leaves (OFF). The presence or absence of leaves is a description of canopy coverage (LEAF), as well as canopy storage in regards to its water holding capacity. This ANOVA test is different from the seasonal ANOVA test because leaves may still be present in the tree canopy despite the start of the fall season. Significant results can indicate that the variations in wetness readings for certain sensor locations are dependent on the presence of foliage.

3) H_0: $\mu_{T\text{-}LEAF} = \mu_{UE\text{-}LEAF} = \mu_{W\text{-}LEAF} = \mu_{LE\text{-}LEAF} = \mu_{B\text{-}LEAF}$

where *LEAF* is the leaf coverage for the tree canopy and includes the cases of either the presence or absence of leaves. The presence of leaves is representative of a dense canopy and includes data for all the rain events where leaves were present during rainfall. The absence of leaves is representative of a sparse canopy and includes data for all the rain events where no leaves were present on the branches during rainfall.

H_A: At least one of the sensor positions differs from the others in mean moisture readings with the presence/absence of leaves.

Three separate ANOVA tests were applied against the following H_0 and H_A for periods of various intensities (*I*), specifically during low intensity, moderate intensity, and high intensity rainstorms. The rainstorm intensity is defined in Table 1. Significant results can indicate that the variations in wetness readings for certain sensor locations are dependent on the rainfall intensity.

4) H_0: $\mu_{T\text{-}I} = \mu_{UE\text{-}I} = \mu_{W\text{-}I} = \mu_{LE\text{-}I} = \mu_{B\text{-}I}$

where *I* is the rainfall intensity and includes data from either low intensity, moderate intensity, or high intensity rainstorms. Low intensity rainstorms include drizzle and light rain showers. Moderate intensity rainstorms include rain showers and moderate rain showers. High intensity rainstorms include heavy rain showers and thunderstorms.

H_A: At least one of the sensor positions differs from the others in mean moisture readings during low/moderate/high intensity rainstorms.

Two separate ANOVA tests are applied against the following H_0 and H_A for intermittent rainfall (int) and continuous rainfall (con). The rainstorm character (*C*) is defined in Table 1. Significant results can indicate that the variations in wetness readings for certain sensor locations are dependent on the rainfall character.

5) H_0: $\mu_{T\text{-}C} = \mu_{UE\text{-}C} = \mu_{W\text{-}C} = \mu_{LE\text{-}C} = \mu_{B\text{-}C}$

where *C* is the rainfall character and includes data from either intermittent or continuous rainstorms. Intermittent rainstorms include drizzle, rain showers, and thunderstorms. Continuous rainstorms include light rain showers, moderate rain showers, and heavy rain showers.

H_A: At least one of the sensor positions differs from the others in mean moisture readings during intermittent/continuous rainstorms.

2.6.2 ANOVA Tests Based on Rain Characteristics

One-way ANOVA tests were computed to determine whether the mean LWS readings (in mm) differed based on rain categories. The rain categories were separated into six groups based on intensity; the categories in order from lowest to highest intensity are drizzle (*D1*), light rain showers (*LRS2*), rain showers (*RS3*), moderate rain showers (*MRS4*), heavy rain showers (*HRS5*), and thunderstorms (*T6*). A general ANOVA test was first performed for all LWS readings across all sensors.

6) H_0: $\mu_{D1} = \mu_{LRS2} = \mu_{RS3} = \mu_{MRS4} = \mu_{HRS5} = \mu_{T6}$

H_A: At least one of the rain categories differs from the others in mean average moisture readings.

To refine whether certain dynamics impacted the variance of the mean LWS readings for different rain categories, further ANOVA tests were computed against a subset of the data. These data subsets were filtered to include only the relevant LWS readings. Dynamics include: sensor position, season (e.g., summer vs. fall) and canopy coverage (e.g., presence of leaves vs. no leaves). The following sets of hypotheses outline the statistical notation for the aforementioned dynamics.

Six separate ANOVA tests were applied against the following H_0 and H_A for periods for data during drizzle (D1), light rain showers (LRS2), rain showers (RS3), moderate rain showers (MRS4), heavy rain showers (HRS5), and thunderstorms (T6). The rain category classification is defined based on both intensity and character and is outlined in Table 1. Significant results can indicate that the variations in wetness readings for certain sensor locations are dependent on rain type.

7) H_0: $\mu_{T\text{-}RC} = \mu_{UE\text{-}RC} = \mu_{W\text{-}RC} = \mu_{LE\text{-}RC} = \mu_{B\text{-}RC}$
where *RC* is the rain category and includes data from either D1, LRS2, RS3, MRS4, HRS5, or T6.

H_A: At least one of the sensor positions differs from the others in mean moisture readings for D1 / LRS2 / RS3 / MRS4 / HRS5 / T6 events.

Two separate ANOVA tests are applied against the following H_0 and H_A for summer data and fall data. Significant results can indicate that the variations in wetness readings for certain rain types are seasonal.

8) H_0: $\mu_{D1\text{-}season} = \mu_{LRS2\text{-}season} = \mu_{RS3\text{-}season} = \mu_{MRS4\text{-}season} = \mu_{HRS5\text{-}season} = \mu_{T6\text{-}season}$
where season is either summer or fall. Summer data includes data from June to September 21st. Fall data includes data from September 22nd to November.

H_A: At least one of the rain categories differs from the others in mean average moisture readings for summer/fall.

Two separate ANOVA tests are applied against the following H_0 and H_A for periods with the presence of leaves and the absence of leaves. The presence or absence of leaves is a description of canopy coverage, as well as canopy storage in regards to its water holding capacity. Significant results can indicate that the variations in wetness readings for certain rain types are dependent on the presence of foliage.

9) H_0: $\mu_{D1\text{-}LEAF} = \mu_{LRS2\text{-}LEAF} = \mu_{RS3\text{-}LEAF} = \mu_{MRS4\text{-}LEAF} = \mu_{HRS5\text{-}LEAF} = \mu_{T6\text{-}LEAF}$
where *LEAF* is the leaf coverage for the tree canopy and includes the cases of either the presence or absence of leaves. The presence of leaves is representative of a dense canopy and includes data for all the rain events where leaves were present during rainfall. The absence of leaves is representative of a sparse canopy and includes data for all the rain events where no leaves were present on the branches during rainfall.

H_A: At least one of the rain categories differs from the others in mean average moisture readings with the presence/absence of leaves.

2.6.3 ANOVA Tests Based on Normalized Time

The basic conjecture is that certain sensors consistently get wet earlier than other sensors. In order to determine the validity of this conjecture, the "normalized time to maximum wetness" is measured. This measurement is how far into an event E_j, a given sensor S_j registered its maximum reading for that event. Let $T(_{i,\,j})$ refers to this normalized time to maximum wetness for Event i, sensor j. For example, if sensor 1 in event 2 achieved its maximum wetness reading at the 4^{th} minute into the event, which had total duration of 10 minutes, the normalized time to maximum wetness T(1,2) will be calculated as 4/10, or 0.4. For each sensor S_j, the mean, μ_j, of all $T(_{i,\,j})$ across all events i is calculated. A smaller mean value would imply that on average, that given sensor got wet earlier into the event.

However, given the different characteristics of the events, it is expected that the within-variance of these $T(_{i,\,j})$ readings for a given sensor S_j to potentially be large. For example, a thunderstorm may cause certain sensors to achieve maximum wetness very early in the event, while a rain shower may cause the same sensor to saturate to its maximal level much later into the event. To quantify this variance, an ANOVA test was performed to determine whether the means of the normalized time to maximum wetness significantly differed based on the sensor. A significant result from post hoc tests between two sensors, will suggest that one of the two sensors gets wet before the other sensor within our given confidence levels.

10) H_0: $\mu_1 = \mu_2 = \ldots = \mu_j$

where μ_j is the mean of all normalized time to maximum wetness values for sensor *j* across all events (*j* = 20).

H_A: At least one of the means of normalized times differs from the other sensors.

To better reduce the within-group variance, several approaches were taken. The first approach is to subset the data based on rain category. The expectation is that different rain types show a typical wetting pattern during different stages of the event. For instance, thunderstorms typically show a pattern of high LWS moisture readings early in the event. Another example is for drizzle events where the moisture dynamics are less variable and the wetness readings typically produce a very flat line when graphically visualized.

Six separate ANOVA tests were applied against the following H_0 and H_A for periods of data during drizzle (D1), light rain showers (LRS2), rain showers (RS3), moderate rain showers (MRS4), heavy rain showers (HRS5), and thunderstorms (T6). The rain category (RC) classification is defined based on both intensity and character and is outlined in Table 1. Significant results can indicate whether certain sensor locations wet first during different types of rainstorms.

11) H_0: $\mu_{1\text{-RC}} = \mu_{2\text{-RC}} = \ldots = \mu_{j\text{-RC}}$

where *RC* is the rain category and includes data from either D1 (*i* = 18), LRS2 (*i* = 18), RS3 (*i* = 24), MRS4 (*i* = 7), HRS5 (*i* = 4), or T6 (*i* = 8). Also, *i* is the number of events in given RC and *j* is the sensor number (*j* = 20).

H_A: At least one of the normalized times differs from the others for certain sensors during D1 / LRS2 / RS3 / MRS4 / HRS5 / T6.

The second approach is based on the observation that wetness phases for high intensity rain events typically show a sharper increase in wetness readings (e.g., wetting phase), followed by a prolonged period of saturation at near maximum wetness overlapped with a gradual decrease during the drying phase. Given that there are temporally localized fluctuations in wetness readings, a maximum wetness reading may be recorded late into an event during the prolonged saturation/drying phase. In order to capture the initial jump in wetness for a given event i, the normalized time was computed to achieve 80% of the maximum wetness increase for a given sensor j ($T_{0.8}(i,j)$). The 80% was an empirically determined threshold that captures the

initial sharp increase in wetness reading. This approach reduces sensitivity to localized fluctuations during saturation, and as such, reduces the variance in the normalized time to maximum wetness readings.

12) H_0: $\mu_{0.8(1)} = \mu_{0.8(2)} = \mu_{0.8(3)} = \ldots = \mu_{0.8(j)}$

where j is the sensor number (j = 20). Note that the normalized times used in these ANOVA tests capture the point in time when the wetness for a given sensor has increased to 80% of its maximum wetness reading.

H_A: At least one of the normalized times differs from the other sensors.

2.6.4 ANOVA Tests Based on Time Intervals

For a given event, the LWS readings for a given sensor are averaged in intervals of X minutes. ANOVA tests were performed to determine whether the means of the average readings of the 20 sensors are significantly different between every two successive intervals (e.g., t_1 vs. t_2 where t_1 is minute 1 to 5 and t_2 is minute 6 to 10 of the same event). The expectation is that for events where there is a sharp increase in leaf wetness, the ANOVA results will show significant difference. If the canopy has reached saturation / steady state, or if the area of the canopy is not getting significantly wet, then the ANOVA results will not be significant. The intent of performing ANOVA tests where the two groups being compared are successive time intervals is to determine whether a given event demonstrates unique wetness patterns.

In order to determine the interval size, the LWS graphs (Appendix B) were reviewed to determine an ideal interval size that captures the variability in the wetness data. Thus, factors, such as rain category and rain intensity for a given event were considered. Notably, a larger interval may not capture significant differences as the variability may be encapsulated within a single interval. Conversely, too small of an interval size may be too granular and produce a lot of non-significant results (noise in dataset). It was determined that for a five-minute interval was the most appropriate time interval for comparison since it captured short-term fluctuations.

For each event, ANOVA tests were computed for each pair of successive five-minute intervals over the same event. Separate ANOVA tests were computed on a subset of data based on the positional locations of the LWS in order to determine the point in time for a given event in which wetness was significant for various regions within the tree canopy.

13) H_0: $\mu_i = \mu_{t+1}$

where *a* five-minute time interval at t_i is compared to the next five-minute interval at t_{i+1}.

H_A: The five-minute time interval differs from the successive five-minute time interval in mean moisture.

2.6.5 ANOVA Tests Based on Wind

Wind data collected from EMOS was converted to azimuth bearings using a 360° azimuth circle with 0° / 360° representing True North (Appendix C). Directions are expressed in degrees of azimuth progressing clockwise through 90° representing due East, 180° representing due South, 270° representing due West, and 360° representing due North. One-way ANOVA tests were computed to determine whether the mean wetness readings differed based on the wind direction category. The wind direction was categorized into quadrants centered on the cardinal directions: North (0° to 44° and 315° to 360°), East (45° to 134°), South (135° to 224°), and West (225° to 314°). The ANOVA test was first performed for all wind readings (azimuth) across all events against the following H_0 and H_A hypothesis. A significant result will demonstrate that at least one of the wind direction categories differs from the others in the mean LWS moisture readings.

14) H_0: $\mu_N = \mu_E = \mu_S = \mu_W$

H_A: At least one of the wind direction categories differs from the others in mean moisture readings.

To refine whether wind speed dynamics impacted the variance of the mean LWS moisture readings for different wind directions, an additional ANOVA test was computed against a subset of the data based on wind speed. As alluded to in §2.3, wind is separated into different wind classes, defined by the International Electrotechnical Commission standard (IEC), and corresponds to low, medium, and high wind (IEC 2012) (Table 5).

Table 5. Chart outlining different wind speeds, ordered from low to high (IEC 2012).

Wind Speed	Standard Range
Low	< 7.5 m·s^{-1}
Medium	7.5 m·s^{-1} to 9.9 m·s^{-1}
High	≥ 10 m·s^{-1}

The effect of wind speed on rainstorms has been linked to runoff and interception processes; several studies have investigated the relationships between rainstorm intensity and wind speed (e.g., Wishmeier and Smith 1958; Pedersen and Hasholt 1995; Bourassa et al. 1997; Helming 2001; Weissman et al. 2001; Draper and Long 2004). However, during the study period, most of the recorded wind speed at EMOS was classified in the low wind speed category, thus, conditions for high wind speeds could not be tested. The maximum wind speed recorded at EMOS was 8.59 m·s^{-1} and most events recorded wind speeds less than 5 m·s^{-1}. Due to this, the wind speed data (*s_wind*) could not be separated based on the standardized classes outlined in Table 6. A histogram was created for the wind speeds recorded at EMOS to determine the frequency distribution; this graphical representation was a guideline for defining the class widths for the range of wind speed data. Wind speed, therefore, was separated into three classes (groups): low (< 5.0 m·s^{-1}), mid-low (5.0 to 7.5 m·s^{-1}), and medium (> 7.5 m·s^{-1}) to determine if there are significant differences within the range of wind speeds recorded at EMOS.

Three separate ANOVA tests were applied against the following H_0 and H_A for periods of data with low, mid-low, and medium wind speeds. Significant results can indicate whether wind speed influences the wetness readings for different wind directions during a given rain event.

15) H_0: $\mu_{N\text{-}s\_wind} = \mu_{E\text{-}s\_wind} = \mu_{S\text{-}s\_wind} = \mu_{W\text{-}s\_wind}$

where *s_wind* is wind speed in m·s^{-1} and this includes the categories of low and medium.

H_A: At least one of the wind direction categories differs from the others in mean moisture readings.

2.7 Rate of Wetness Change

Based on the observation of the LWS graphs (Appendix B) that rain events have distinct wetting and drying phases, it presented the opportunity to determine the point of saturation (point in which sensors reached maximum wetness). It was observed that different rain categories displayed unique wetting and drying slopes throughout the event. Thus, a comparison of the wetting and drying slopes across different rain types and sensor locations can provide insight on whether the observed patterns are unique to certain rain conditions. For example, it is expected that for sensors that for high intensity rain storms (e.g., thunderstorms), sensors would get wet faster compared to low intensity rainstorms (e.g., drizzle). Thus, a larger slope would likely be computed in the case of higher intensity rainstorms. Further, the division between the wetting and drying slope is defined as the point of saturation since the sensor is no longer getting more wet. The drying slope is distinguished from the wetting slope with a negative rate of change, and likewise, a larger slope would indicate a faster drying rate.

As described in §2.4, it is difficult to identify the start and end times for the wetting and drying phase. Thus, a 15-minute moving average was applied to the one-minute LWS data across all events. The application of a moving average to time-series data is to smooth out short-term fluctuations and highlight longer-term trends in the LWS graphs. Given a series of numbers (i.e., LWS readings for an event) and a fixed subset size (i.e., 15-minutes), the first element of the moving average is obtained by taking the average of the initial fixed subset of the number series. Then the subset is modified by shifting forward; that is, excluding the first number of the series and including the next number following the original subset in the series. This creates a new subset of numbers, which is averaged. This process is repeated over the entire set of data for each rain event; the data produced from these subsets is referred to as the moving average.

Once the start and end times for the wetting and drying phases were determined using the moving average plots for each event, the original recorded LWS data between those start and end times were filtered out and graphed. A line of best fit was generated for each of the observed wetting and drying phases using the original LWS data set and the slope was computed based on the following equation (Eq. 4).

$$m = \frac{(w_{t2} - w_{t1})}{(t_2 - t_1)} \tag{4}$$

Equation 4 is used to compute the wetting and drying slope where the rate of change is determined as the change in LWS wetness (Δw) over the change in time (Δt). The values used in this slope calculation are obtained from the start and end times in the rolling average using wetness data from the original dataset.

3. RESULTS

3.1 Historical and Current Patterns on Seasonal Trends

Ontario experiences continental climate and is defined by the seasonal trend of precipitation and annual runoff increasing from northwest to southeast (Environment Canada 2010). The year 2009 (year of study period) presented above seasonal averages for precipitation (mean total precipitation of 776 mm) and slightly below seasonal averages for temperature (mean temperature of 8.5°C) (Figure 18). Therefore, the year 2009, relative to the 25-year long-term normal, was a wet year with regards to precipitation while temperature deviated only slightly from the long-term. Below is a temperature-precipitation graph (Figure 18) illustrating the seasonal trends for the past 25 years (1987 to 2012) in Toronto, Ontario, Canada. Data in Figure 18 was obtained from Environment Canada's weather station at Pearson Airport and is based on long-term averages of monthly temperature and precipitation records.

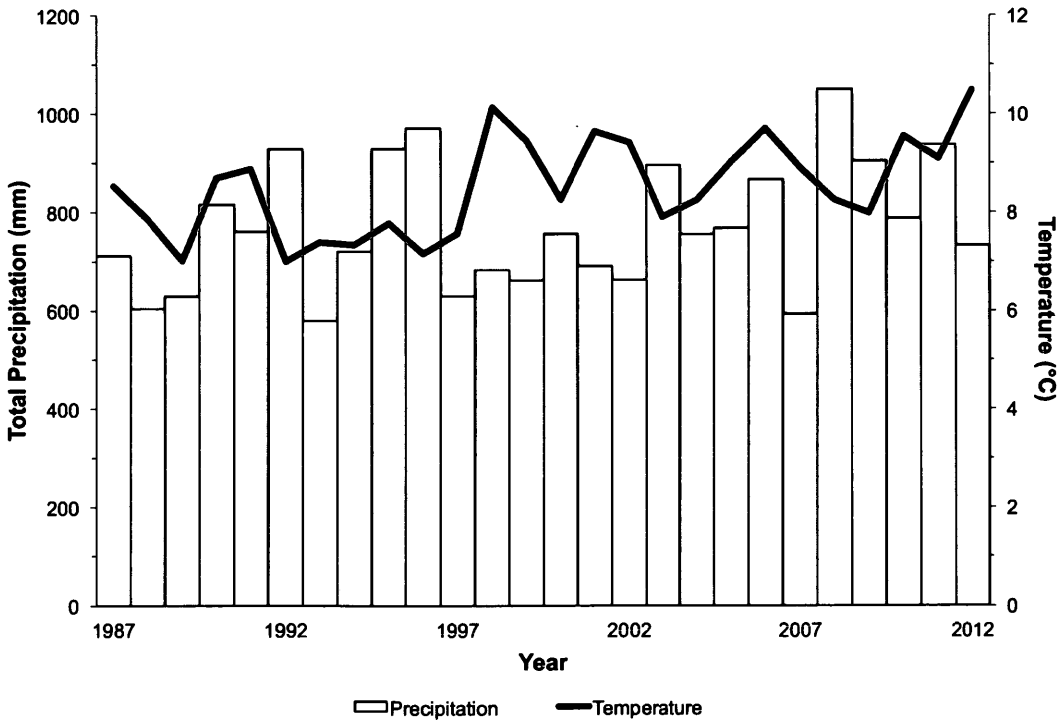

Figure 18. A graph illustrating the seasonal trends for both precipitation and temperature over the past 25 years (1987-2012) in Toronto, Ontario where the bars represent the total annual precipitation and the line represents the mean annual temperature. The average total annual precipitation over the 25-year period is 769.6 mm and the average mean annual temperature recorded over the 25-year period is 8.5°C. Data was retrieved from Environment Canada's weather station at Pearson Airport (43° 40.415', 079° 37.000' W).

The year 2009 was characterized as a season with above averages for precipitation (Figure 19, 20). More specifically, during the study period (June to November 2009), there were a total of 79 rain events (Appendix A) and the bulk of these events were classified as low intensity storms (e.g., drizzle, light rain showers) (Table 6). The monthly average temperatures during the study period (with the exception of July and September) stayed near normal across the province, varying from their expected values by an average of only half a degree below normal (Figure 21). Note that the spacing of the months along the x-axis in the following graphs illustrating data collected from the study site is not equal due to an unequal distribution of events in each month. Table 6 highlights that the months of June, September, and November experienced fewer rain events compared to the months of July, August, and October.

Table 6. An outline of the total number of rainstorm events recorded for each month during the study period and for each type of rain category.

	D1	LRS2	RS3	MRS4	HRS5	T6	Total
June	2	1	3	0	0	2	8
July	3	6	4	0	1	2	16
August	5	2	2	2	1	5	17
September	2	2	4	2	0	0	10
October	4	5	7	2	1	0	19
November	2	2	4	1	0	0	9
Total	18	18	24	7	3	9	79

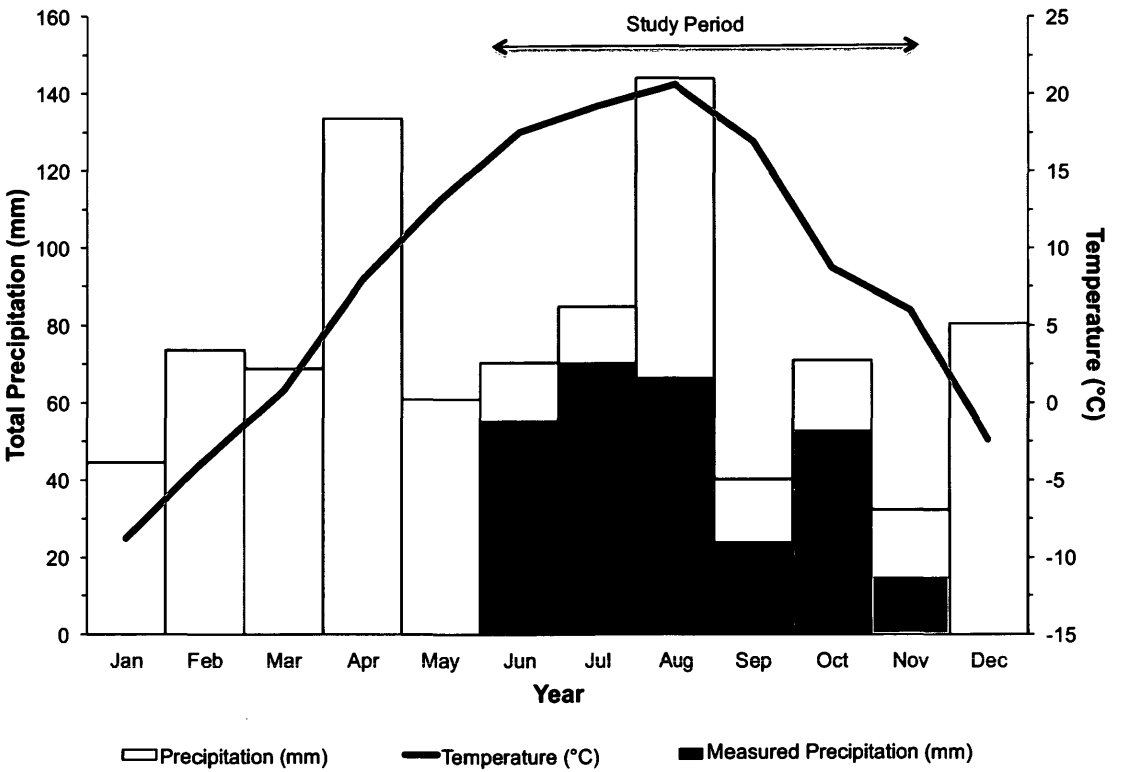

Figure 19. A graph illustrating the seasonal trends for both precipitation and temperature over the study period (2009) in Toronto, Ontario where the bars represent total precipitation (data from white bars is from Environment Canada and data from blue bars is from the tipping bucket rain gauge installed at the study site) and the line represents the mean temperature. Note that the snow precipitation in the winter months from Environment Canada was converted to SWE for comparison. The weather trends during the study period (June to November 2009) are summarized: the summer season experienced heavy precipitation with abnormally high rainfall totals recorded in the latter half of July and August. With regards to temperature, after a cool June and July, seasonal temperatures of over 30°C arrived for the remainder of the summer. Fall marked above-normal seasonal temperatures, with the exception of October temperatures remaining seasonal. As for precipitation, the fall months were drier than seasonal norms for September and November, but rainfall was both numerous and intense in October and storms were accompanied by strong winds.

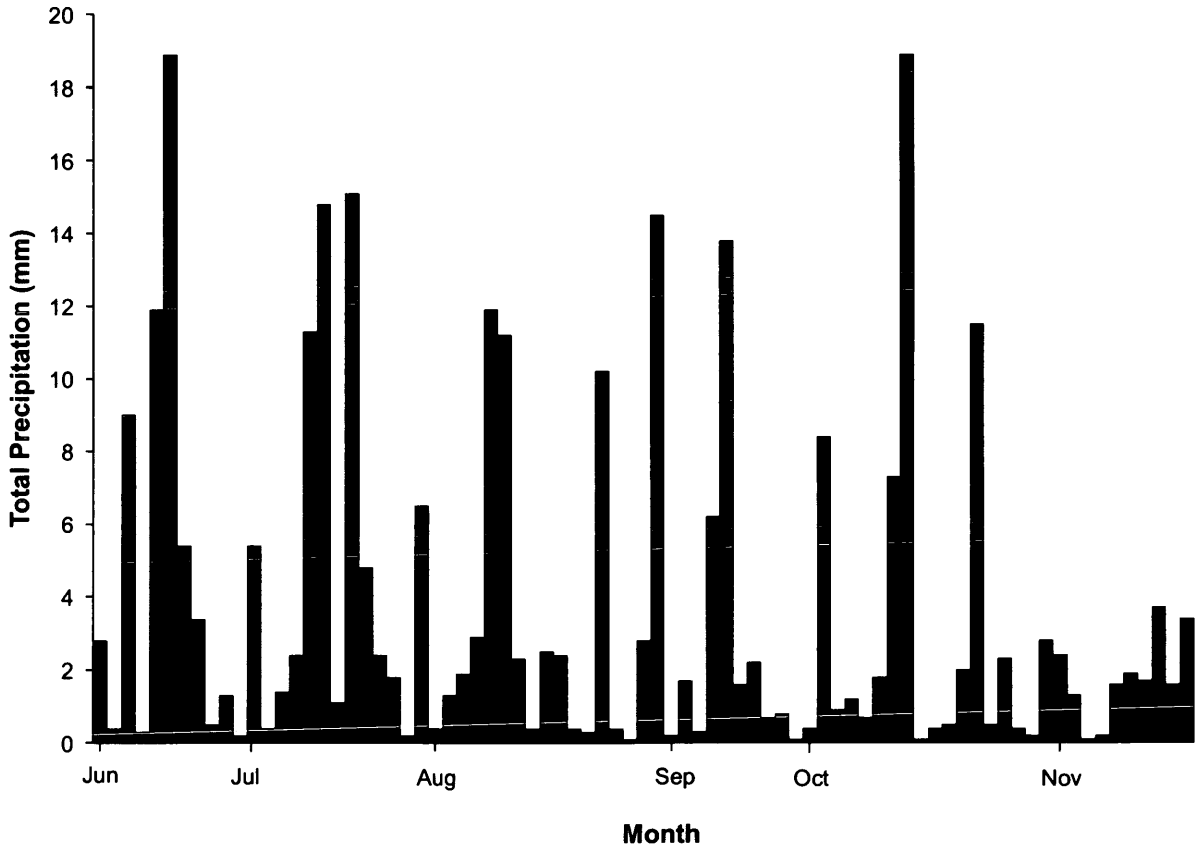

Figure 20. The temporal distribution of net precipitation (in mm) recorded during the study period (June to November 2009) is outlined above, where each bar represents the total amount of rainfall for one rain event. Data was obtained from the tipping bucket rain gauge installed at the study site.

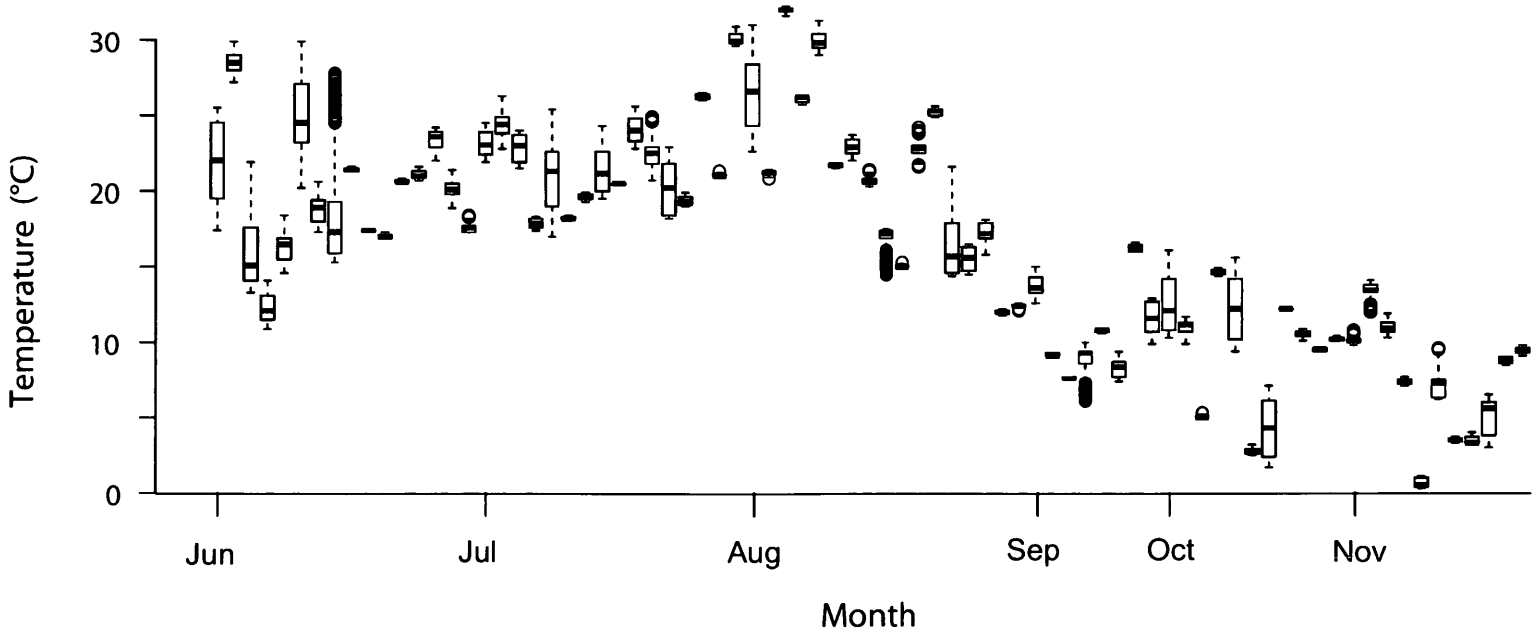

Figure 21. The temporal distribution of air temperature (°C) for each rain event recorded during the study period (June to November 2009) is outlined above in boxplots, where each bar represents a rain event. The thick horizontal line represents the median temperature, the lower end of the box presents the lower quartile, and the higher end of the box represents the upper quartile. The whiskers that extend downwards and upwards represent the minimum-recorded temperature and the maximum-recorded temperature respectively. This uses data recorded by the relative humidity sensor installed at the weather station 3 m from the study site.

The summer season (June to September 21st) were active months for thunderstorms; the humid air that pushed northwards from the Gulf of Mexico drove the development of thunderstorms. However, July experienced exceptionally cooler temperatures (mean of 19.8°C); as a result, the cooler air did not intrude on the Gulf air. Thus, the cool, moist and unstable air mass allowed for increased convective activity, which pushed monthly rainfall amounts well above average (monthly total of 69.6 mm of rainfall). A persistent upper-level low-pressure system brought highly localized and intense thunderstorms to southeastern Ontario during the final week of the month. Over the last week of July (seven-day period from 23-29July), a humid and unstable air mass was present and thus resulted in several isolated thunderstorms throughout the week. From 26-29July, the study site experienced two intense thunderstorms (wetting all 20 LWS in less than 15 minutes).

This weather trend in the latter half of July extended into August bringing about violent summer storms and heavy rainfall. A bout of warm and humid air on August 20, combined with a weather disturbance moving in from the American Midwest, produced heavy rainstorm events and tornadoes in southwestern parts of Ontario moving eastward. Although the study site did not experience tornado storms, Toronto was hit with thunderstorms that dissipated over the week as drizzle.

The fall season (September 22nd to November) during the study period presented very different weather patterns. September was characterized by above-normal temperatures and below-normal total precipitation; September recorded an average monthly temperature of 6.3°C and total precipitation was measured at 27.6 mm of rainfall. The warmer weather was accompanied by a dry spell that affected southern Ontario until the latter half of September. Most of the precipitation recorded in September occurred during the last two weeks of the month due to the jet stream pattern that gradually shifted towards a more north-to-south flow at the end of the month, in conjunction with the deep low-pressure system moving over the Great Lakes. The coupling effect of the two aforementioned changes in the pressure system ushered in a much cooler air mass that produced rain showers and low winds (4.8 $m \cdot s^{-1}$) (Figure 22).

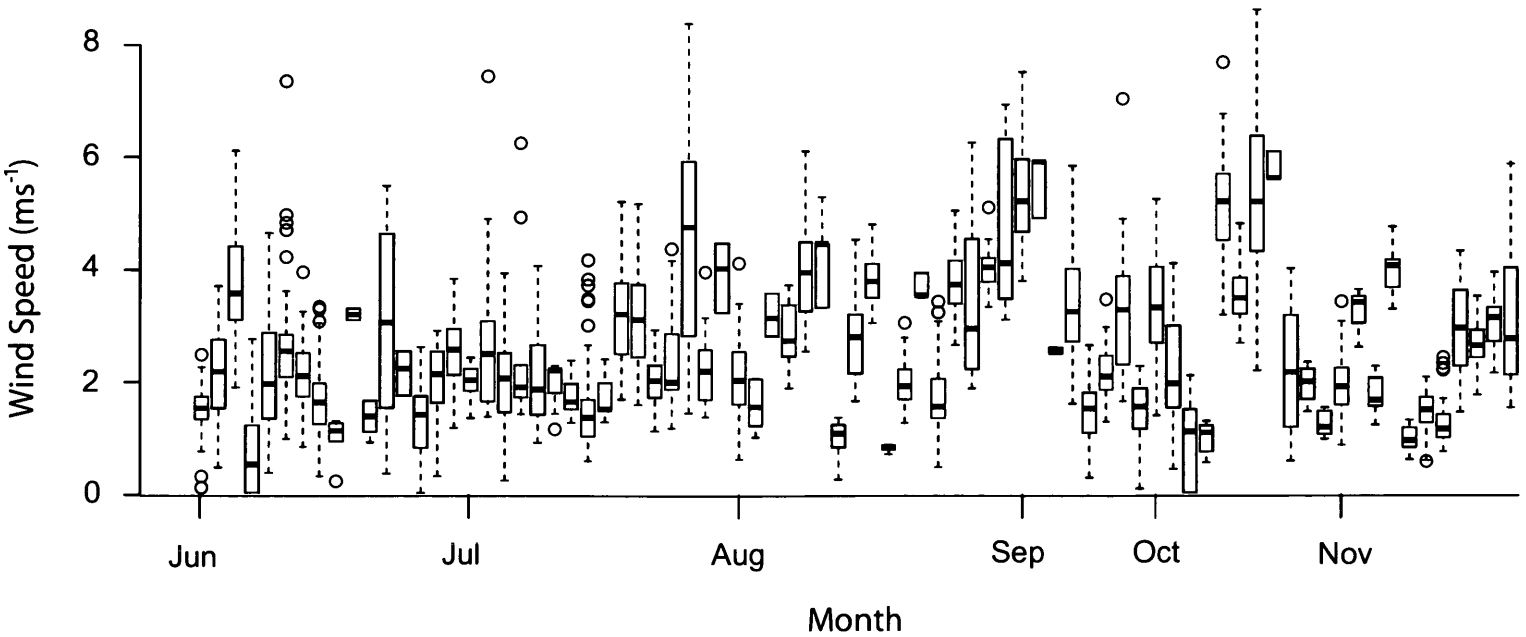

Figure 22. The temporal distribution of wind speed ($m \cdot s^{-1}$) for each rain event recorded during the study period (June to November 2009) is outlined above in boxplots, where each bar represents a rain event. The thick horizontal line represents the median wind speed, the lower end of the box presents the lower quartile, and the higher end of the box represents the upper quartile. The whiskers that extend downwards and upwards represent the minimum-recorded wind speed and the maximum-recorded wind speed respectively. This uses data recorded by the anemometer installed at the York University EMOS weather station.

October brought a number of heavier rainfalls (e.g., moderate rain showers and heavy rain showers), with one event (on October 9) producing almost 20 mm of rain over a 30-minute time span. The month ended with an intense disturbance moving from American Midwest to Husband Bay, resulting in gusty winds from the southwest and heavy rainfall. During this period, the study site experienced a stronger average wind speed (6.2 $m \cdot s^{-1}$) compared to the other recorded events (Figure 22); however, the storms during the final week of October were less intense (e.g., drizzle and light rain showers).

November was a record-breaking month in terms of temperatures (monthly mean average of 7.2°C) and sunshine (118.2 hours of sunshine; fourth sunniest November since 1937) (Figure 23). The warm, dry air resulted in November establishing a new record for a snow-free month for the first time in recorded history (Environment Canada 2009).

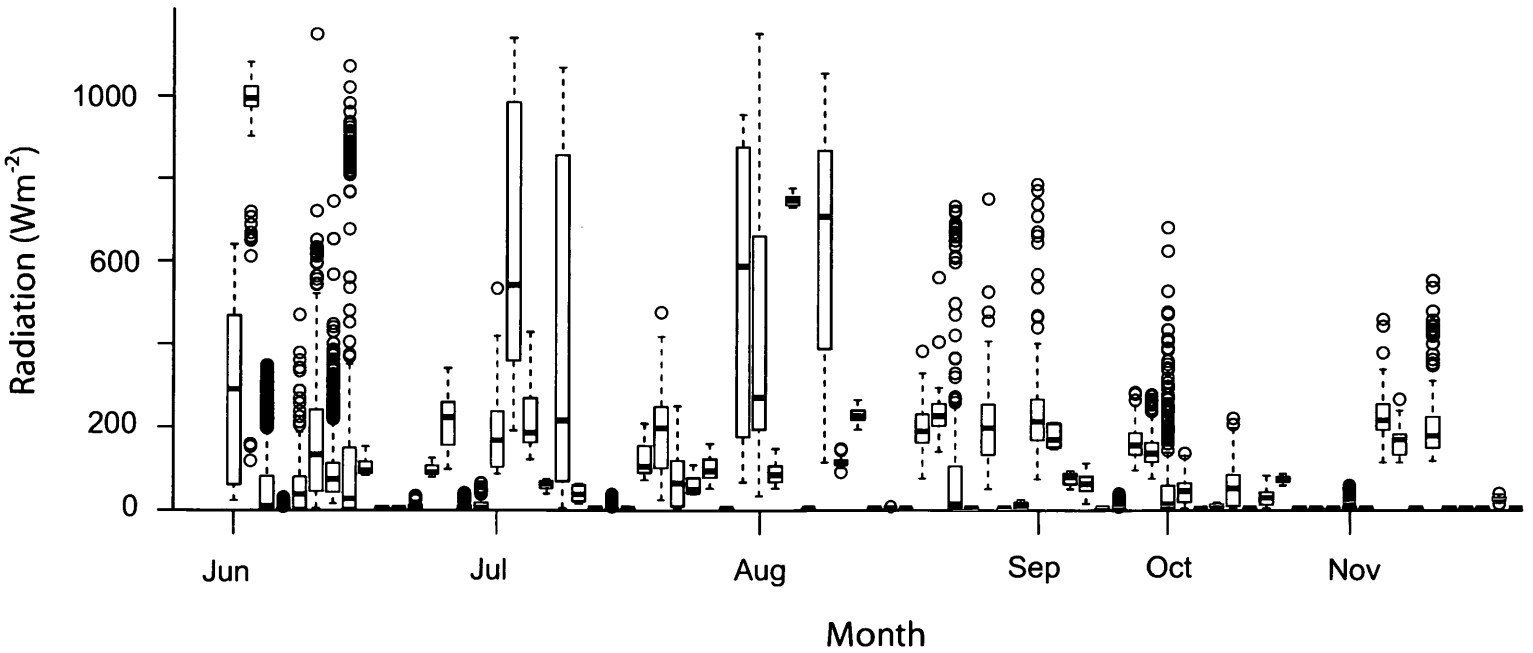

Figure 23. The temporal distribution of solar radiation ($W \cdot m^{-2}$) for each rain event recorded during the study period (June to November 2009) is outlined above in boxplots, where each bar represents a rain event. The thick horizontal line represents the median solar radiation, the lower end of the box presents the lower quartile, and the higher end of the box represents the upper quartile. The whiskers that extend downwards and upwards represent the minimum-recorded solar radiation and the maximum-recorded solar radiation respectively. This uses data recorded by the pyranometer sensor installed at the weather station 3 m from the study site.

Figure 24 outlines the number of storms by season, rain intensity level, and rain character category. Notice the minimal number of high intensity and continuous storms. The predominance of intermittent rainfall indicates the prevalence of convective rain, which occurs from convective clouds. These rainstorms fall over an area for a relatively short time, as convective clouds have limited horizontal extent, and are characterized by showers that have rapidly changing intensity. Also, the total number of storms in the summer and fall seasons was similar. During the six-month period, the shortest storm was of five-minute duration on 2 July 2009 (event 10); the longest rain event was on 29 June 2009 (event 8), which was 1332 minutes (approximately 22 hours) long. Rainstorm durations across the 79 recorded rain events averaged a length of approximately 3.5 hours in duration.

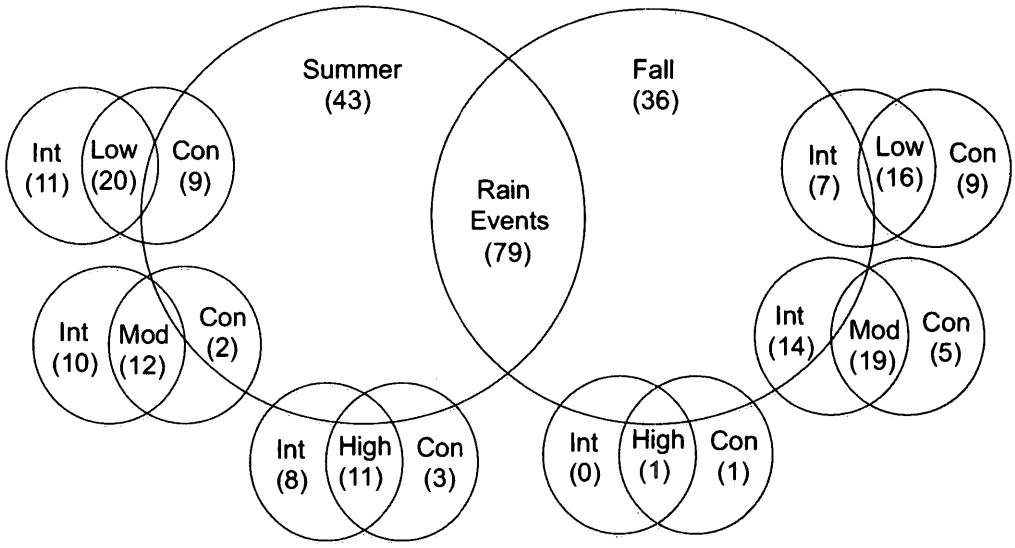

Figure 24. A Venn diagram illustrating the total number of rainstorm events recorded for different seasons (summer and fall), rain intensity levels (low, moderate (mod), and high), and rain character categories (intermittent (int) and continuous (con)) during the study period. The values in brackets are the total number of rain events under each given condition.

The spatial distribution of moisture during a low intensity rain event (i.e., drizzle and light rain showers) revealed moisture remained isolated along the upper edge and rarely reaches the bottom of the canopy during the storm. This finding was highlighted in the soil moisture readings recorded in the understory (beneath the tree canopy). Soil moisture remained dry with zero or near zero readings during low intensity rainfall.

3.2 ANOVA Results

ANOVA tests were computed to address the five goals of this project (§1.4). In summary, the presence of leaves significantly reduces the amount of moisture recorded for sensors positioned lower in the tree canopy (e.g., W, LE, B). This trend coincides with the change in season where the tree canopy is dense during summer months, but sparse (and eventually leafless) during fall months. These results indicate the seasonal influence on instantaneous canopy wetness.

Further, the upper edge sensors experienced significant wetting compared to the other sensor positions in the tree canopy. With regard to rain category, wetness was significantly different for the two extremes in rain intensity, specifically drizzle and thunderstorms. During drizzle and thunderstorm events, sensors positioned in the upper edge of the tree canopy differed significantly from the bottom sensors. These results demonstrate that both sensor position and rain intensity effect the variability observed in the instantaneous canopy wetness.

ANOVA tests on normalized time data demonstrated that the upper edge sensors get wet in a given rain event earlier than sensors positioned lower in the tree canopy. However, variations in the point in time in which the upper edge sensors wet differs only in the case of drizzle events. When computing ANOVA tests on successive five-minute intervals for each event, it was determined that the observed wetness differed significantly during thunderstorm events at intervals where the sensors reach a point of saturation.

With regard to wind, although medium wind speed, originating from the North and East direction, produced significant results, the data set was small (i.e., three thunderstorms experienced medium wind speeds while the remaining storms had recorded wind speeds classified in the low category) and therefore results obtained from these ANOVA tests were limited. The following subsections outline the results from the aforementioned ANOVA tests in further detail.

3.2.1 ANOVA on Season

Computing ANOVA tests on sensor position and rain category allowed for comparison of seasonal influences. ANOVA test where sensor position is the independent variable and wetness readings were the dependent variable (ANOVA test #2) were performed for events that occurred in the summer and fall seasons separately.

For events that occurred during the summer season from June to September 21st (event 1 to 43) rejected the null hypothesis. Thus, at least one of the sensor positions differed from the other in mean moisture during the summer ($F = 26.51$, $p = 2.00\times10^{-16}$). The Tukey test indicated that all pairwise combinations with UE and W positions were significantly different: UE-T ($p = 1.00\times10^{-7}$), UE-W ($p = 2.03\times10^{-6}$), UE-LE ($p = 1.00\times10^{-7}$), UE-B ($p = 1.00\times10^{-7}$), W-T ($p = 2.03\times10^{-2}$), W-LE ($p = 1.06\times10^{-3}$), and W-B ($p = 1.26\times10^{-3}$).

In the fall season from September 22nd to November (event 44 to 79), the null hypothesis was also rejected ($F = 28.83$, $p = 2.00\times10^{-16}$). The Tukey test indicated that all pairwise groups with UE were significantly different: UE-T ($p = 1.00\times10^{-7}$), UE-W ($p = 6.10\times10^{-6}$), UE-LE ($p = 1.00\times10^{-7}$), and UE-B ($p = 1.00\times10^{-7}$).

Results from the ANOVA tests comparing the two seasons during the study period (summer and fall) indicated that there are significant differences in moisture for various positions in the tree canopy for different seasons. This result prompted another ANOVA test on the presence and absence of leaves in the tree canopy (ANOVA test #3) since changes in canopy density was observed as the study period progressed. The leaves started to fall off the tree canopy (resulting in a more sparse tree canopy under study) in October; by October 26th the tree was leafless. Events that occurred after October 26, 2009 were classified in the category of absence of leaves for this ANOVA test.

ANOVA test where sensor position is the independent variable and wetness readings were the dependent variable (ANOVA test #3) were computed for the two conditions of absence and presence of leaves. For rain events that occurred with the presence of leaves in the tree canopy (events 1 to 65), the ANOVA test rejected the null hypothesis. Thus, at least one of the sensor positions differed from the other in mean moisture during events where leaves were present ($F = 35.30$, $p = 2.00\times10^{-16}$). The Tukey test indicated that all pairwise groups with UE were significantly different: UE-T ($p = 1.00\times10^{-7}$), UE-W ($p = 2.00\times10^{-7}$), UE-LE ($p = 1.00\times10^{-7}$), and UE-B ($p = 1.00\times10^{-7}$).

For rain events that occurred with the absence of leaves in the tree canopy (events 66 to 79) also indicated that at least one of the sensor positions differed from the others in mean moisture ($F = 19.49$, $p = 1.12\times10^{-12}$). The Tukey test indicated that only the UE paired with the bottom sensors differed significantly ($p = 1.00\times10^{-7}$).

The presence and absence of leaves ANOVA tests (ANOVA test #3) indicated that the UE region of the canopy is significantly different in wetness from the bottom of the canopy despite changes in canopy density. However, observed wetness differences in various regions of the tree canopy under the two leaf conditions (leaves on and leaves off) are significant.

In order to determine if there are seasonal affects on moisture for different rain types, ANOVA tests were computed where the independent variable was rain category and the dependent variable was sensor wetness for events that occurred in the summer and fall months separately (ANOVA test #8).

By running an ANOVA test on only the summer months, it resulted in the null hypothesis not being rejected. This implied that the mean moisture recorded for all rain types were not significantly differed from the others ($F = 1.69$, $p = 1.62\times10^{-1}$). Note that during the fall seasons, there were no thunderstorms recorded. ANOVA tests for the fall months, however, resulted in the null hypothesis being rejected ($F = 23.47$, $p = 2.95\times10^{-9}$). The Tukey test resulted in all pairwise combinations for LRS2 and RS3 to be significantly different: LRS2-RS3 ($p = 4.00\times10^{-7}$), LRS2-MRS4 ($p = 5.30\times10^{-6}$), LRS2-HRS5 ($p = 1.10\times10^{-6}$), RS3-MRS4 ($p = 1.56\times10^{-5}$), and RS3-HRS5 ($p = 2.70\times10^{-6}$). Therefore, results indicated significant differences in moisture recorded for LRS2 and RS3 in the fall.

Due to observed results from the ANOVA test on canopy density based on sensor position (ANOVA test #3), additional ANOVA tests were computed for the presence and absence of leaves (ANOVA test #9). ANOVA tests for the presence of leaves did not reject the null hypothesis, meaning that the mean moisture for all rain categories was not significantly different when leaves were in the canopy ($F = 1.32$, $p = 2.71\times10^{-1}$). However, ANOVA tests for the absence of leaves resulted in the null hypothesis being rejected ($F = 26.85$, $p = 2.26\times10^{-8}$). The Tukey test resulted in all pairwise combinations of LRS2 and RS3 to be significantly different: LRS2-RS3 ($p = 2.20\times10^{-6}$), LRS2-MRS4 ($p = 6.80\times10^{-6}$), LRS2-HRS5 ($p = 2.20\times10^{-6}$), RS3-MRS4 ($p = 2.51\times10^{-5}$), and RS3-HRS5 ($p = 6.00\times10^{-6}$). Note that since there were no recorded thunderstorms during the fall months, this indicated the absence of thunderstorms during the period when the leaves have fallen from the tree canopy. Results therefore indicate that the presence and absence of leaves do influence tree canopy wetness for different rain categories. In the case of LRS2 and RS3, the absence of leaves results in significant differences in canopy moisture.

3.2.2 ANOVA on Sensor Positions

ANOVA test where sensor location was the independent variable and wetness readings were the dependent variable (ANOVA test #1) indicated that at least one of the sensor positions differed significantly from the other positions in mean moisture at a 95% confidence interval ($F = 9.69$, $p = 1.78\times10^{-7}$). The Tukey test indicated that upper edge when paired with the other positional groups produced significant results: UE-T ($p = 2.30\times10^{-5}$), UE-W ($p = 4.98\times10^{-2}$), UE-

LE ($p = 9.52\times10^{-4}$), and UE-B ($p = 2.10\times10^{-6}$). Figure 25 illustrates the boxplot for the ANOVA results; notably, UE has a mean of 687 mm, which is significantly more than the other sensor positions. As such, UE gets significantly wetter than the other sensors with 95% confidence across all rain events.

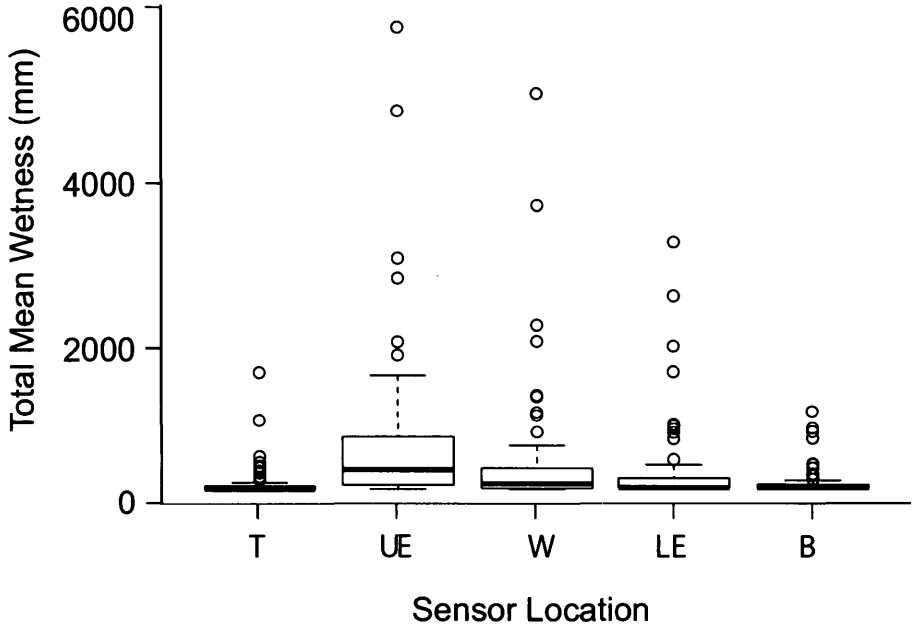

Figure 25. The distribution of total mean wetness (mm) is outlined above in boxplots, where each bar represents a positional group for the LWS sensors (top (T), upper edge (UE), within (W), lower edge (LE), and bottom (B)). This boxplot illustrates the ANOVA test results that compare the variance between the wetness for different sensor positions. The thick horizontal line represents the median total mean wetness, the lower end of the box presents the lower quartile, and the higher end of the box represents the upper quartile. The whiskers that extend downwards and upwards represent the minimum-recorded total mean wetness and the maximum-recorded total mean wetness respectively.

3.2.3 ANOVA on Rain Categories

ANOVA test where the rain category was the independent variable and wetness readings were the dependent variable (ANOVA test #6) indicated that at least one of the rain categories differed significantly from the other rain categories in mean moisture at a 95% confidence interval ($F = 56.61$, $p = 2.00\times10^{-16}$). The Tukey test resulted in all pairwise combinations with drizzle and three other pairwise combinations were significantly different: D1-LRS2 ($p = 1.00\times10^{-7}$), D1-RS3

($p = 1.00\times10^{-7}$), D1-MRS4 ($p = 1.00\times10^{-7}$), D1-HRS5 ($p = 1.00\times10^{-7}$), D1-T6 ($p = 1.00\times10^{-7}$), LRS2-HRS5 ($p = 5.73\times10^{-5}$), LRS2-T6 ($p = 1.94\times10^{-2}$), and RS3-HRS5 ($p = 4.88\times10^{-2}$).

Figure 26 illustrates the boxplot for the ANOVA results for the mean moisture wetness across all sensor positions (an average across all 20 sensors); notably, for drizzle events, the mean is 0.53 mm, which is significantly less than the other rain categories. As such, the wetness recorded during drizzle events is significantly different compared to other rain categories with 95% confidence across all sensor locations.

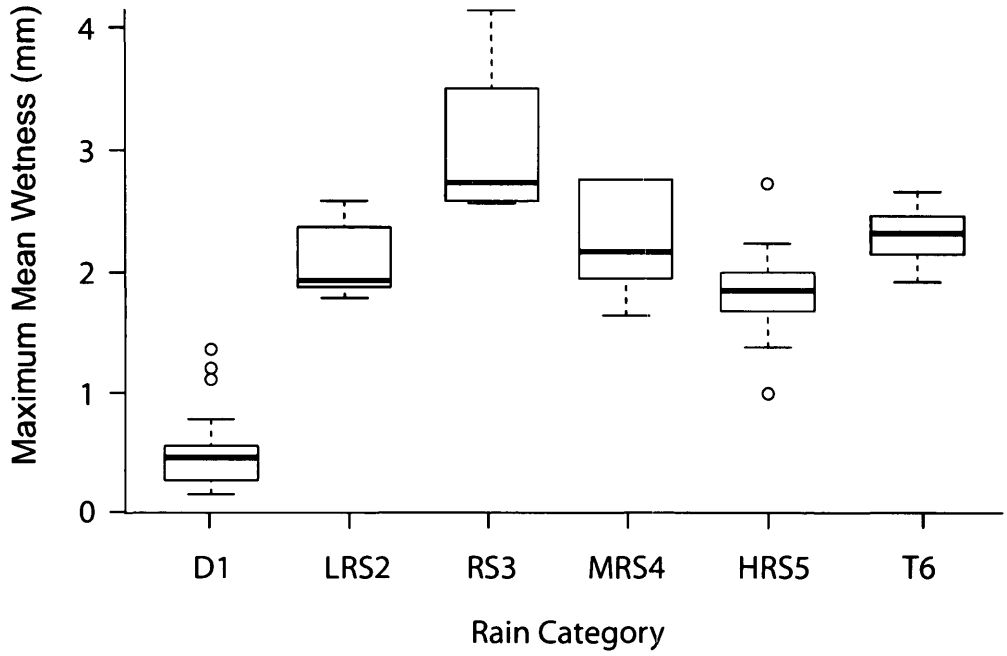

Figure 26. The distribution of maximum mean wetness (mm) is outlined above in boxplots, where each bar represents a rain category (drizzle (D1), light rain showers (LRS2), rain showers (RS3), moderate rain showers (MRS4), heavy rain showers (HRS5), and thunderstorms (T6)). This boxplot illustrates the ANOVA test results that compare the variance between the maximum wetness recorded across all 20 LWS sensors for the different rain categories. The thick horizontal line represents the median maximum mean wetness, the lower end of the box presents the lower quartile, and the higher end of the box represents the upper quartile. The whiskers that extend downwards and upwards represent the minimum-recorded maximum mean wetness and the maximum-recorded maximum mean wetness across all sensors respectively.

Given that the ANOVA tests on sensor positions indicated that sensor position has an effect on canopy moisture, ANOVA tests for each rain category (ANOVA test #7) were performed to determine if the wetness readings varied significantly for each sensor position under different types of rainfall. ANOVA tests on drizzle rain events rejected the null hypothesis, which implied that at least one of the sensor positions differed from the others in mean moisture ($F = 3.90$, $p = 5.89\times10^{-3}$). The Tukey test resulted in only one pairwise group to be significantly different: UE-B ($p = 1.59\times10^{-2}$).

Similar ANOVA tests were computed for light rain showers, rain showers, moderate rain showers, and heavy rain showers; the separate ANOVA tests on events categorized under these four rain types did not reject the null hypothesis: LRS2 ($F = 3.83$, $p = 5.89\times10^{-2}$), RS3 ($F = 3.14$, $p = 1.70\times10^{-2}$), MRS4 ($F = 3.87$, $p = 1.19\times10^{-2}$), and HRS5 ($F = 2.40$, $p = 1.19\times10^{-1}$). This implied that the variance between mean moisture for all sensor positions in these four rain categories were not significantly different.

Thunderstorm events resulted in the null hypothesis being rejected, which implied that at least one of the sensor positions differed from the others in mean moisture ($F = 6.32$, $p = 4.87\times10^{-4}$). The Tukey test resulted in three pairwise groups to be significantly different: UE-T ($p = 1.89\times10^{-3}$), UE-LE ($p = 3.96\times10^{-2}$), and UE-B ($p = 6.86\times10^{-4}$).

As described in Table 1, the six rain categories can also be classified based on rain intensity and rain character. Interestingly, the results from the ANOVA tests for each rain category that compared wetness variability for the different sensor positions (ANOVA test #7) highlighted that drizzle events performed differently compared to the other rain types. Thus, comparison of intensity and character can provide an alternate approach to studying relationships for the various rain categories. Separate ANOVA tests were computed for the three rain intensity levels (low, medium, and high) (ANOVA test #4) and two rain character types (intermittent and continuous) (ANOVA test #5).

For rain events that were low intensity, the null hypothesis was rejected; this demonstrated that at least one of the sensor positions differed from the others in mean moisture ($F = 10.73$, $p = 8.45\times10^{-8}$). The Tukey test indicated that all pairwise combinations with UE were significantly different: UE-T ($p = 1.9\times10^{-6}$), UE-W ($p = 7.2\times10^{-4}$), UE-LE ($p = 7.4\times10^{-6}$), and UE-B ($p = 1.60\times10^{-6}$).

In the case of medium intensity rain events, the null hypothesis was rejected ($F = 5.48$, $p = 3.79\times10^{-4}$). The Tukey test indicated that 2 pairwise groups with UE were significantly different: UE-T ($p = 1.08\times10^{-3}$) and UE-B ($p = 1.12\times10^{-3}$). Likewise, high intensity rain events also rejected the null hypothesis ($F = 4.44$, $p = 3.50\times10^{-3}$); the Tukey test indicated that the same two pairwise

groups with UE in the ANOVA test for medium intensity rain were significantly different: UE-T (p = 7.50×10^{-3}) and UE-B (p = 6.32×10^{-3}).

For all rainstorms intensity levels (ANOVA test #4), the ANOVA tests indicated that the UE region of the canopy is significantly different from the bottom and top in regards to wetness. This implies although the moisture from the top and bottom of the tree canopy significantly differs from moisture recorded at the upper edge of the canopy, the different rain intensities do not influence the moisture dynamics significantly.

With regard to rain character (ANOVA test #5), the ANOVA test for intermittent rain resulted in the null hypothesis being rejected. This indicated that at least one of the sensor positions differed from the others in mean moisture (F = 4.19, p = 2.67×10^{-3}). The Tukey test resulted in 2 pairwise groups that were significantly different: UE-T (p = 7.47×10^{-3}) and UE-B (p = 4.72×10^{-3}). In the case of continuous rain, the null hypothesis was also rejected (F = 7.43, p = 1.93×10^{-5}). Similar to the intermittent results, the Tukey test resulted in the same 2 pairwise groups to be significantly different: UE-T (p = 4.86×10^{-5}) and UE-B (p = 1.18×10^{-4}).

The ANOVA test results on rain intensity (ANOVA test #4) and rain character (ANOVA test #5) highlight that the UE region of the canopy is significantly different in wetness from the bottom and top region of the canopy. However, results indicate that both the intensity and character of rain does not influence the moisture dynamics significantly, but rather the classification of rain type affects the canopy wetness. Therefore, the type of rainfall influences the observed canopy moisture in the upper edge region of the tree canopy.

3.2.4 ANOVA on Time

ANOVA test to determine whether the means of the normalized time to maximum wetness differed based on sensor location (ANOVA test #10) rejected the null hypothesis. This implied that during a rain event, the sensors that do get wet are wetting significantly (F = 4.14, p = 5.84×10^{-9}). The Tukey test results illustrated that four upper edge sensors (LWS6, LWS7, LWS8 and LWS9) differed significantly and therefore got wet earlier into the rain event when compared with sensors in positions lower in the tree canopy (Table 7).

Table 7. The Tukey test results for ANOVA test #10 where each pairwise combination are presented in the triangular matrix where boxes shaded in red indicate that the p-values are significant with a 95% confidence interval.

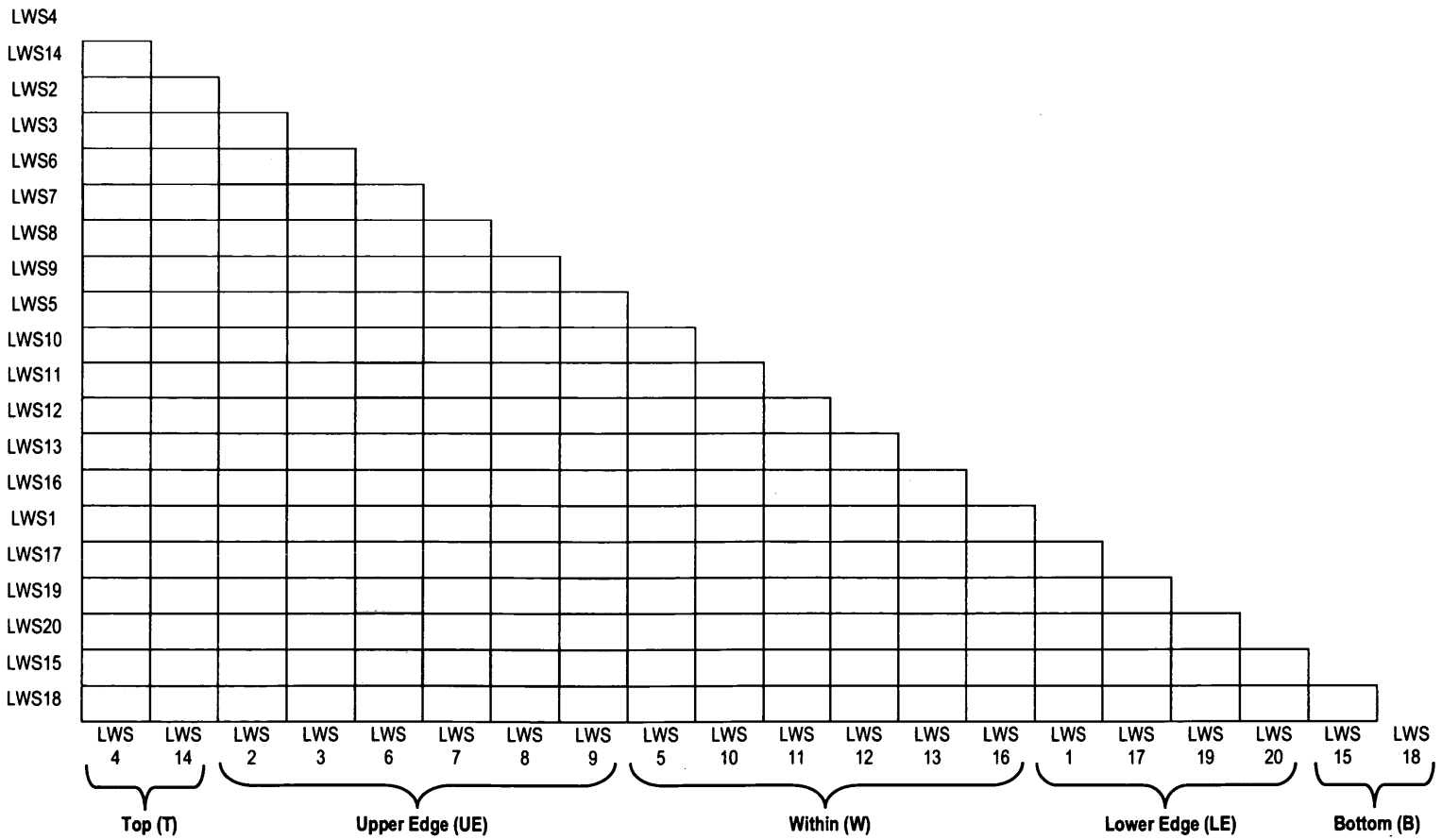

As demonstrated in the ANOVA test on rain categories (ANOVA test #6), the type of rain event can result in significant differences in wetness. Thus, ANOVA tests on the means of the normalized times for each rain category were computed separately (ANOVA test #11).

ANOVA tests on the normalized times for drizzle events produced results that rejected the null hypothesis, which implied that during a rain event, of the sensors that do get wet, at least one of those sensors wets significantly ($F = 6.60$, $p = 1.04\times10^{-14}$). Results from the Tukey test indicated that four upper edge sensors (LWS6, LWS7, LWS8, LWS9) and one within sensor (LWS10) significantly got wet first compared to other sensors positioned lower in the tree canopy (Table 8). However, for other rain categories, the null hypothesis was not rejected: LRS2 ($F = 1.80$, $p = 2.16\times10^{-2}$), RS3 ($F = 1.39$, $p = 1.28\times10^{-1}$) MRS4 ($F = 0.82$, $p = 6.75\times10^{-1}$), HRS5 ($F = 1.49$, $p = 1.21\times10^{-1}$), and T6 ($F = 0.93$, $p = 5.45\times10^{-1}$). This demonstrates that the rain type does influence which sensors get wet first during a rain event, but the differences in the mean normalized times observed across all rain categories is only significant for drizzle events.

Table 8. The Tukey test results for ANOVA test #11 where each pairwise combination are presented in the triangular matrix where boxes shaded in red indicate that the p-values are significant with a 95% confidence interval.

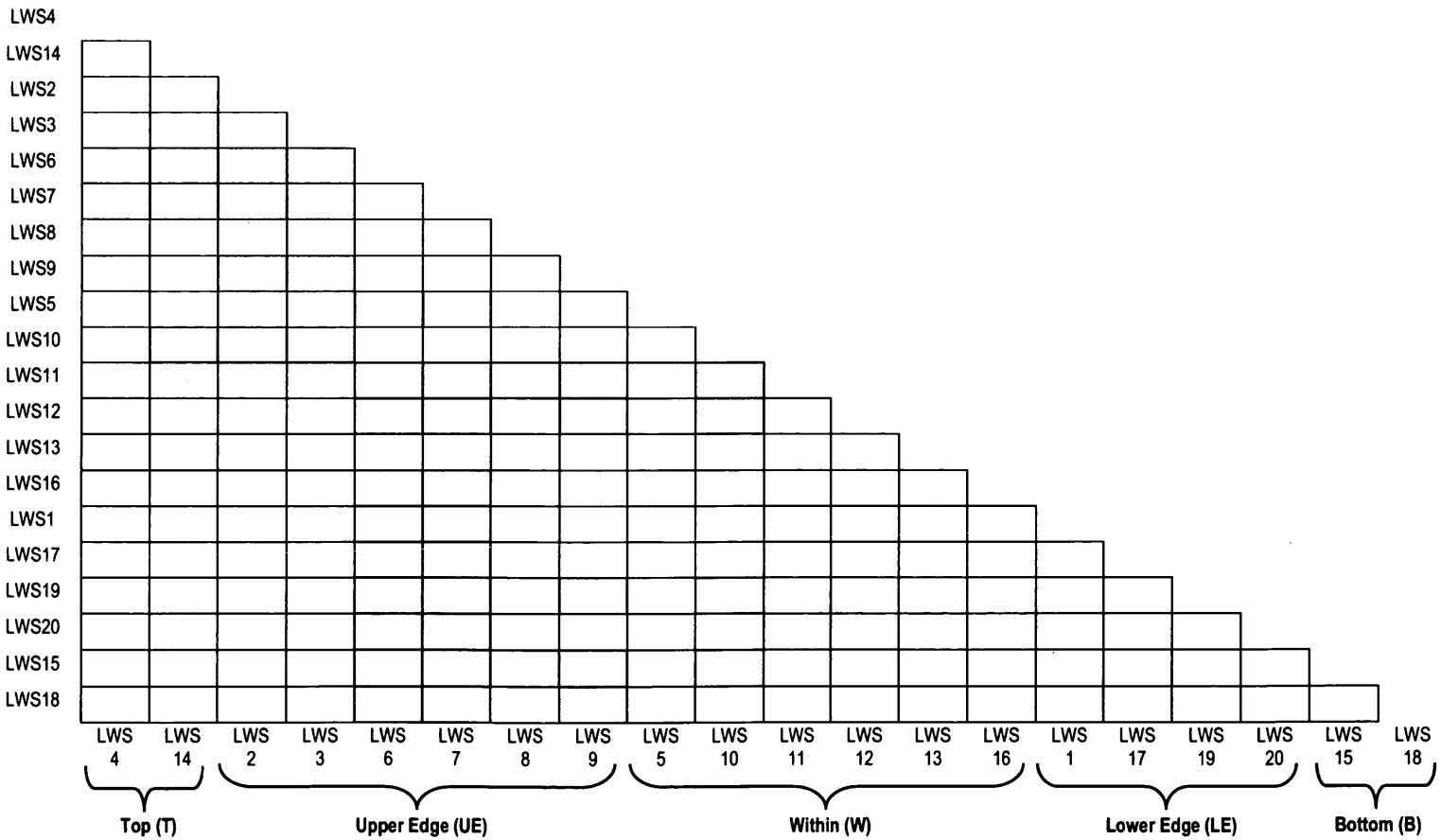

In order to capture the initial incline in moisture during a given rain event, ANOVA was computed on the normalized time defined as the time in which 80% of the maximum wetness increase for a given sensor was achieved (ANOVA test #12). The results from these tests presented very similar results to tests outlined in the ANOVA tests using the maximum wetness (ANOVA test #10). This ANOVA test rejected the null hypothesis ($F = 6.14$, $p = 1.73 \times 10^{-13}$) and the Tukey test indicated that several sensors get wet earlier into the rain event, but take longer to reach its maximum wetness (Table 9). Therefore, computing ANOVA on the 80% maximum wetness captures the initial sharp increase in moisture (wetting phase) to determine if these peaks in moisture are significant (sensor wetness has reached its point of saturation). Since several more pairwise sensor combinations produced significant results, this indicates that sensors tend to gradually saturate later into the event. Further, results from ANOVA test #10 and #12 demonstrate that the four UE sensors (LWS 6, LWS7, LWS8, and LWS9) behave differently compared to the other sensors. This could be due to the presence of the bird's nest that was between the other two UE sensors (LWS 2 and LWS 3).

Table 9. The Tukey test results for ANOVA test #12 where each pairwise combination are presented in the triangular matrix where boxes shaded in red indicate that the p-values are significant with a 95% confidence interval.

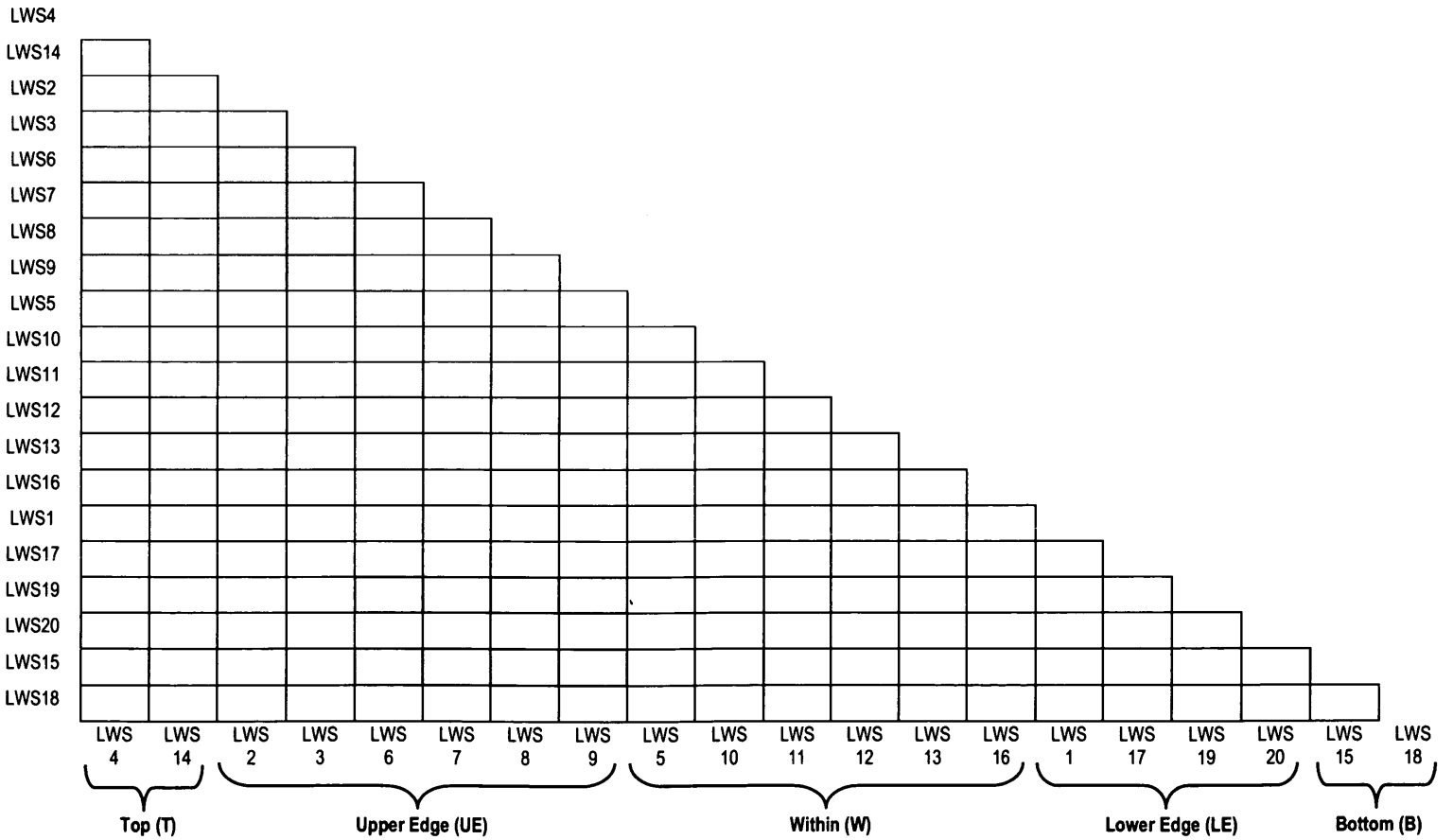

ANOVA tests were performed comparing each consecutive five-minute interval for a given rain event (ANOVA test #13). Results indicated that only in long duration thunderstorms (event 6, 8, 27), there is a significant change in wetness. A commonality between the significant intervals for these three thunderstorms is that these intervals occur near the point of saturation (saturation points observed from ANOVA test #10 and #12). Table 10 outlines the results in further detail.

Table 10. The Tukey test results for ANOVA test #13 where the pairwise combinations that produced significant differences are described.

Pairwise Combination	*F*	p
Event 6, $t_{47} - t_{48}$	12.31	1.18×10^{-3}
Event 6, $t_{48} - t_{49}$	13.35	7.78×10^{-4}
Event 6, $t_{49} - t_{50}$	8.67	5.50×10^{-3}
Event 8, $t_{60} - t_{61}$	16.42	2.42×10^{-4}
Event 27, $t_3 - t_4$	11.39	1.71×10^{-3}
Event 27, $t_4 - t_5$	13.19	8.27×10^{-4}
Event 27, $t_5 - t_6$	11.32	1.76×10^{-3}

Given the results in the earlier ANOVA tests (ANOVA tests #1 - #12), sensor position, rain category, and season were important to consider when studying the ANOVAs for these consecutive five-minute intervals. Notably from ANOVA test #10, four upper edge sensors (LWS 6, LWS7, LWS8, and LWS9) behaved differently from the other two sensors in the same positional group (LWS 2 and LWS 3 were positioned closer to the boundary between UE-LE sensors). Thus, LWS 2 and LWS3 is extracted into its own positional group called "edge boundary" (EB) in order to reduce the within variance of the upper edge data.

The ANOVA tests computed in ANOVA test #13 were re-run based using the new positional groups and compared across events of the same rain category and season. With regards to the positional groupings described in Table 1, the UE sensor position was now separated into two new edge groups: UE-2 (LWS 6, LWS7, LWS8, and LWS9) and EB (LWS2 and LWS3). Results from this ANOVA tests captured the observed peaks in the LWS graphs (Appendix B) and highlighted the point in time in a given event where moisture significantly differs. Results are summarized in Table 11 below.

Table 11. The general trends for ANOVA test #13 based on sensor position, rain category, and season where TI_s refers to point in a given event where the consecutive five-minute time interval is significant as a percentage out of the total event duration.

Condition	Summer TI_s (% into event)	Fall TI_s (% into event)
D1		
T		
UE-2	5.2	4.2
EB		
W	94.6	
LE		
B		
LRS2		
T	99.5	95.8
UE-2	3.8	3.5
EB	91.2	88.2
W	64.8	51.9
LE	85.6	83.7
B	97.2	91.8
RS3		
T	86.1	82.1
UE-2	3.0	2.6
EB	75.2	73.2
W	44.2	40.1
LE	73.5	69.9
B	76.1	72.0
MRS4		
T	80.0	77.2
UE-2	2.9	2.4
EB	71.1	67.2
W	38.1	37.9
LE	65.2	60.1
B	71.0	66.2
HRS5		
T	60.0	52.8
UE-2	2.3	2.0
EB	63.2	60.4
LE	35.1	30.9
W	55.0	51.9
B	58.2	56.0
T6		
T	45.8	
UE-2	1.4	
EB	54.2	
W	28.1	
LE	49.0	
B	53.4	

Results from this ANOVA test indicate the general moisture direction within a tree canopy for different time stages (intervals) within a rain event. Further, the ANOVA results demonstrate the time in which wetness is significant (highlight wetting phases and point of saturation). Water appears to be entering the tree canopy at the UE-2 region and wetting significantly early into the event for all rain types and across both seasons. However, in the case of thunderstorms, although UE-2 gets wet significantly first, the other positional groups wet significantly relatively early in the rain event compared to other the other five rain types. Also, the changing canopy density in the fall influences the significant wetness intervals and therefore result in wetting at different stages of the rain event for the same rain category.

3.2.5 ANOVA on Wind

ANOVA tests were performed comparing the wind direction (in the pre-defined quadrants of N, E, S, and W) for a given rain event where the independent variable was wind direction and the dependent variable was LWS wetness (ANOVA test #14, Figure 27). Results indicated no significant differences for the different wind directions since the null hypothesis was not rejected ($F = 1.89$, $p = 2.78\times10^{-1}$). Three separate ANOVA tests were computed for events that recorded low wind speeds ($F = 0.81$, $p = 9.78\times10^{-1}$), mid-low wind speeds ($F = 0.92$, $p = 9.96\times10^{-1}$), and medium wind speeds ($F = 4.11$, $p = 4.92\times10^{-2}$) where the medium wind speed ANOVA tests rejected the null hypothesis. A Tukey test was computed to determine which wind direction categories differed significantly; results indicated that medium wind speed from the North direction was significantly different from all other pairwise combinations: N-E ($F = 3.99$, $p = 4.78\times10^{-2}$), N-S ($F = 4.47$, $p = 4.82\times10^{-2}$), and N-W ($F = 4.63$, $p = 4.95\times10^{-2}$). However, it was observed that wind direction and wind speed from the three nearby Environment Canada weather stations recorded very different results from the data retrieved from EMOS.

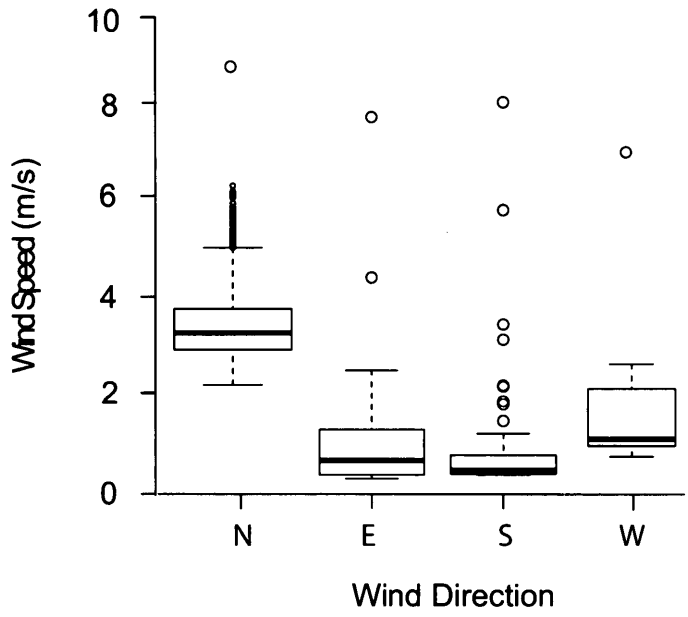

Figure 27. The distribution of mean wind speed ($m \cdot s^{-1}$) is outlined above in boxplots, where each bar represents a wind direction quadrant (North (N), East (E), South (S), and West (W)). This boxplot illustrates the ANOVA test results that compare the variance between the mean wind speeds recorded across all events for the four directional quadrants. The thick horizontal line represents the median mean wind speed, the lower end of the box presents the lower quartile, and the higher end of the box represents the upper quartile. The whiskers that extend downwards and upwards represent the minimum-recorded mean wind speed and the maximum-recorded mean wind speed across all events respectively.

3.3 Wetting and Drying Phases

Graphs illustrating the LWS moisture readings for all 79-rain events illustrated a distinct wetting pattern in the sensor moisture readings for each type of rain category (Figure 28). Leaf wetness for drizzle events is relatively consistent throughout the event as seen in Figure 28a where the leaf moisture for each successive minute increases only slightly in magnitude from its previous minute in the event. This pattern is visualized as a plateau or flat line with minimal fluctuations. For light rain showers (Figure 28b), there is a lag time before sensors get considerably wet while for rain showers (Figure 28c), the peaks of wetness fluctuate throughout the event. In the case of moderate rain showers, patterns observed are very similar to rain showers but have higher wetness recorded (Figure 28d). For heavy rain showers and thunderstorms all sensors wet and reach saturation or near-saturation state (Figure 28 e, f). However, thunderstorms have very distinctive wetness peaks and the wetting and drying phases are clearly defined (Figure 28f). These observed trends reflect the results outlined in Table 11 and Table 12.

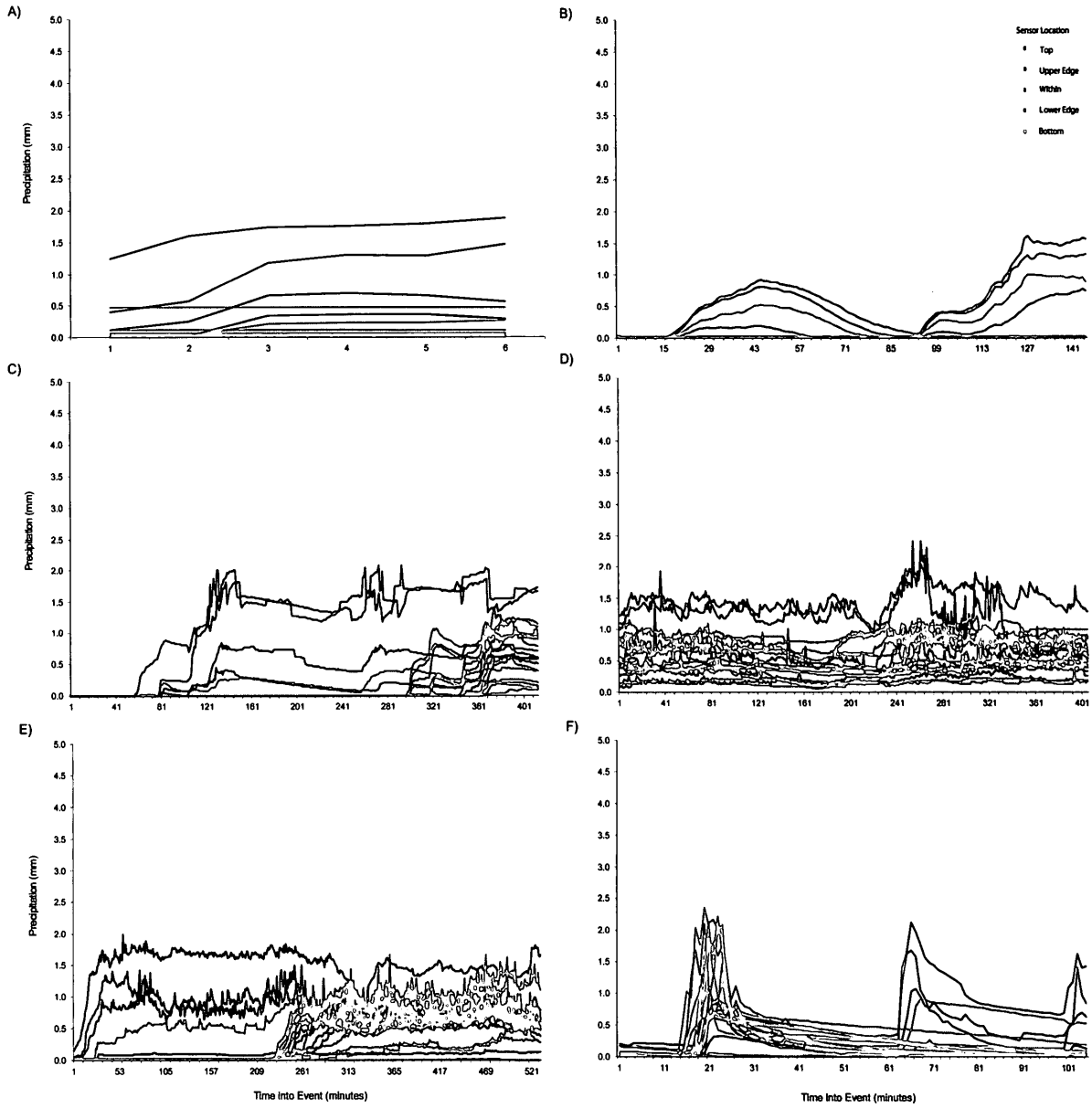

Figure 28. Leaf wetness graphs of the 20 LWS moisture readings for various events where each graph illustrates the general wetting pattern observed for each rain category: A) drizzle, B) light rain showers, C) rain showers, D) moderate rain showers, E) heavy rain showers, and F) thunderstorms.

Table 12. Average slopes recorded for the wetting and drying phases across all rain events based on sensor position.

Rain Category		Sensor Position T	UE	W	LE	B
D1						
	Wet		0.44	0.16		
	Dry		-0.04			
LRS2						
	Wet	0.05	0.13	0.13	0.08	0.05
	Dry	-0.06	-0.03	-0.10	-0.01	
RS3						
	Wet	0.08	0.18	0.19	0.08	0.05
	Dry	-0.05	-0.05	-0.08	-0.01	-0.01
MRS4						
	Wet	0.09	0.22	0.20	0.13	0.08
	Dry	-0.04	-0.04	-0.04	-0.01	-0.01
HRS5						
	Wet	0.10	0.28	0.25	0.13	0.10
	Dry	-0.04	-0.05	-0.06	-0.05	
T6						
	Wet	0.13	0.42	0.28	0.26	0.23
	Dry	0.06	-0.08	-0.20	-0.09	-0.17

The wetting and drying slope for each sensor position was computed to determine if each rain category had an unique slope that defined the point of saturation. Notably, thunderstorm events experienced the fastest change in wetness for all positional groups and therefore reached saturation faster compared to the other rain categories. The upper edge sensors also had the largest positive, while the within sensors had the largest negative slopes (Table 12). This indicates that the upper edge sensors wet quicker, but the within sensors dry faster.

The lag time between the end of the rainstorm and the drying off period is dependent on air temperature, relative humidity, and solar radiation. During conditions with cooler temperatures (e.g., November rain events), the drying phase for the same rain type took longer to dry (on average, approximately 6 hours after the rain event all sensors were dry). Conversely, on warmer days (e.g., July and August rain events), the drying phase for the same rain type took considerably less time for all sensors to be dry (on average, approximately 2 hours after the rain event all sensors were dry). In some incidences, the sensors, although recording the presence of moisture, had the same moisture reading as the previous minute for a longer time interval (e.g., LWS07 recorded 0.5 mm of moisture from minute 10 to minute 25 of the drizzle event). This observed scenario implies that evapotranspiration is occurring, or at the very least, the amount of input is equal to the output since the moisture readings are the same during this time interval.

4. DISCUSSION AND ANALYSIS

As outlined in §1.4, the effects of canopy storage for five dynamics were considered: 1) sensor position, 2) rain category type, 3) season, 4) time of saturation, and 5) wind. During rain events, the upper edge of the tree was significantly different in wetness compared to all other positional groups (ANOVA test #1). Also, the upper edge sensors also significantly wetted first compared to the four other tree canopy positions (ANOVA test #10, #12, and #13). This suggests that intercepted rainfall likely enters the tree canopy along the upper edge of the canopy. Also, results from the normalized times for the 80% of the maximum wetness (ANOVA test #12) demonstrated that four of the UE sensors (UE-2: LWS 6, LWS7, LWS8, and LWS9) behaved significantly different from the other two UE sensors (EB: LWS 2 and LWS 3) in the same category. This highlights that even within a positional group there is variance in wetness. Clearly, the amount of wetness recorded for a tree canopy is influenced by the position in which the wetness reading is collected.

An unexpected result from the normalized time ANOVA tests (ANOVA test #10 and ANOVA test #12) involved the top (T) sensors (LWS 4 and LWS 14) reaching their maximum wetness very late into the rainstorm. Since the sensors positioned at the top of the tree canopy were located at a higher elevation than the UE sensors, one would assume that the T sensors should be wetting sooner than the results indicate. A likely explanation for this is that T sensors were not at the tips of the top-most branches due to branch flexibility and thus some leaves are to be found above these sensors causing potential rain shadow effects (Figure 8).

The wetness recorded for various rain types differs significantly (ANOVA test #6) where drizzle events experience wetness significantly different from all other rain types. This supports the classification of drizzle by the American Meteorological Society where rainfall is separated into two classes of drizzle and rain where rain includes the other five rain types in Table 1. Drizzle is an unique class of rainfall because of its smaller diameter in drop size by definition (AMS 2000). Unlike the other rain categories, drizzle events do not wet all sensor positions. Drizzle events often only wet the upper edge sensors and moisture evapotranspires before reaching the ground surface (ANOVA test #7). This observation was supported by the soil moisture readings recorded for the canopy understory where soil moisture was almost negligible (Appendix C). Interestingly, since rain intensity and character are descriptive of rain category types, it was expected that there would be significant differences in wetness for these dynamics. However, ANOVA tests comparing the various rain intensities and characters based on sensor

position and rain category separately did not result in significant results. Therefore, rain intensity and rain character do not influence canopy moisture.

During the study period, there were three incidents (one in June, July and August) where a series of successive thunderstorms occurred. In these situations, the sensors not only saturated but also did not dry completely before the next thunderstorm. Although throughfall was not measured in this project, research indicates that during these scenarios, it is observed that the canopy saturates and a portion of the rainfall will drip through the canopy as throughfall (Gash 1979; Staelens et al. 2008). Further, the remaining rainfall is either stored in the canopy or lost as evaporation during the rainfall event (Gash 1979). Thus, when rainfall events are greater than 6 mm, there is a higher tendency for water to leave as throughfall and moisture already in the canopy begins to exit via leaf drip (Williams et al. 1987).

Analysis of these successive groups of thunderstorms during the months of June, July, and August were computed by comparing rain data from the two seasons of summer and fall. With regard to season, it was expected that moisture should vary for rain events occurring in the summer versus fall months. This was due to variations in canopy density where tree canopies in summer season have dense and full leaf coverage while in the fall season, the tree canopies begin to change drastically with the falling of leaves (creating a sparse and eventually leafless tree canopy). Results therefore suggest that the tree phenology has a strong influence on interception during large rainfall events (given the patterns observed for the aforementioned successive thunderstorms in the summer season.

With the absence of leaves, it was observed that the Tukey test results differed significantly with only the pairwise comparison of UE-B being significant (ANOVA test #4 and #9). Also, this would suggest that in winter months, where there are no leaves for all deciduous trees, the upper edge sensors would still wet first before the bottom sensors and water propagates through the canopy along the branches to reach the bottom. Therefore, the differences in tree phenology (or canopy densities) can influence the quantity of moisture and the direction in which moisture moves through the tree canopy. Additionally, this highlights the importance of considering canopy density in interception modeling and suggests the possibility of incorporating the Leaf Area Index (LAI) into interception modeling (van Dijk and Bruijnzeel 2001).

A limiting factor to any interception model, however, is the presence of dew or frost. Dew accumulates through the night; this moisture from the air is seen as small droplets on the plant leaves approximately two to three hours past sunrise. Therefore, when the temperature of the leaf drop bellows dew point of the surrounding air, the water is able to condense on the leaf and if the dew point is below freezing, then the water will condense directly into a solid (frost via sublimation). Dew formation causes the release of latent heat, therefore warming the surface

and surrounding air. However, as night begins, temperature can drop rapidly through radiative cooling of the ground, and once dew starts to form, the rate of the temperature drop decreases dramatically. For this study, dew was observed in the evening and was often mistaken as small isolated drizzle events. However, the LWS thresholds defined by Decagon Inc. (2007) and field notes allowed for dew moisture to be filtered out from rainfall moisture in the GIS database. Further, as seen in the experimental data by Decagon Inc. (2007) (Figure 9), dew and frost can be mistaken as rainfall for low intensity storms since the quantity of moisture is small. Another notable remark to consider is that plants also exude moisture, which will form droplets on the leaves in the morning when humidity is high. This is termed guttation, when plants release excess water from the tips of leaves and this moisture can be confused with dew (since both phenomena occur at the same time) or drizzle events (if rain occurred in the morning). This influence was more difficult to remove from the study for rain events that occurred during morning hours.

During a rain event, there are certain times in which moisture is significantly different from successive intervals (ANOVA test #13). The time into the event in which the significant intervals were observed was computed as a percentage out of the total duration of a given rain event. This suggests the point in time certain positional groupings record significant wetness readings and also captures the wetting phases that experience significant changes in moisture. With drizzle events resulting in several positional groups remaining dry, this implies that moisture remains stationary on the leaf surface for a prolonged time. Since in most drizzle events, only the upper edge records a wetness reading, it suggests that the moisture recorded in the UE region evapotranspire before reaching positions lower in the tree canopy. Further, since thunderstorm events experience significant wetness across all sensor positions midway into the rain event, it indicates that not only all sensors have wetted, but also the entire tree canopy has reached a point of saturation. This suggests that additional inputs to the tree canopy would not adhere to the leaf surface, but rather drip to the sensors positioned below, eventually escaping to the soil surface in the tree's understory.

It was difficult to assess the effect of wind (direction and speed) on canopy wetness due to the lack of data (e.g., only three medium wind speed readings and no high wind speed readings), which resulted in the use of alternate wind speed divisions (§2.3). Further, since an anemometer unfortunately could not be installed at the study site, it was assumed that the wind data at the study site was consistent with the wind data recorded by EMOS. Note, however, the potential of local eddies at the study site due to the presence of the building. Herwitz and Slye (1995) discussed the influence of wind on interception by describing how wind not only moves the moisture towards the object intercepting the rainfall, but also, in the case of trees, helps to dry

out the leaves faster by wicking off water to leaves below. This implies that sensors located further down in a tree canopy with regards to sensor position would experience the influence of wind as the wind pushes the moisture from leaves above to drop its surface water to leaves below. Therefore, moisture readings recorded at lower positions may not necessarily be new moisture inputs to the tree canopy. This demonstrates that the pathway in which intercepted rainfall moves within the canopy is highly variable during rainstorms accompanied by high wind speeds. However, for this study, under the conditions observed at the study site, wind does not influence canopy moisture (ANOVA test #14). Although there may be some indication of the effects of wind speed when analyzing medium wind speed data, wind data that was descriptive of the actual study site was unavailable, and thus further research is required to make conclusions on wind effects on interception.

The wetting and drying phase is very difficult to distinguish since leaves in the canopy can wet and dry simultaneously with inputs offsetting the evapotranspiration that is occurring within the tree canopy. Further, since canopy surfaces do experience evaporation directly off the surface into the atmosphere, it is difficult to capture all the methods that contribute to interception loss. Despite this, studying the start and end time of the wetting and drying phases using the LWS graphs of the moving average helped to visualize these divisions and points of saturation. Interestingly, each rain type has a distinct pattern in wetness with wetting and drying slopes that are descriptive of the rate of wetness change observed in the LWS graphs. Drizzle events experience the least amount of rainfall and changes in wetness are close to the dry state. Thus, the wetting and drying slopes are very low. Conversely, thunderstorms experience the largest quantity of rainfall and changes in wetness vary significantly (ANOVA test #13) throughout the storm. The wetting and drying phases for thunderstorms are distinct with a steep incline and decline representing the slopes respectively. For thunderstorms, the upper edge sensors reach saturation the fastest, but the within sensors return to its dry state the fastest. For all events, the bottom sensors wet the latest into the event and take the longest to dry off.

Given the unique patterns and trends for the different rain categories, this present the opportunity to characterize wetness for a given set of conditions. More specifically, if the slope of the wetting and drying phases are known and the rain type or season is defined, then it is possible to model a general trend of how the tree canopy wets during that given rain event. For instance, information is provided for a summer rain event with a wetting slope of 0.40 for the upper edge sensors and a drying slope of -0.18 for the within sensors where all the positional groups wet at the half-way into the rain event. Given the aforementioned information, this rain event is likely a thunderstorm (e.g., ANOVA test #8, ANOVA test #9, ANOVA test #10, ANOVA test #13). Although this study does not, by any means, allow for prediction of meteorological

trends, this study highlights that different rain types behave differently in regards to leaf wetness and characterizes the behaviour of surface leaf wetness during various rain types. This study demonstrated that the moisture dynamics in a tree canopy are heterogeneous and analyzing a tree canopy at the individual leaf scale aids in the understanding of the wetting and drying phases for a given rain event. Further, the importance of studying interception at a higher spatial and temporal resolution is reiterated in order to capture tree canopy heterogeneity and to characterize canopy moisture.

5. CONCLUSIONS

Quantifying canopy moisture using leaf sensors to capture instantaneous leaf surface moisture data allowed for assessment of moisture dynamics within a tree canopy during and following a rain event. This method introduced an approach to track the movement of water throughout a rainstorm in order to understand how a tree is wetted during different rain types. This study highlighted the following five conclusions.

(1) Instantaneous leaf wetness within a tree canopy is influenced by season.

(2) The upper edge of a tree canopy wets first and the sequence of sensors wetting is dependent on the rain type.

(3) All rain types behave differently with regards to leaf wetness and have unique wetting and drying phases (slopes), which allow for characterization of canopy moisture dynamics for various rain types.

(4) Thunderstorm events experience an earlier point of saturation compared to all other rain types and drizzle events do not experience canopy saturation. Also, the upper edge sensors wet the fastest while the within sensors dry the quickest.

(5) The influence of wind speed on instantaneous wetness within the canopy could not be determined given insufficient wind data for the study site.

Since variations from the summer and fall season affect the canopy density, comparison of rain events occurring during the summer and fall seasons resulted in significant differences where rain events in the fall resulted in fewer significant differences in wetness. The variations in canopy density prompted for a comparison between rain events that occurred with and without leaves in the tree canopy. Results demonstrated that in conditions with the absence of leaves, the significant differences observed with all UE pairwise combinations were no longer present, which supports the expectation that a leafless tree would experience relatively the same likelihood of permeating moisture to any other sensor position. Clearly, leaf drip is the dominant method of interception for a tree canopy in the summer.

During a rain event, moisture typically enters the tree canopy along the upper edge of the canopy and the wetness observed in the upper edge regions significantly differ from all other positional groups. Drizzle events, compared to the other rain categories, differ significantly in mean wetness and thunderstorm events result in all sensor positions experiencing significant wetness earlier into a rain event.

Drizzle events did not experience canopy saturation with several positional groups remaining dry. Further, thunderstorm events experienced significant wetness across all sensor positions midway into the rain event and often, the entire tree canopy reached a point of saturation during a thunderstorm. For all rain types, the upper edge sensors wetted earlier than all other positional groups and reached saturation the fastest.

Although several studies have indicated the influence of wind affecting canopy storage, due to the presence of local eddies and the inability to install an anemometer at the study site, it is difficult to conclude the influence of wind on the instantaneous wetness within the canopy. Thus, further research is required on wind in order to determine if wetness significantly differs for various wind speeds and wind directions.

Results from this study highlight that the amount of intercepted rainfall can vary greatly as the dispersion of precipitation (positional groups of LWS) and rain type influence the observed differences in canopy moisture. The application of 4D GIS to visualize moisture changes within the tree canopy allowed for the characterization of the wetting and drying phases for a given rain event. Further research is required on the heterogeneity of moisture in a tree canopy for other tree species and for a larger area (e.g., forests that comprise of multiple tree canopies). Installing LWS to capture the temporary adherence of water to the leaf surface is an innovative approach to measure leaf moisture within a non-fruiting bearing tree canopy; results from this study can be used to infer the behaviour of leaf flow within the tree canopy for various rain types. This study offers initial insight on the complex internal moisture dynamics of a tree canopy and highlights the importance of understanding interception at a finer spatial and temporal resolution.

REFERENCES CITED

Addington, R.N., R.J. Mitchell, R. Oren, and L.A. Donovan. 2004. Stomatal sensitivity to vapor pressure deficit and its relationship to hydraulic conductance in *Pinus palustris*. *Tree Physiology* **24**:561-569.

Ahokas, E., S. Kaasalainen, J. Hyyppa, and J. Suomalainen. 2006. Calibration of the Optech ALTM 3100 laser scanner intensity data using brightness targets. ISPRS Commission I Symposium, July 3-6, 2006, Marne-la-Vallee, France, International Archives of Photogrammetry, Remote Sensing and Spatial Information Sciences, 36(A1).

Ahrens, C.D. 2007. Meteorology today: an introduction to weather, climate, and the environment. NY: Central Learning, p.296.

American Forests. 1996. CITYgreen urban ecosystem analysis software. American Forests. Washington, D.C.

American Meteorological Society (AMS). 2000. Glossary of Meteorology, 2nd ed. Boston, MA: AMS, p.216.

Anderson, A.E., M. Weiler, Y. Alilia, and R.O. Hudson. 2010. Piezometric response in zones of a watershed with lateral preferential flow as a first-order control on subsurface flow. *Hydrologic Processes* **24**(16):2237-2247.

Baltsavias, E.P. 1999. Airborne laser scanning: basic relations and formulas. *ISPRS Journal of Photogrammetry & Remote Sensing* **54**:199-214.

Bang, S., H.H. Thi, K.W. Kim, M.H. Nguyen, and D.M. Dang. 2008. Arsenic-contaminated groundwater in the Mekong River Delta of Vietnam. Proceedings of the International Symposia on Geoscience Resources and Environments of Asian Terranes (GREAT 2008), 4th IGCP 516, and 5th APSEG; November 24-26, 2008, Bangkok, Thailand.

Barry, R.G. and R.J. Chorley. 2003. Atmosphere, Weather and Climate. NY: Routledge, p.115.

Batzer, J.C. and M.L. Gleason. 2008. Spatial heterogeneity of leaf wetness duration in apple trees and its influence on performance of a warning system for sotty blotch and flyspeck. *Plant Disease* **92**(1):164-170.

Bedient, P.B. and W.C. Huber. 1992. Hydrology and floodplain analysis. 2nd ed. Massachusetts: Addison-Wesley, p.261.

Bergkamp, G., B. Orlando, I. Burton. 2003. Change: adaptation of water resources management to climate change. IUCN, Gland, Switzerland.

Bluman, A.G. 2006. A Brief Version: Elementary Statistics: A Step by Step Approach, 3rd edition. UK: McGraw-Hill Publishing Company, p.660.

Bosch, J.M. and J.D. Hewlett. 1982. A review of catchment experiments to determine the effect of vegetation changes on water yield and evapotranspiration. *Journal of Hydrology* **55**:3-23.

Bourassa, M.A., M.H. Freilich, D.M. Legler, W.T. Liu, and J.J. O'Brien. 1997. Wind observation from new satellite and research vessels agree. *EOS Transaction of American Geophysical Union* **78**:597-602.

Brady, N.C. and R.R Weil. 2002. The nature and properties of soil. 13th ed. Upper Saddle River, NJ: Pearson Education, p.606.

Brenna, R. and T.L. Webster. 2006. Object-oriented land cover classification of lidar-derived surfaces. *Canadian Journal of Remote Sensing* **32**(2):162-172.

Bruijnzeel, L.A. 2004. Hydrological functions of tropical forests: not seeing the soil for the trees? *Agriculture, Ecosystems and Environment* **104**:185-228.

Buttle, J.M. and A.G. Farnsworth. 2012. Measurement and modeling of canopy water partitioning in a reforested landscape: the Ganaraska forest, southern Ontario, Canada. *Journal of Hydrology* **466-467**:103-114.

Buttle, J.M. and P.M. Lafleur. 2007. Anatomy of an extreme event: the July 14-15, 2004 Peterborough rainstorm. *Canadian Water Resources Journal* **32**:59-74.

Calder, I.R. 1997. Water use by forests, limits and controls. *Tree Physiology* **18**:625-631.

Calder, I.R. 2005. Blue revolution: integrated land and water resource management, 2nd ed. London, U.K.: Earthscan, p.229.

Calder, I.R. 2007. Forests and water – ensuring forest benefits outweigh water costs. *Forest Ecology and Management* **251**:110-120.

Campbell, N.A. and J.B. Reece. 2005. Biology, 7th edition. San Francisco, California: Benjamin Cummings, p.433.

Cappiella, K., T. Schueler, and T. Wright. 2005. Urban watershed forestry manual: Part 1. Methods for increasing forest cover in a watershed. Newtown Square PA: United States Department of Agriculture, Forest Service, Northeastern Area, State and Private Forestry.

Crockford, R.H., and D.P. Richardson. 2000. Partitioning of rainfall into throughfall, stemflow and interception: effect of forest type, ground cover and climate. *Hydrological Processes* **11**:1509-1523.

Decagon Devices. 2007. Dielectric Leaf Wetness Sensor: Operator's Manual, Version 3. Pullman, WA: Decagon Devices Inc. p.19.

Dombroski, A. and M. Gleason. 2005. Temperature optima of a Cercospora sp causing leaf spot on Japanese tree lilac. *Phytopathology* **95**(6):S25.

Draper, D.W. and D.G. Long. 2004. Simultaneous wind and rain retrieval using SeaWinds data.

IEEE Transactions on Geoscience and Remote Sensing **42**(7):1411-1423.

Eakins, B.W. and G.F. Sharman. 2010. Volumes of the world's oceans from ETOPO1. Boulder, CO: NOAA national geophysical data center, p. 218.

Environment Canada. 1987. Federal water policy. Toronto, ON: Government of Canada, p. 37.

Environment Canada. 2009. Weather report. Toronto, ON: Government of Canada, p.31.

Environment Canada. 2010. Weather report. Toronto, ON: Government of Canada, p.37.

Environment Canada. 2011. AWARE: The atmosphere, the weather and flying. Toronto, ON: Government of Canada, p. 247.

Freeborn, J.R. and D.J. Sample. 2012. Residential stormwater: methods for decreasing runoff and increasing stormwater infiltration. *Journal of Green Building* **7**(2):15-30.

Freeman, G.F. 1920. Studies in evaporation and transpiration. *Botanical Gazette* **70**(3):190-210.

Fuentes, J.D. and T.J. Gillespie. 1992. A gas exchange system to study the effects of leaf surface wetness on the deposition of ozone. *Atmospheric Environment* **26**:1165-1173.

Gash, J.H.C. 1979. An analytical model of rainfall interception by forests. *Quarterly Journal of the Royal Meteorological Society* **105**:43-55.

Gash, J.H.C., C.R. Lloyd, and G. Lachaud. 1995. Estimating sparse forest rainfall interception with an analytical model. *Journal of Hydrology* **170**(1-4):79-86.

Gerhold, H.D. 2007. Tree Lilac (*Syringa reticulata*) cultivars tested as street trees: second report. *Arboriculture and Urban Forestry* **33**(3):182-184.

Green, J.S.A. 2006. Transfer properties of the large-scale and the general circulation of the atmosphere. *Quarterly Journal of the Royal Meteorological Society* **96**(408):157-185.

Hamlet, A.F., P.W. Mote, M.P. Clark, D.P. Lettenmaier. 2007. Twentieth-Century Trends in Runoff, Evapotranspiration, and Soil Moisture in the Western United States. *Journal of Climate* **20**:1468-1486.

Hanlon, E.A. 2009. Farming in the future – reaping ecosystem services. Southwest Florida agriculture and farming for ecosystem services workshop. Southwest Florida Research and Education Center, Immokalee, Florida. 10 November 2009.

Hatfield, J.L. and J.H. Prueger. 2011. Spatial and Temporal Variation in Evapotranspiration. *In:* Evapotranspiration – From Measurements to Agricultural and Environmental Applications.

Held, I.M. and B.J. Hoskins. 1985. Large-scale eddies and the general circulation of the troposphere. *Advances in Geophysics* **28**(A):3-31.

Helming, K. 2001. Wind speed effects on rain erosivity. *In:* D.E. Stott, R.H. Mohtar, and G.C.

Steinhardt (eds.). Sustaining the Global Farm. Select papers from the 10th International Soil Conservation Organization Meeting held May 24-29, 1999 at Purdue University and the USDA-ARS National Soil Erosion Research Laboratory.

Henshall, W.R. and R.M. Beresford. 1997. Performance of wetness sensors used in plant disease forecasting. *Plant Diseases* **50**:107-111.

Herbst, M., P.T.W. Rosier, D.D. Mcneil, R.J. Harding and D.J. Gowing. 2008. Seasonal variability of interception evaporation from the canopy of a mixed deciduous forest. *Agricultural and Forest Meteorology* **148**(11):1655-1667.

Herwitz, S. and R. Slye. 1995. Three-dimensional modeling of canopy tree interception of wind-driven rainfall. *Journal of Hydrology* **168**:205-226.

Hopp, L. and J.J. McDonnell. 2011. Examining the role of throughfall patterns on subsurface stormflow generation. *Journal of Hydrology* **409**:460-471.

Horton, R.E. 1919. Rainfall interception. *Monthly Weather Review* **49**:603-623.

Huber, L. and T.J. Gillespie. 1992. Modeling leaf wetness in relation to plant disease epidemiology. *Annual Review of Phytopathology* **30**:553-577.

International Electrotechnical Commission standard (IEC). 2012. Technical Reports on Wind Speed Standards. UK: IEC Publications, p.143.

Isenburg, M.L., Y. Liu, J. Shewchuk, J. Snoeyink, and T. Thirion. 2006. Generating raster DEM from mass points via TIN streaming. In: Proceedings of GIScience '06, Munster, Germany, September 20-23. P.186-198.

Jetten, V.G. 1996. Interception of tropical rain forest: performance of a canopy water balance model. *Hydrological processes* **10**(6):671-685.

Kilian, J., N. Haala, and M. Englich. 1996. Capture and evaluation of airborne laser scanner data. *International Archives of Photogrammetry, Remote Sensing and Spatial Information Sciences* **31**(B3):383-388.

Kloefkorn, W. 2011. Japanese lilac: June. *Midwest Quarterly-A Journal Of Contemporary Thought* **52**(4):335.

Konrad, W., M. Ebner, C. Traiser, and A. Roth-Nebelsick. 2011. Leaf surface wettability and implications for drop shedding and evaporation from forest canopies. *Pure Applied Geophysics* **169**:835-845.

Kume, T., J.M. Odair, K. Kuraji, K. Tanaka, T. Horiuchi, M. Suzuki, and T. Kumagai. 2008. Estimation of canopy water storage capacity from sap flow measurements in a Bornean tropical rainforest. *Journal of Hydrology* **352**:288-295.

Laird, S.G., C.R. Ford, S.H. Laseter, and J.M. Vose. 2011. Long-term forest management and

climate effects on streamflow. The Fourth Interagency Conference on Research in the Watersheds, 26-30 September 2011, Fairbanks, AK.

Lam, N.S.N, and D.A. Quattrochi. 1992. On the issues of scale, resolution, and fractal analysis in the mapping sciences. *The Professional Geographer* **44**:88-98.

Lankreijer, H.J.M., M.J. Hendriks, and W. Klaassen. 1993. A comparison of models simulating rainfall interception of forests. *Agricultural and Forest Meteorology* **64**:187-199.

Lawrence, D.M., P.E. Thornton, K.W. Oleson, and G.B. Bonan, 2007: The Partitioning of Evapotranspiration into Transpiration, Soil Evaporation, and Canopy Evaporation in a GCM: Impacts on Land–Atmosphere Interaction. Journal of Hydrometeorology **8**:862-880.

Le Duc, M.C. 1992. A design methodology for geoinformatic systems. *Computer, Environment, and Urban Systems* **16**:403-413.

Lewis, J. 2002. Stemflow estimation in a redwood forest using model-based stratified random sampling. *Environmetrics* **14**(6):559-571.

Leyton, L., E. R. C. Reynolds, and F. B. Thompson. 1967. Rainfall interception in forest and moorland, pp. 163-178. *In:* W. E. Sopper and H.W. Lull, International Symposium on Forest Hydrology. New York: Pergamon Press, Inc.

Liu, S. 1997. A new model for the prediction of rainfall interception in forest canopies. *Ecological Modeling* **99**:151-159.

Liu, S.G. 2001. Evaluation of the Liu model for predicting rainfall interception in forests world-wide. *Hydrological Processes* **15**(12):2341-2360.

Llorens, P., 1997. Rainfall interception by a Pinus sylvestris forest patch overgrown in a Mediterranean mountainous abandoned area. II. assessment of the applicability of Gash's analytical model. *Journal of Hydrology* **199**(3-4):346-359.

Lloyd, C.R. 1990. The temporal distribution of Amazonian rainfall and its implications for forest interception. *Quarterly Journal of the Royal Meterlogical Society* **116**:1487-1494.

Lloyd, C.R., J.H.C. Gash, W.J. Shuttleworth. 1988. The measurement and modeling of rainfall interception by Amazonian rain forest. *Agricultural and Forest Meterology* **43**:277-294.

Massman, W.J. 1983. The derivation and validation of a new model for the interception of rainfall by forests. *Agricultural Meteorology* **28**:261-286.

McCulloch, J.S.G. and M. Robinson. 1993. History of forest hydrology. *Journal of Hydrology* **150**:189-216.

Ministry of Environment. 2011. Ontario's climate change progress report: adaptation strategy and action plan 2011-2014. Toronto, ON: Government of Canada, p. 30.

Miralles, D.G., J.H. Gash, T.R.H. Holmes, R.A.M. de Jeu, and A.J. Dolman. 2010. Global canopy

interception from satellite observations. *Journal of Geophysical Research* **115**(D16122):8.

Mooney, H.A., C. Field, C.V. Yanes, and C. Chu. 1983. Environmental controls on stomatal conductance in a shrub of the humid tropics. *Proceedings of the National Academy of Sciences of the United States of America* **80**(5):1295-1297.

Mulder, J.P.M. 1985. Simulating interception focusing standard meterological data. *In:* Hutchison, B.A. and B.B. Hicks (ed.), The Forest-Atmosphere Interaction, Reidel, Drodrecht. p.177-196.

Muzylo, A., F. Valente, F. Domingo, and P. Llorens. 2012. Modelling rainfall partitioning with sparse Gash and Rutter models in a downy oak stand in leafed and leafless periods. *Hydrological Processes* **26**:3161-3173.

Oke, T.R. 1987. Boundary Layer Climates. New York: Routledge, p.435.

Pan, Z., G. Liu, and C. Zhou. 2003. Dynamic analysis of evapotranspiration based on remote sensing in Yellow River Delta, *Journal of Geographical Sciences* **13**(4):408-415.

Pearce, A.J. and L.K. Rowe. 1981. Rainfall interception in a multi-storied evergreen mixed forest: estimates using Gash's analytical model. *Journal of Hydrology* **49**:341-353.

Pedersen, H.S., and B. Hasholt. 1995. Influence of wind speed on rainsplash erosion. *Catena* **24**:39-4.

Perks, A., T. Winkller, and B. Stewart. 1996. The adequacy of hydrological networks: a global assessment. *Technical Reports in Hydrology and Water Resources* **52**:56.

Pidwirny, M. 2006. Evaporation and transpiration: fundamentals of physical geography, 2nd ed. Okanagan, BC: University of BC, p.271.

Riekerk, H., H.L. Gholz, D.G. Neary, L.V. Korhnak, and S.G. Liu. 1995. Evapotranspiration of pineflatwoods in Florida. Final report to USDA forest service southern forest experiment station, p.37.

Raper, J. 1989. 3D applications in Geographic Information Systems. London: Taylor & Francis, p.156.

Rutter, A.J., K.A. Kershaw, P.C. Robins, A.J. Morton. 1971. A predictive model of rainfall interception in forests. I. Derivation of the model from observations in a plantation of Corsican pine. *Agricultural Meteorology* **9**:367-384.

Rutter, A.J., A.J. Morton, and P.C. Robins. 1975. A predictive model of rainfall interception in forests. II. generalization of the model and comparison with observation in some coniferous and hardwood stands. *Journal of Applied Ecology* **12**:367-380.

Rutter, A.J. and A.J. Morton. 1977. A predictive model of rainfall interception in forests. III.

Sensitivity of model to stand parameters and meteorological variables. *Journal of Applied Ecology* **14**:567-588.

Ruudi, V.D.E., A.M.J. Coenders-Gerrits, R. Nikoli, and H.H.G. Savenije. 2012. The importance of proper hydrology in forest cover-water yield debate: commentary on Ellison et al. (2012) *Global Change Biology* **18**:806-820. *Global Change Biology* **18**:2677-2680.

Salmon, J.R. and P.A. Taylor. 2012. Errors and uncertainties associated with missing wind data. *Wind Energy* **15**(7):889-901.

Schmidt, R.A. and D.R. Gluns. 1991. Snowfall interception on branches of three conifer species. *Canadian Journal of Forestry Resources* **21**:1262-1269.

Schmidt, R.A. and C.A. Troendle. 1992. Sublimation of intercepted snow as a global source of water vapor. *In:* Proceedings for the 60th Annual Western Snow Conference, April 14-16, 1992, Jackson, Wyo., p.1-9.

Schuepp, P.H., M.Y. Leclerc, J.I. Macpherson, and R.L. Desjardins. 1990. Footprint prediction of scalar fluxes from analytical solutions of the diffusion equation. *Boundary Layer Meteorology* **50**:355-374.

Siles, P. V. Philippe, E. Dreyer, J.M. Harmand. 2010. Rainfall partitioning into throughfall, stemflow and interception loss in a coffee (Coffea arabica L.) monoculture compared to an agroforestry system with Inga densiflora. *Journal of Hydrology* **395**(1-2):39-48.

Smelser, N.J. and P.B. Baltes. 2001. International Encyclopedia of the Social & Behavioral Sciences. Oxford: Pergamon Press, p.13504.

Song, J.H., S.H. Han, K. Yu, and Y.I. Kim. 2002. Assessing the possibility of land-cover classification using lidar intensity data. ISPRS Proceedings, 9-13 September, Graz, vol. 34, p.1-4.

Spittlehouse, D.L. and R.D. Winkler. 2002. Modeling snowmelt in a forest and clearcut. In: Proc. 25th Conf. Agric. For. Meteorol., May 20-24, 2002, Norfolk Va. Am. Meteorol. Soc., Boston, Mass., p.121-122.

Staelens, J., A. De Schrijver, K. Verheyen and N.E.C. Verhoest. 2008. Rainfall partitioning into throughfall, stemflow, and interception within a single beech. Canopy: influence of foliation, rain event characteristics, and meteorology. *Hydrological Processes* **22**:33-45.

Sutanto, S.J., J. Wenninger, A.M.J. Coenders-Gerrits, and S. Uhlenbrook. 2012. Partitioning of evaporation into transpiration, soil evaporation and interception: a comparison between isotope measurements and a HYDRUS-1D model. *Hydrology and Earth System Sciences* **16**:2605-2616.

Sutton, J.C., T.J. Gillespie, and P.D. Hildebrand. 1984. Monitoring weather factors in relation to plant disease. *Plant Disease* **68**:78-84.

Sutton, D.J., Z.J. Kabala, A. Francisco, and D. Vasudevan. 2001. Limitation and potential of commercially available Rhodamine WT as a groundwater tracer. *Water Resources* **37**:1641-1656.

Symonds, G.W.D. 1973. Tree Identification Book: A New Method for the Practical Identification and Recognition of Trees. NY: William Morrow Paperbacks, p.272.

Takahashi, M. T.W. Giambelluca, R.G. Mudd, J.K. DeLay, M.A. Nullet, and G.P. Asner. 2010. Rainfall partitioning and cloud water interception in native forest and invaded forest in Hawaii volcanoes National Park. *Hydrological Processes* **25**(3):448-464.

Taylor, P.A., and J.R. Salmon. 1993. A model for the correction of surface wind data for sheltering by upwind obstacles. *Journal of Applied Meteorology* **32**:1683-1694.

Todd, A.K., J.M. Buttle, and C.H. Taylor. 2006. Hydrologic dynamics and linkages in a wetland dominated basin. *Journal of Hydrology* **319**:15-35.

Trenberth, K.E. 1992. Climate System Modeling. Cambridge: Cambridge University Press, p.788.

Tversky, B., J. Morrison, M. Betrancourt. 2002. Animation: can it facilitate? *International Journal of Human Computer Studies* **57**:247-262.

United Nations Environment Programme. 2011. UNEP Year Book: Emerging Issues in Our Global Environment 2011. United Kingdom: United Nations, p.78.

Valente, F., J.S. David, and J.H.C. Gash. 1997. Modelling interception loss for two sparse eucalypt and pine forests in central Portugal using reformulated Rutter and Gash analytical models. *Journal of Hydrology* **190**(1-2):141-162.

Van der Wal, A.F. 1978. Moisture as a factor in epidemiology and forecasting. In: Koslowski, T.T. Water deficits and plant growth – water and plant disease. New York: Academic Press, p.253-295.

Van Dijk, A.I.J.M. and L.A. Bruijnzeel. 2001.Modelling rainfall interception by vegetation of variable density using an adapted analytical model: part 1 – model description. *Journal of Hydrology* **247**:230-238.

Van Dijk, A.I.J.M. and R.J. Keenan. 2007. Planted forests and water in perspective. *Forest Ecology and Management* **251**:1-9.

Voigt, G.K. 1960. Distribution of rainfall under forest stands. *Forestry Science* **6**:2-10.

Vose, J.M., G. Sun, C.R. Ford, M. Bredemeier, K. Otsuki, X.H. Wei, Z.Q. Zhang, and L. Zhang. 2011. Forest ecohydrological research in the 21st century: what are the critical needs? *Ecohydrology* **4**:146-158.

Ward, R.C. and Robinson, M. 2000. Principles of Hydrology, 4th edition. UK: McGraw-Hill Publishing Company, p.449.

Weissman, D.E., M.A. Bourassa, and J. Tongue. 2001. Effects of rain rate and wind magnitude

on SeaWinds scatterometer wind speed errors. *Journal of Atmospheric and Oceanic Technology* **19**:738-746.

Whitehead, D. and F.M. Kelliher. 1991. A canopy water balance model for a *Pinus radiata* stand before and after thinning. *Agricultural Forestry and Meteorology* **55**:109-126.

Williams, A.G., M. Kent, and T.L. Ternan. 1987. Quantity and quality of bracken throughfall, stemflow, and litterflow in a Dartmoor catchment. *Journal of Applied Ecology* **24**:217-230.

Williams, J. 1997. Weather Book. NY: Routledge, p.158.

Winkler, R.D., R.D. Moore, T.E. Redding, D.L. Spittlehouse, D.E. Carlyle-Moses, and B.D. Smerdon. Hydrological processes and watershed response. *Forestry* **6**:133-177.

Wishmeier, W.H. and D.D. Smith. 1958. Rainfall energy and it's relationship to soil loss. *Transactions of the American Geophysical Union* **39**:295-291.

Xiao, Q., E.G. McPherson, S.L. Ustin, M.E. Grismer, and J.R. Simpson. 2000. Winter Rainfall Interception by Two Mature Open-Grown Trees in Davis, California. *Hydrological Processes* **14**(4):763-784.

Xiao, Q. and E.G. McPherson. 2003. Rainfall interception by Santa Monica's municipal urban forest. *Urban Ecosystems* **6**: 291–302.

Zeng, N., J.W. Shuttleworth, and J.H.C. Gash. 2000. Influence of temporal variability of rainfall on interception loss, part 1: point analysis. *Journal of Hydrology* **228**:228-241.

Zhai, X., R.J. Greatbatch, and J. Sheng. 2006. Diagnosing the role of eddies in driving the circulation of the northwest Atlantic Ocean. *Geophysical Research Letters* **31**(L22304):1-4.

Zingari, P.C. and M. Achouri. 2010. Five years after Shiga: recent developments in forest and water policy implementation. *Forest and Water* **218**:120-128.

Zinke, P.J. 1967. Forest interception studies in the United States. *In:* Sopper, W.E. and H.W. Lull (ed.). International Symposium on Forest Hydrology, Pergamon Press, Oxford, p.137-161.

Zotarelli, L., M.D. Dukes, R. Munoz-Carpena. 2009. Soil water distribution and nitrate leaching of drip irrigation controlled by soil moisture sensors. *Agricultural News* **4**:1-8.

APPENDIX A

Table 13. A list of details pertaining to the 8 rain events in June 2009; the start/end times for each event, total precipitation recorded (in mm), and the rain category type is listed in detail below.

Event ID	Start Date/Time (yyyy-mm-dd / hh:mm)	End Date/Time (yyyy-mm-dd / hh:mm)	Total Precipitation (mm)	Rain Category
1	2009-06-11 14:13	2009-06-11 21:05	2.8	LRS2
2	2009-06-14 17:34	2009-06-14 20:21	0.4	D1
3	2009-06-17 14:28	2009-06-18 10:45	9.0	RS3
4	2009-06-19 03:10	2009-06-19 10:27	0.3	D1
5	2009-06-20 03:02	2009-06-20 22:45	11.9	RS3
6	2009-06-25 11:45	2009-06-25 18:30	18.9	T6
7	2009-06-28 10:16	2009-06-28 20:55	5.4	RS3
8	2009-06-29 13:01	2009-06-30 11:13	3.4	T6

Table 14. A list of details pertaining to the 16 rain events in July 2009; the start/end times for each event, total precipitation recorded (in mm), and the rain category type is listed in detail below.

Event ID	Start Date/Time (yyyy-mm-dd / hh:mm)	End Date/Time (yyyy-mm-dd / hh:mm)	Total Precipitation (mm)	Rain Category
9	2009-07-01 21:40	2009-07-01 22:05	0.5	LRS2
10	2009-07-02 07:15	2009-07-02 07:20	1.3	LRS2
11	2009-07-07 03:00	2009-07-07 03:20	0.2	D1
12	2009-07-11 09:21	2009-07-11 10:30	5.4	LRS2
13	2009-07-17 20:29	2009-07-17 20:43	0.4	D1
14	2009-07-21 16:47	2009-07-21 19:55	1.4	LRS2
15	2009-07-22 23:17	2009-07-23 03:40	2.4	LRS2
16	2009-07-23 05:50	2009-07-23 12:35	11.3	HRS5
17	2009-07-23 22:00	2009-07-23 22:45	14.8	RS3
18	2009-07-24 16:29	2009-07-24 17:40	1.1	LRS2
19	2009-07-25 14:45	2009-07-25 17:30	15.1	RS3
20	2009-07-26 11:14	2009-07-26 12:10	4.8	RS3
21	2009-07-26 15:10	2009-07-26 18:50	2.4	T6
22	2009-07-26 22:30	2009-07-26 22:55	1.8	RS3
23	2009-07-28 04:48	2009-07-28 05:12	0.2	D1
24	2009-07-29 02:29	2009-07-29 11:10	6.5	T6

Table 15. A list of details pertaining to the 17 rain events in August 2009; the start/end times for each event, total precipitation recorded (in mm), and the rain category type is listed in detail below.

Event ID	Start Date/Time (yyyy-mm-dd / hh:mm)	End Date/Time (yyyy-mm-dd / hh:mm)	Total Precipitation (mm)	Rain Category
25	2009-08-02 05:57	2009-08-02 06:28	0.4	D1
26	2009-08-04 13:16	2009-08-04 14:32	1.3	T6
27	2009-08-04 20:11	2009-08-04 21:55	1.9	T6
28	2009-08-08 18:03	2009-08-09 01:30	2.9	T6
29	2009-08-09 11:15	2009-08-09 11:55	11.9	RS3
30	2009-08-09 20:12	2009-08-09 21:35	11.2	MRS4
31	2009-08-10 03:40	2009-08-10 05:30	2.3	MRS4
32	2009-08-10 17:04	2009-08-10 17:18	0.4	D1
33	2009-08-11 13:41	2009-08-11 17:40	2.5	HRS5
34	2009-08-12 12:51	2009-08-12 13:30	2.4	RS3
35	2009-08-17 15:28	2009-08-17 15:42	0.4	D1
36	2009-08-18 03:53	2009-08-18 05:05	0.3	LRS2
37	2009-08-20 16:50	2009-08-20 19:50	10.2	T6
38	2009-08-21 13:10	2009-08-21 13:24	0.4	D1
39	2009-08-22 13:42	2009-08-22 14:18	0.1	D1
40	2009-08-26 05:20	2009-08-26 09:20	2.8	LRS2
41	2009-08-28 23:26	2009-08-29 03:55	14.5	HRS5

Table 16. A list of details pertaining to the 10 rain events in September 2009; the start/end times for each event, total precipitation recorded (in mm), and the rain category type is listed in detail below.

Event ID	Start Date/Time (yyyy-mm-dd / hh:mm)	End Date/Time (yyyy-mm-dd / hh:mm)	Total Precipitation (mm)	Rain Category
42	2009-09-05 06:55	2009-09-05 07:15	0.2	D1
43	2009-09-21 15:57	2009-09-21 19:15	1.7	RS3
44	2009-09-23 15:27	2009-09-23 15:40	0.3	LRS2
45	2009-09-26 15:08	2009-09-27 03:55	6.2	MRS4
46	2009-09-28 06:38	2009-09-28 10:05	13.8	MRS4
47	2009-09-28 17:15	2009-09-28 19:05	1.6	RS3
48	2009-09-29 03:25	2009-09-29 04:25	2.2	RS3
49	2009-09-29 11:00	2009-09-29 11:50	0.7	RS3
50	2009-09-29 17:41	2009-09-29 20:40	0.8	LRS2
51	2009-09-30 14:29	2009-09-30 14:35	0.1	D1

Table 17. A list of details pertaining to the 19 rain events in October 2009; the start/end times for each event, total precipitation recorded (in mm), and the rain category type is listed in detail below.

Event ID	Start Date/Time (yyyy-mm-dd / hh:mm)	End Date/Time (yyyy-mm-dd / hh:mm)	Total Precipitation (mm)	Rain Category
52	2009-10-01 13:57	2009-10-01 14:08	0.4	D1
53	2009-10-02 11:45	2009-10-02 20:35	8.4	MRS4
54	2009-10-02 22:25	2009-10-02 23:55	0.9	RS3
55	2009-10-03 06:45	2009-10-03 12:25	1.2	LRS2
56	2009-10-03 17:50	2009-10-03 18:25	0.7	LRS2
57	2009-10-04 12:49	2009-10-04 16:05	1.8	RS3
58	2009-10-06 19:02	2009-10-07 01:20	7.3	RS3
59	2009-10-09 12:49	2009-10-10 00:15	18.9	MRS4
60	2009-10-13 04:35	2009-10-13 08:21	0.1	LRS2
61	2009-10-20 21:39	2009-10-20 22:12	0.4	D1
62	2009-10-22 10:25	2009-10-22 15:55	0.5	LRS2
63	2009-10-23 06:15	2009-10-23 09:45	2.0	RS3
64	2009-10-23 11:20	2009-10-23 23:05	11.5	HRS5
65	2009-10-24 15:49	2009-10-24 15:58	0.5	D1
66	2009-10-28 00:39	2009-10-28 04:50	2.3	RS3
67	2009-10-28 09:00	2009-10-28 10:05	0.4	LRS2
68	2009-10-29 01:31	2009-10-29 02:14	0.2	D1
69	2009-10-30 08:24	2009-10-30 13:00	2.8	RS3
70	2009-10-31 02:25	2009-10-31 03:38	2.4	RS3

Table 18. A list of details pertaining to the 9 rain events in November 2009; the start/end times for each event, total precipitation recorded (in mm), and the rain category type is listed in detail below.

Event ID	Start Date/Time (yyyy-mm-dd / hh:mm)	End Date/Time (yyyy-mm-dd / hh:mm)	Total Precipitation (mm)	Rain Category
71	2009-11-02 17:03	2009-11-02 19:30	1.3	LRS2
72	2009-11-03 14:46	2009-11-03 15:18	0.1	D1
73	2009-11-04 07:08	2009-11-04 08:12	0.2	D1
74	2009-11-04 16:46	2009-11-04 19:10	1.6	LRS2
75	2009-11-04 23:30	2009-11-05 02:05	1.9	RS3
76	2009-11-05 07:20	2009-11-05 10:30	1.7	RS3
77	2009-11-19 05:10	2009-11-19 10:00	3.7	RS3
78	2009-11-19 16:05	2009-11-19 17:40	1.6	RS3
79	2009-11-19 22:10	2009-11-20 02:20	3.4	MRS4

APPENDIX B

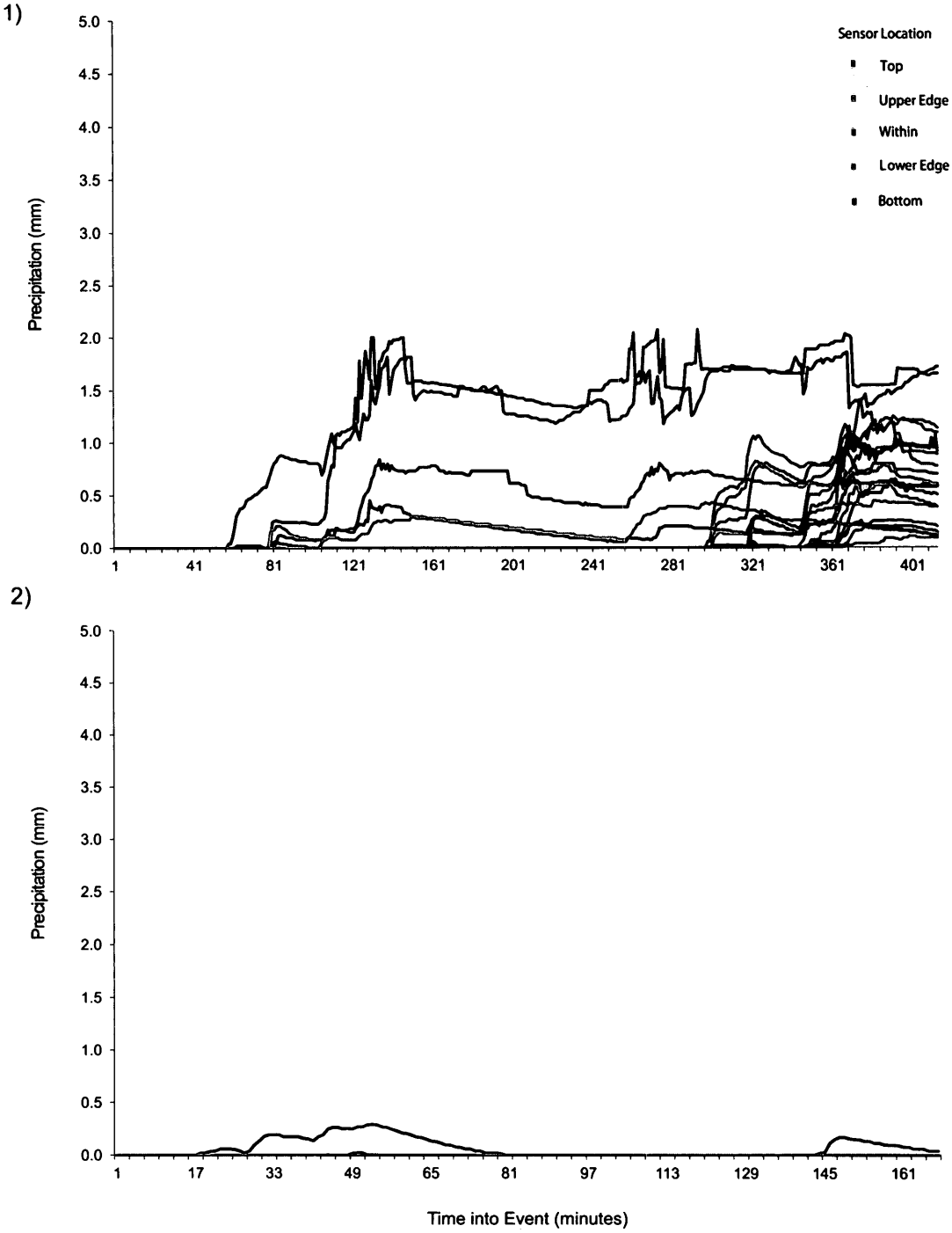

Figure 29. LWS wetness readings recorded for Event 1 (on June 11, 2009 from 14:13 to 21:05) and Event 2 (on June 14, 2009 from 17:34 to 20:21).

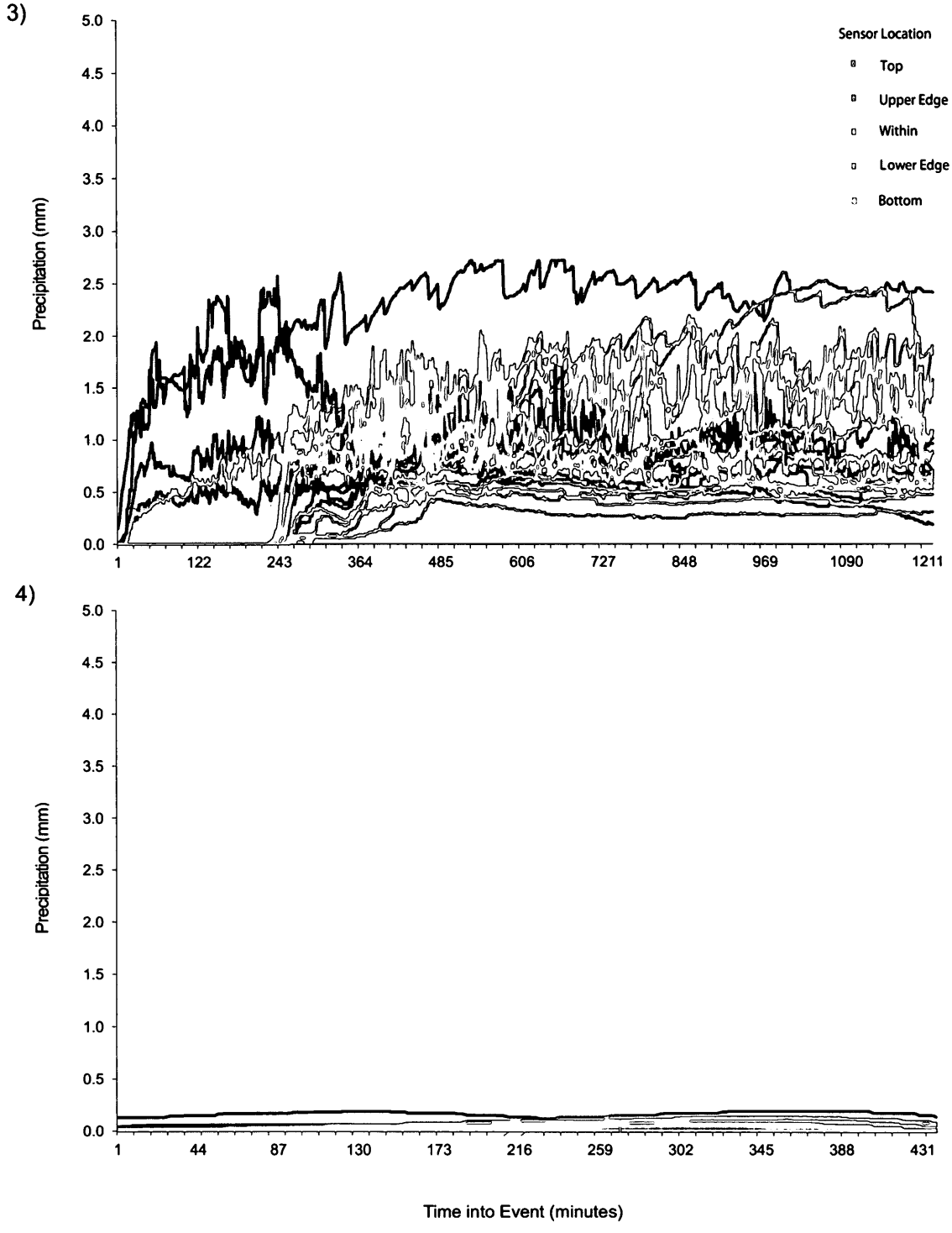

Figure 30. LWS wetness readings recorded for Event 3 (on June 17, 2009 to June 18, 2009 from 14:28 to 10:45) and Event 4 (on June 19, 2009 from 03:10 to 10:27).

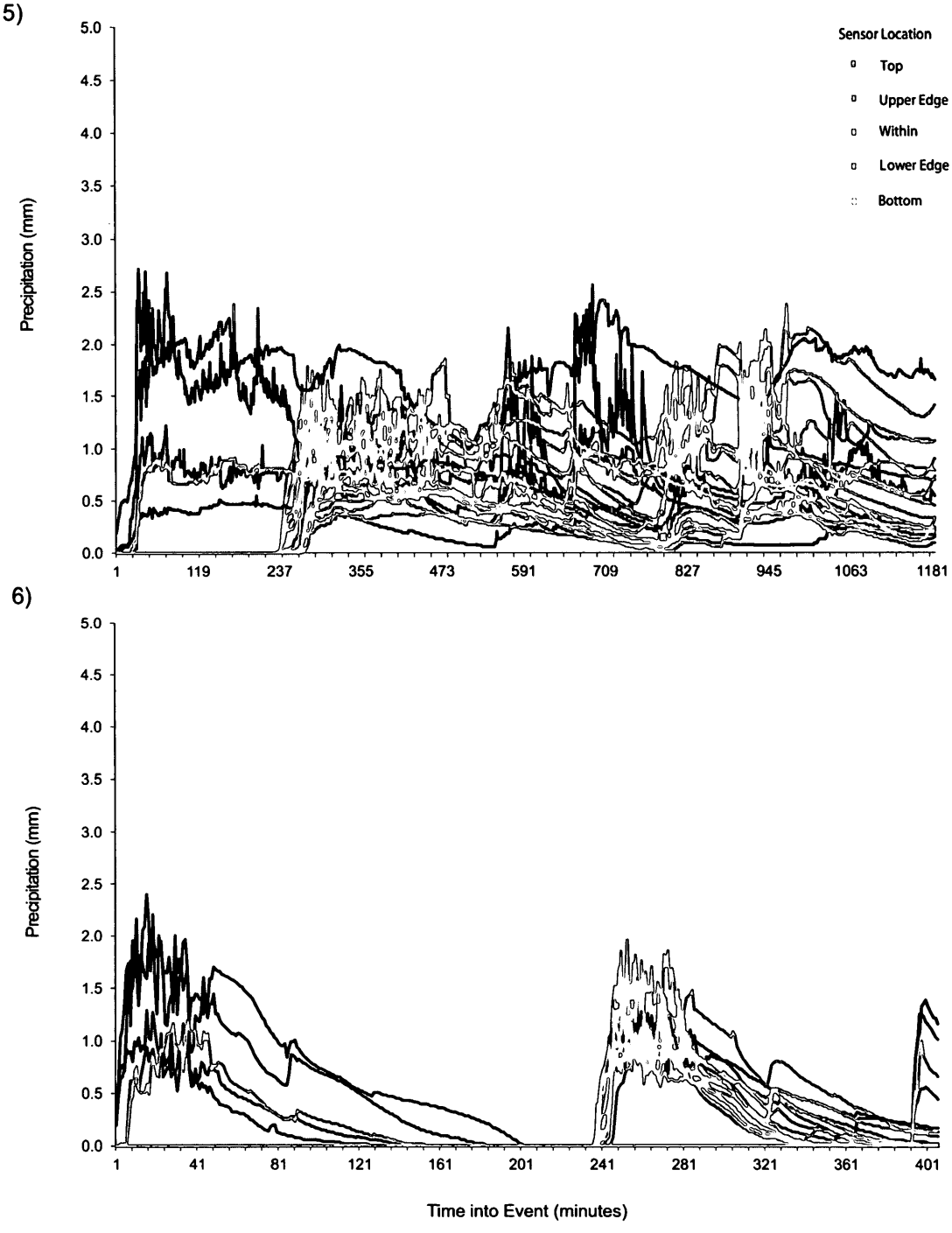

Figure 31. LWS wetness readings recorded for Event 5 (on June 20, 2009 from 03:02 to 22:45) and Event 6 (on June 25, 2009 from 11:45 to 18:30).

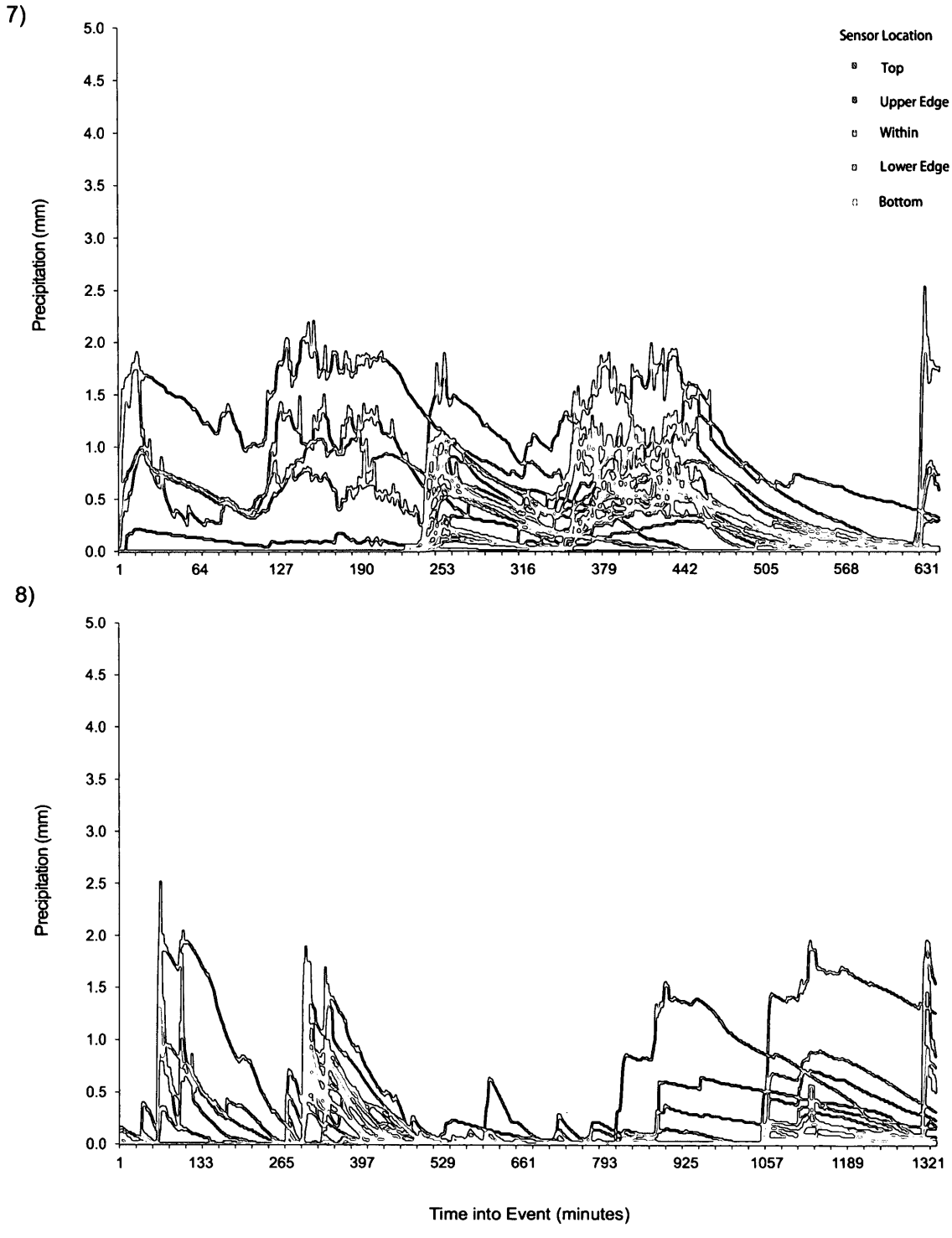

Figure 32. LWS wetness readings recorded for Event 7 (on June 28, 2009 from 10:16 to 20:55) and Event 8 (on June 29, 2009 to June 30, 2009 from 13:01 to 11:13).

9)

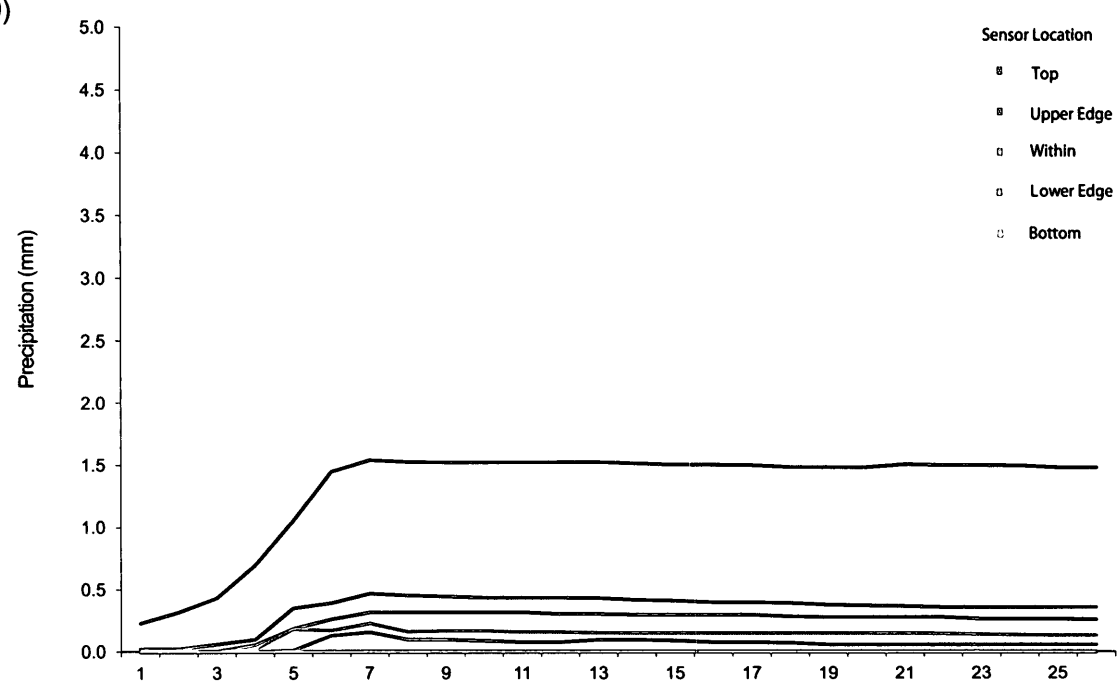

10)

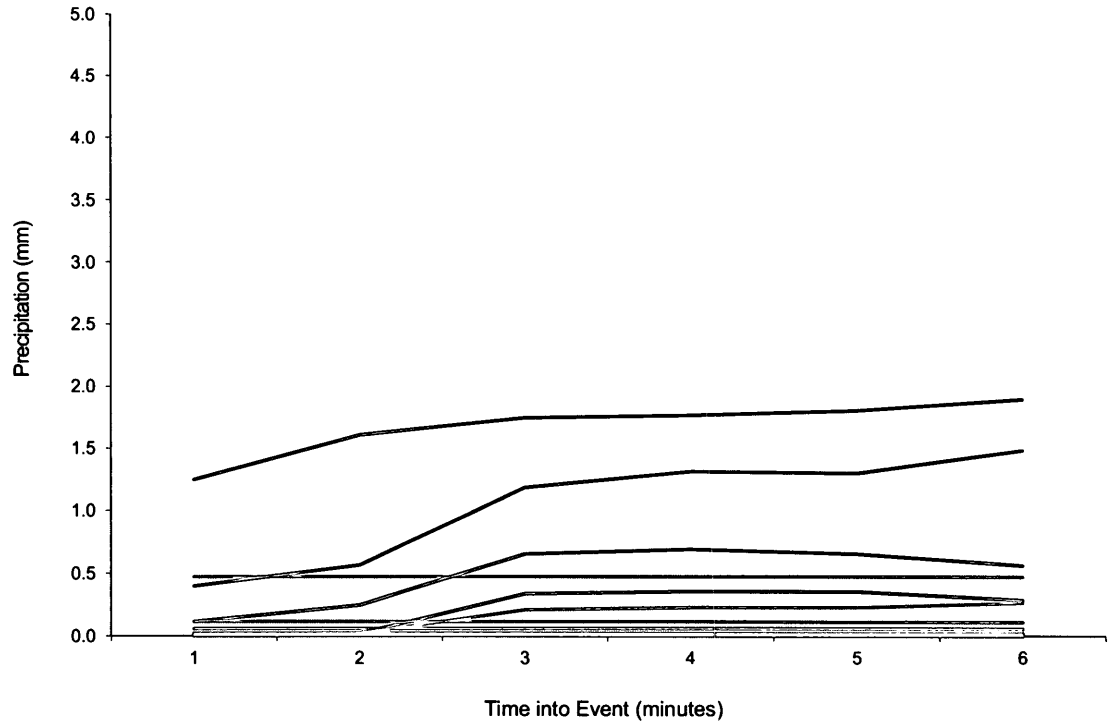

Figure 33. LWS wetness readings recorded for Event 9 (on July 1, 2009 from 21:40 to 22:05) and Event 10 (on July 2, 2009 from 07:15 to 07:20).

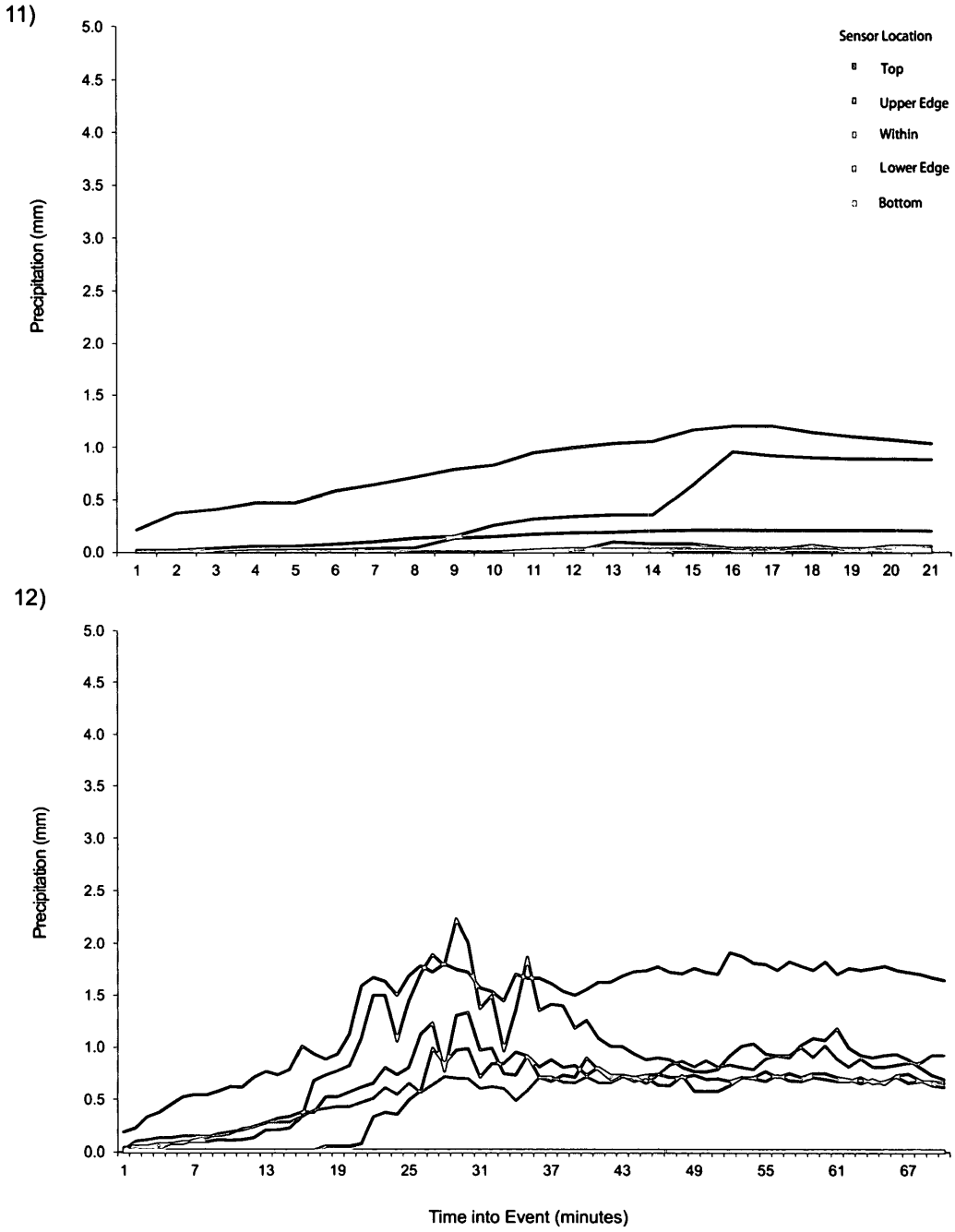

Figure 34. LWS wetness readings recorded for Event 11 (on July 7, 2009 from 03:00 to 03:20) and Event 12 (on July 11, 2009 from 09:21 to 10:30).

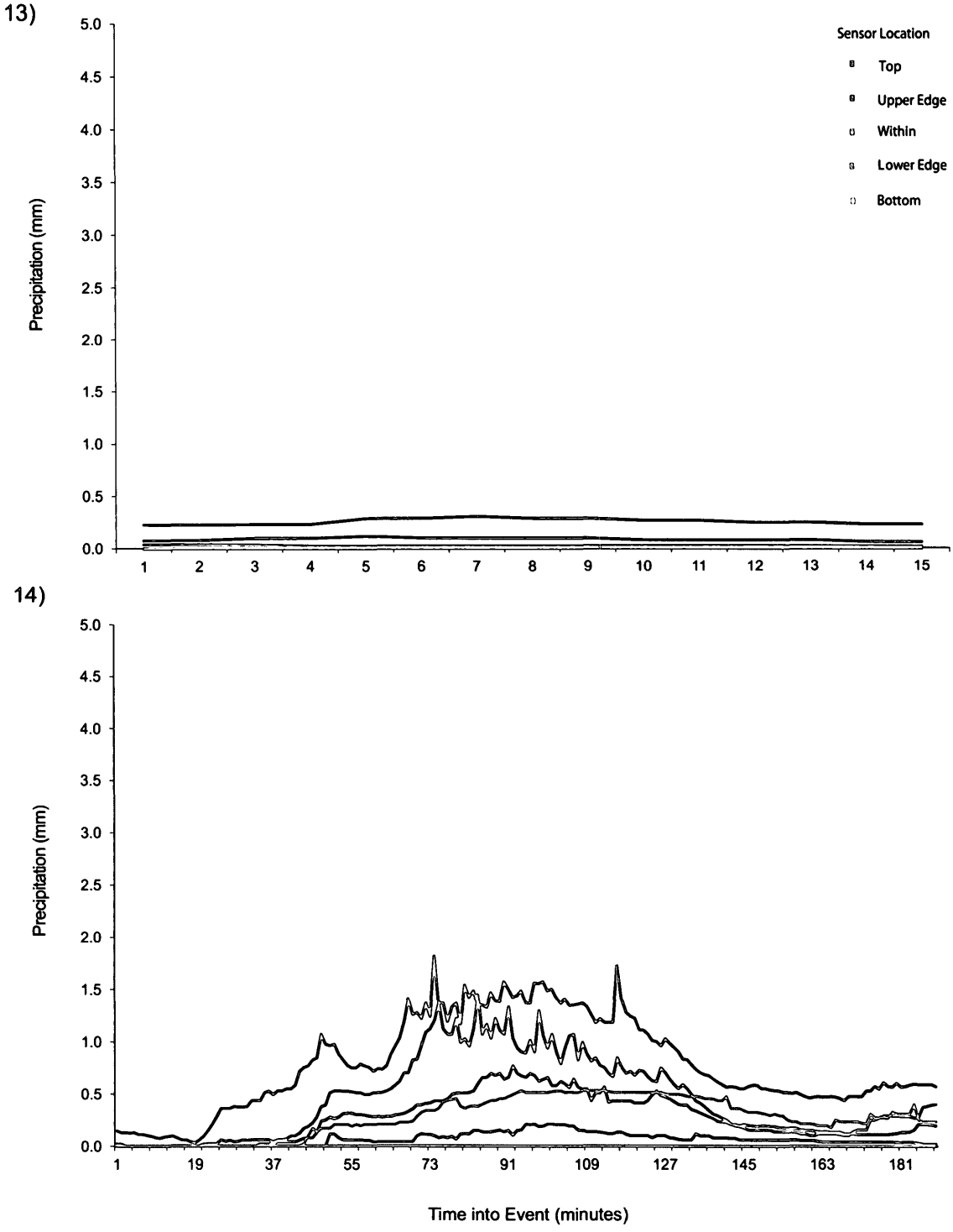

Figure 35. LWS wetness readings recorded for Event 13 (on July 17, 2009 from 20:29 to 20:43) and Event 14 (on July 21, 2009 from 16:47 to 19:55).

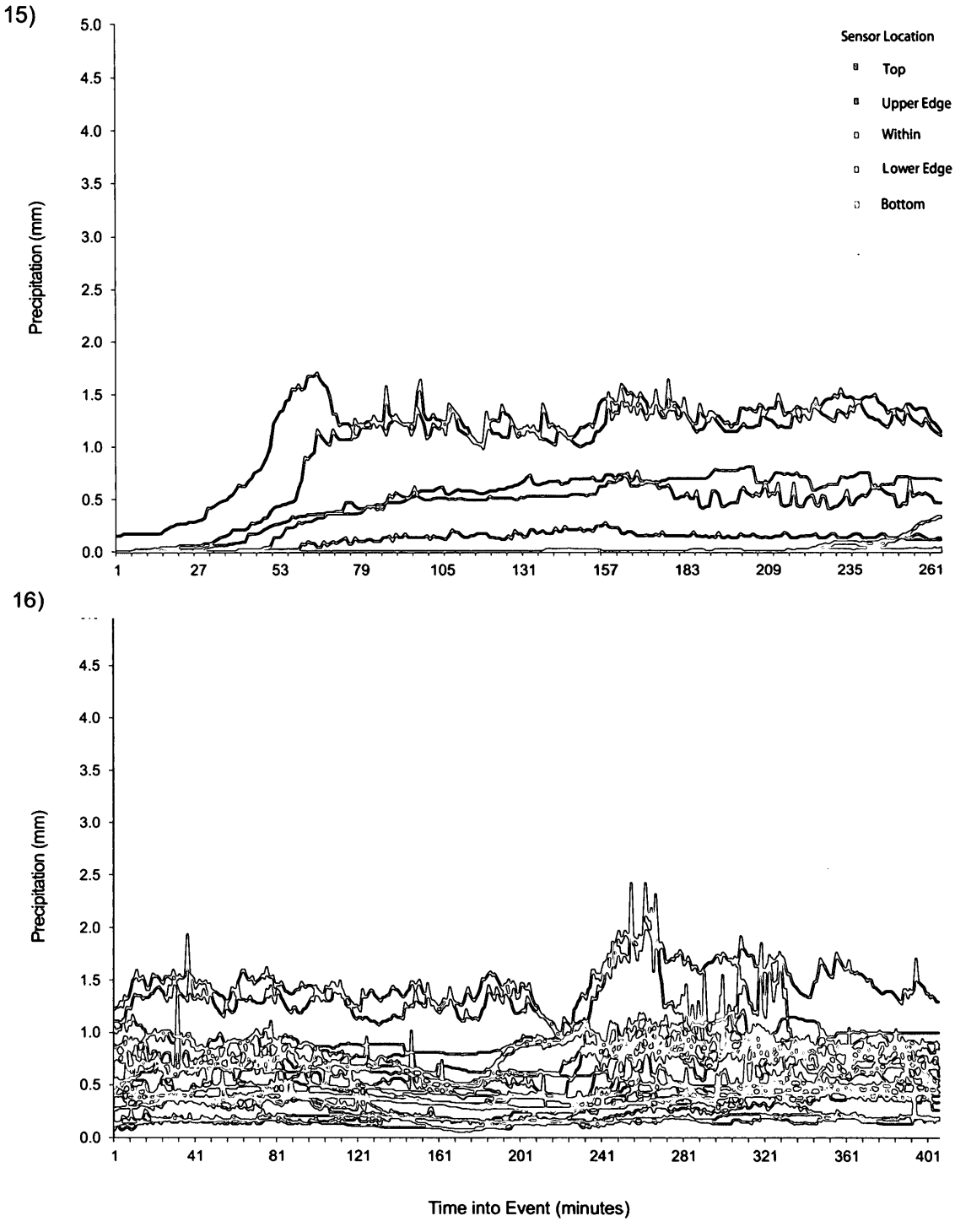

Figure 36. LWS wetness readings recorded for Event 15 (on July 22, 2009 to July 23, 2009 from 23:17 to 03:40) and Event 16 (on July 23, 2009 from 05:50 to 12:35).

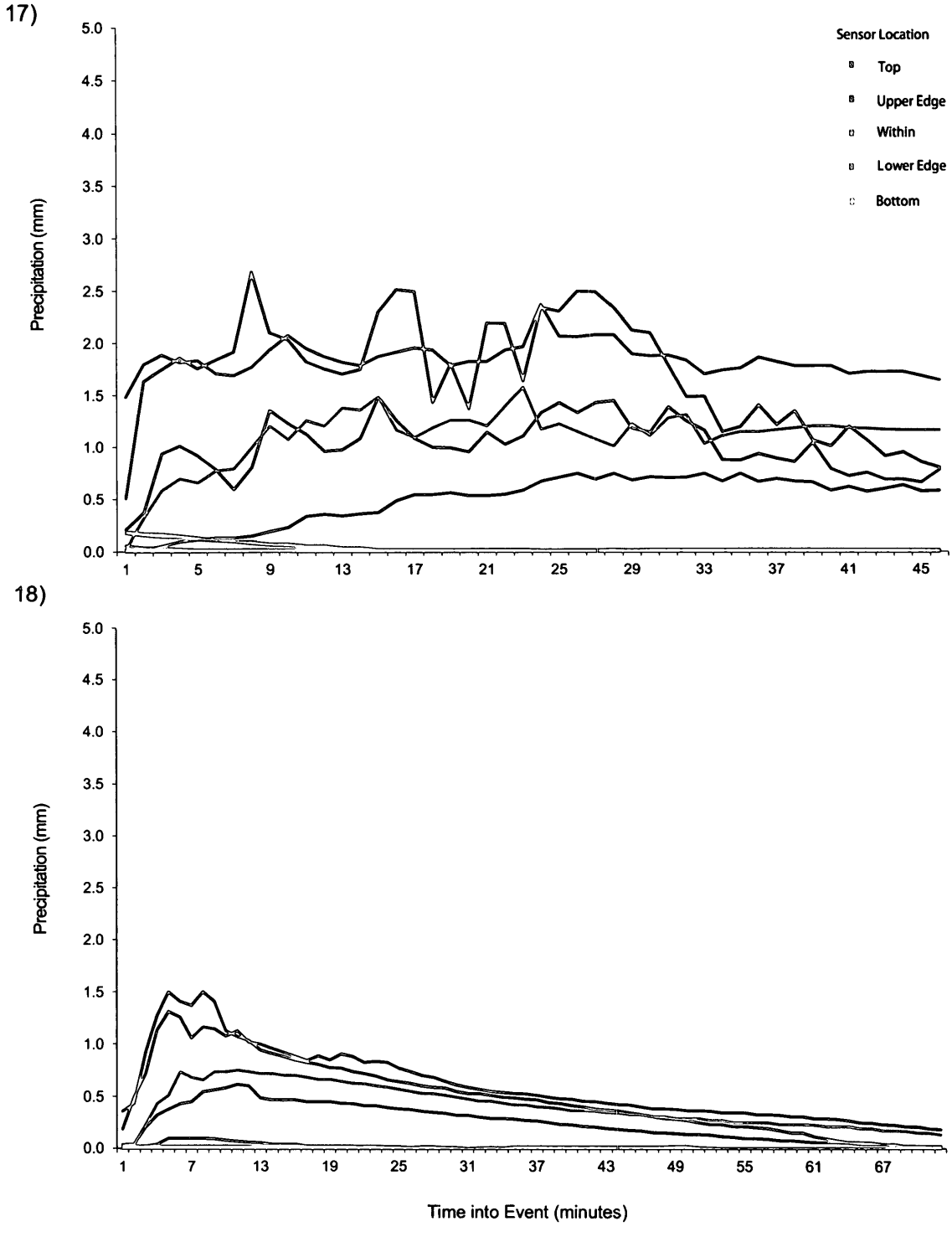

Figure 37. LWS wetness readings recorded for Event 17 (on July 23, 2009 from 22:00 to 22:45) and Event 18 (on July 24, 2009 from 16:29 to 17:40).

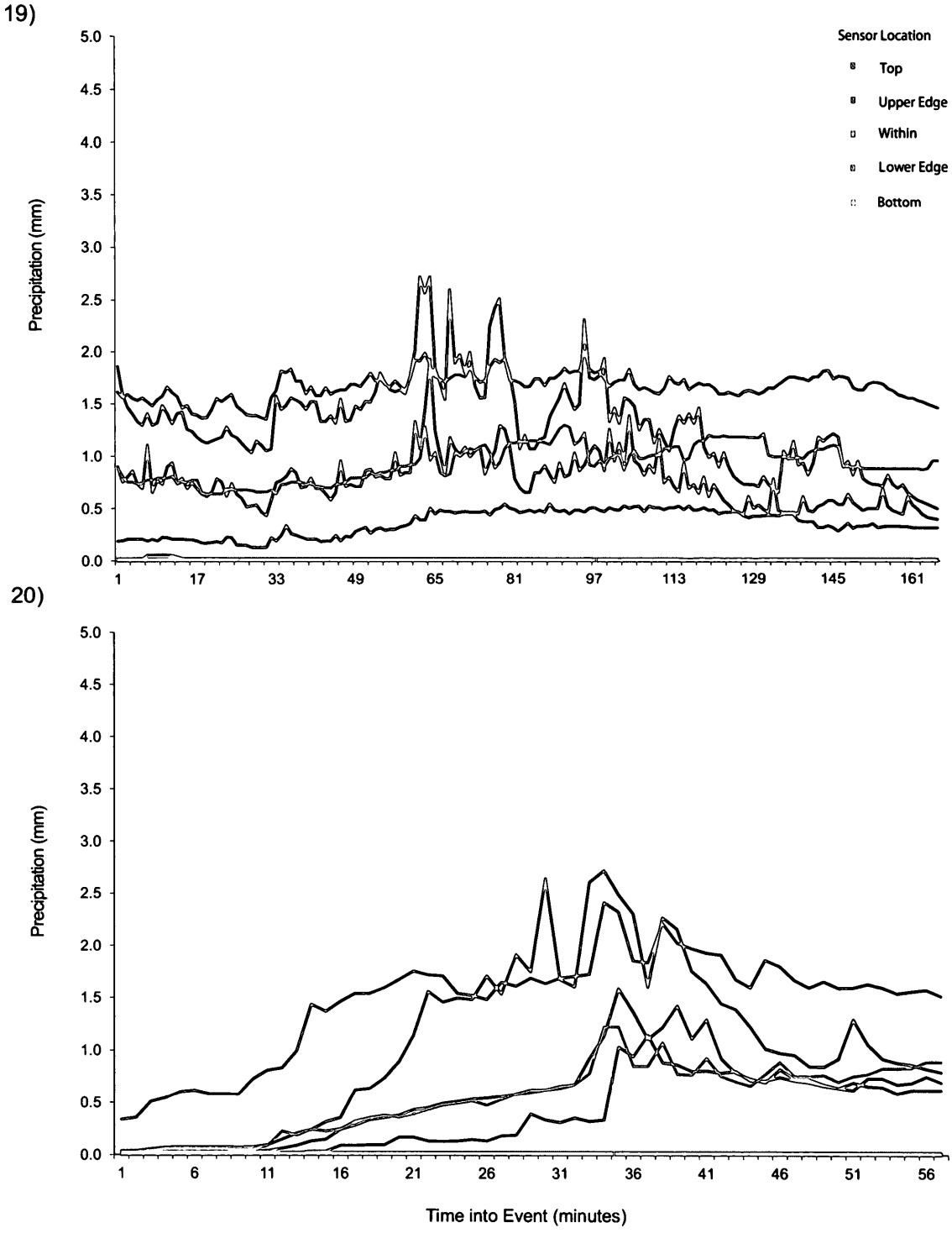

Figure 38. LWS wetness readings recorded for Event 19 (on July 25, 2009 from 14:45 to 17:30) and Event 20 (on July 26, 2009 from 11:14 to 12:10).

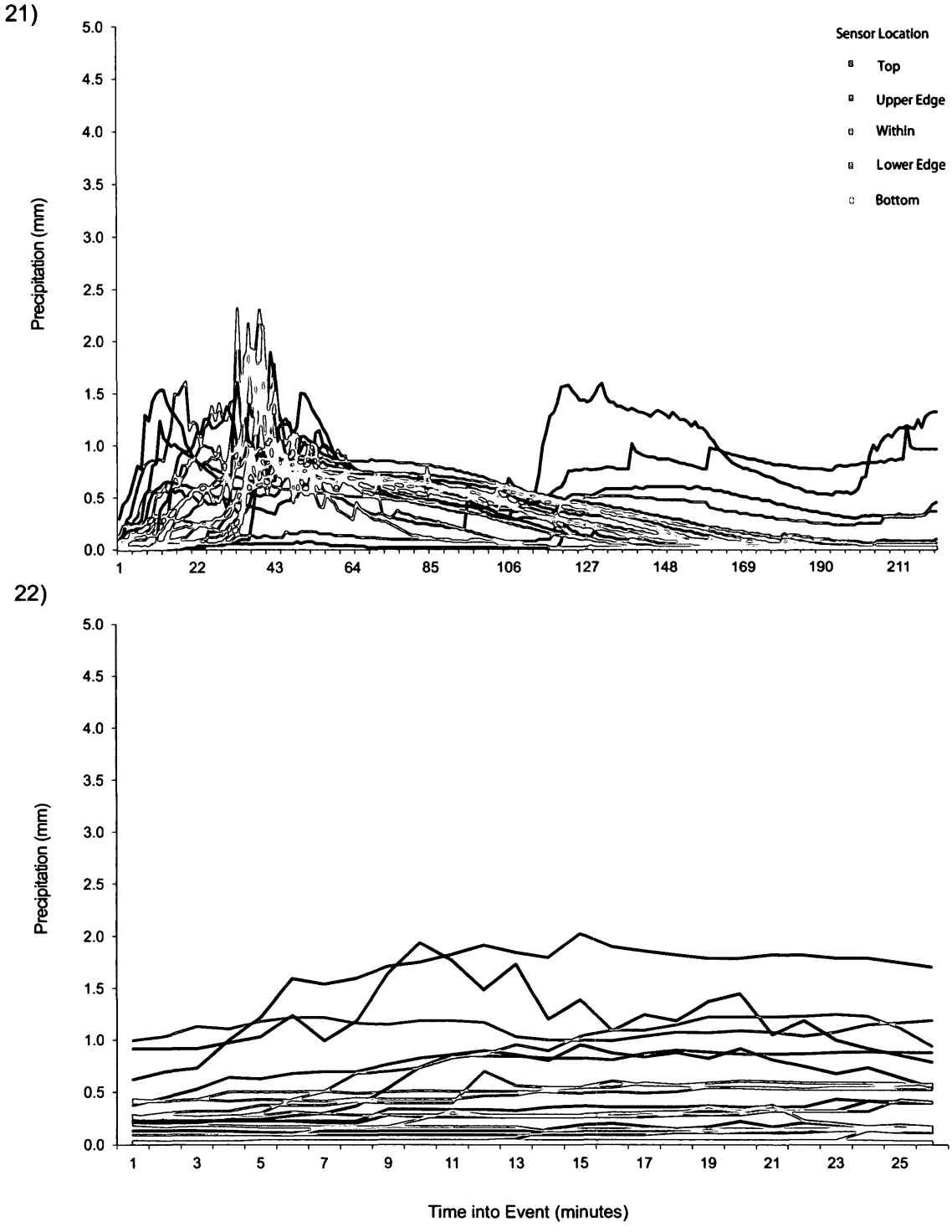

Figure 39. LWS wetness readings recorded for Event 21 (on July 26, 2009 from 15:10 to 18:50) and Event 22 (on July 26, 2009 from 22:30 to 22:55).

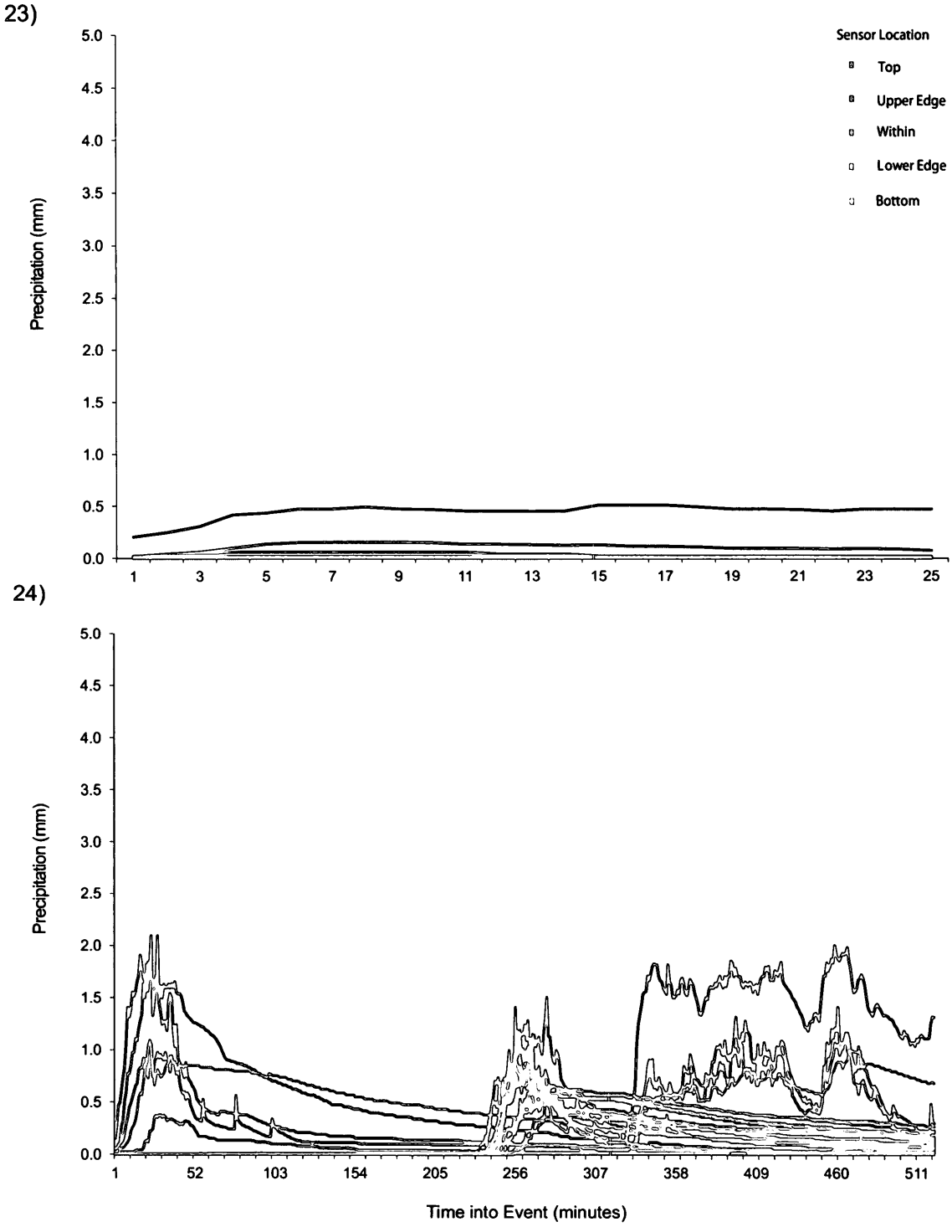

Figure 40. LWS wetness readings recorded for Event 23 (on July 28, 2009 from 04:48 to 05:12) and Event 24 (on July 29, 2009 from 02:29 to 11:10).

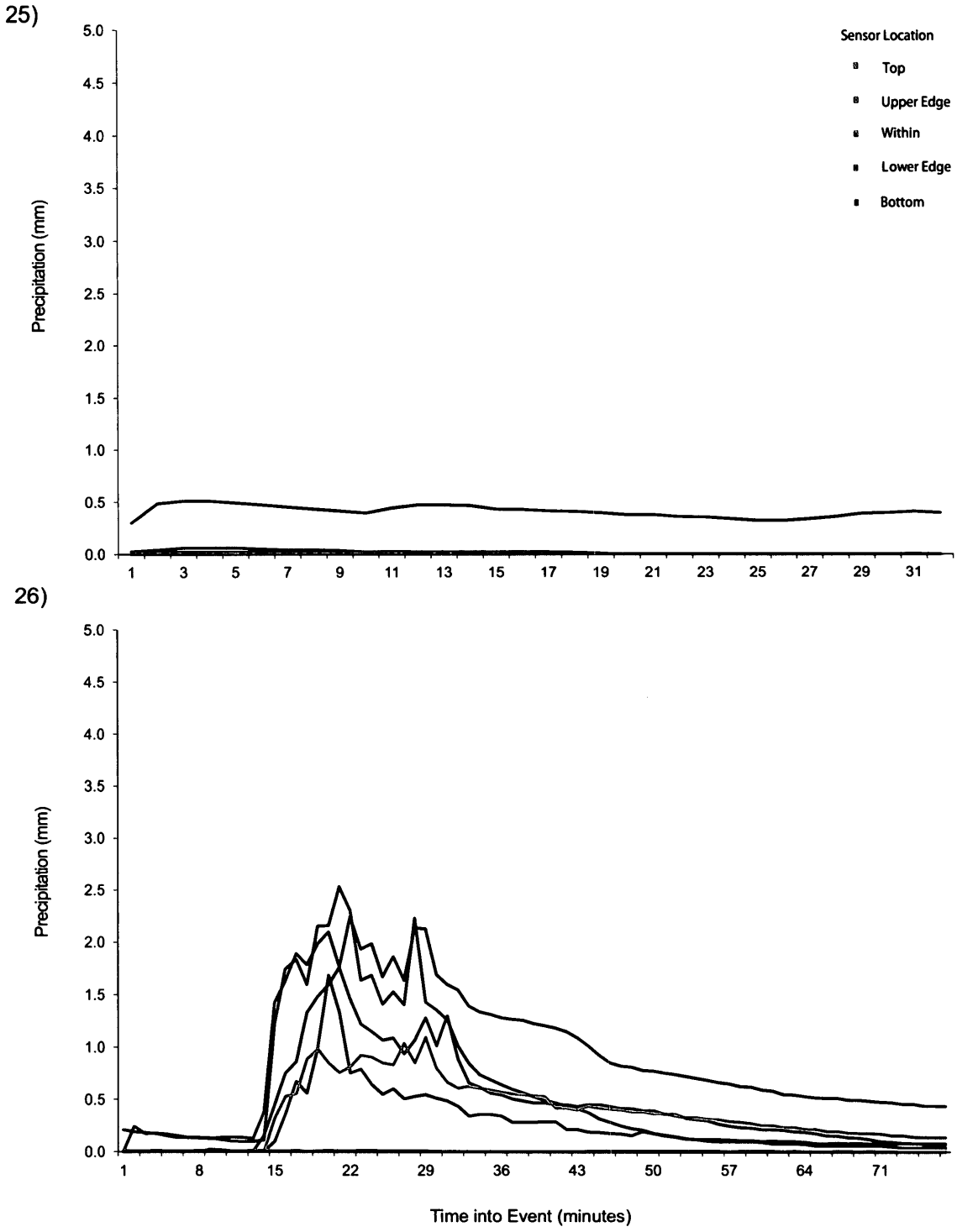

Figure 41. LWS wetness readings recorded for Event 25 (on August 2, 2009 from 05:57 to 06:28) and Event 26 (on August 4, 2009 from 13:16 to 14:32).

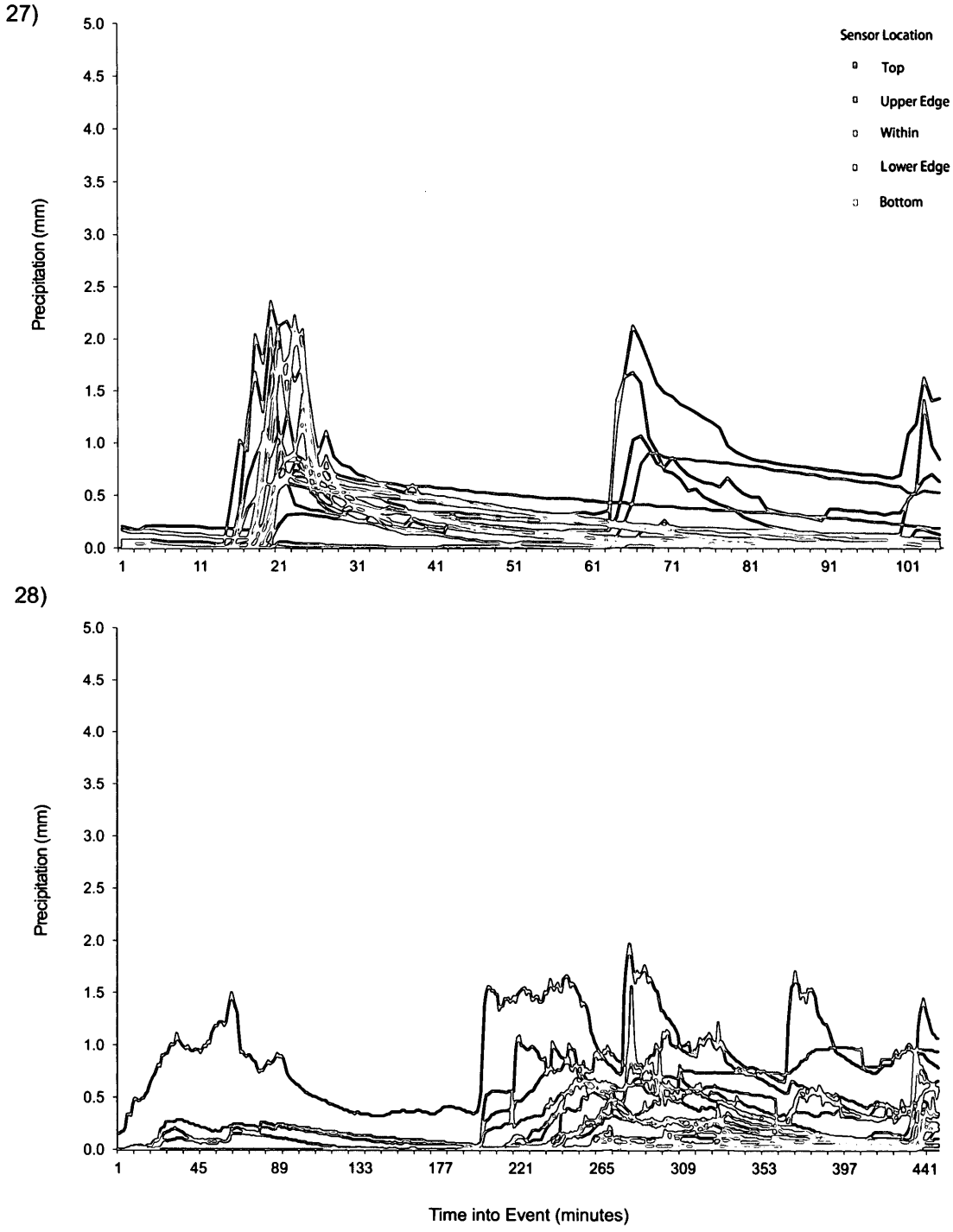

Figure 42. LWS wetness readings recorded for Event 27 (on August 4, 2009 from 20:11 to 21:55) and Event 28 (on August 8, 2009 from 18:03 to 01:30).

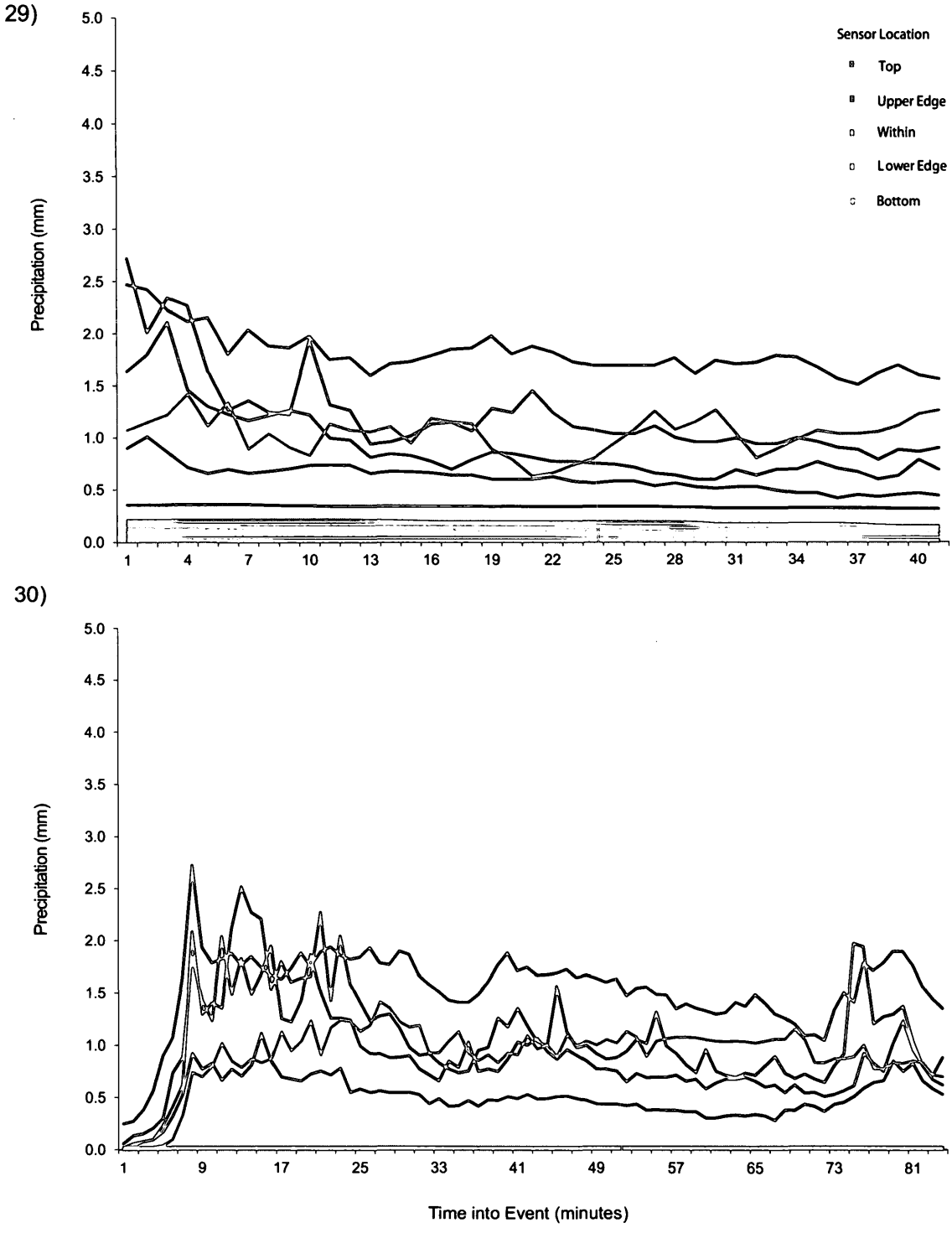

Figure 43. LWS wetness readings recorded for Event 29 (on August 9, 2009 from 11:15 to 11:55) and Event 30 (on August 9, 2009 from 20:12 to 21:35).

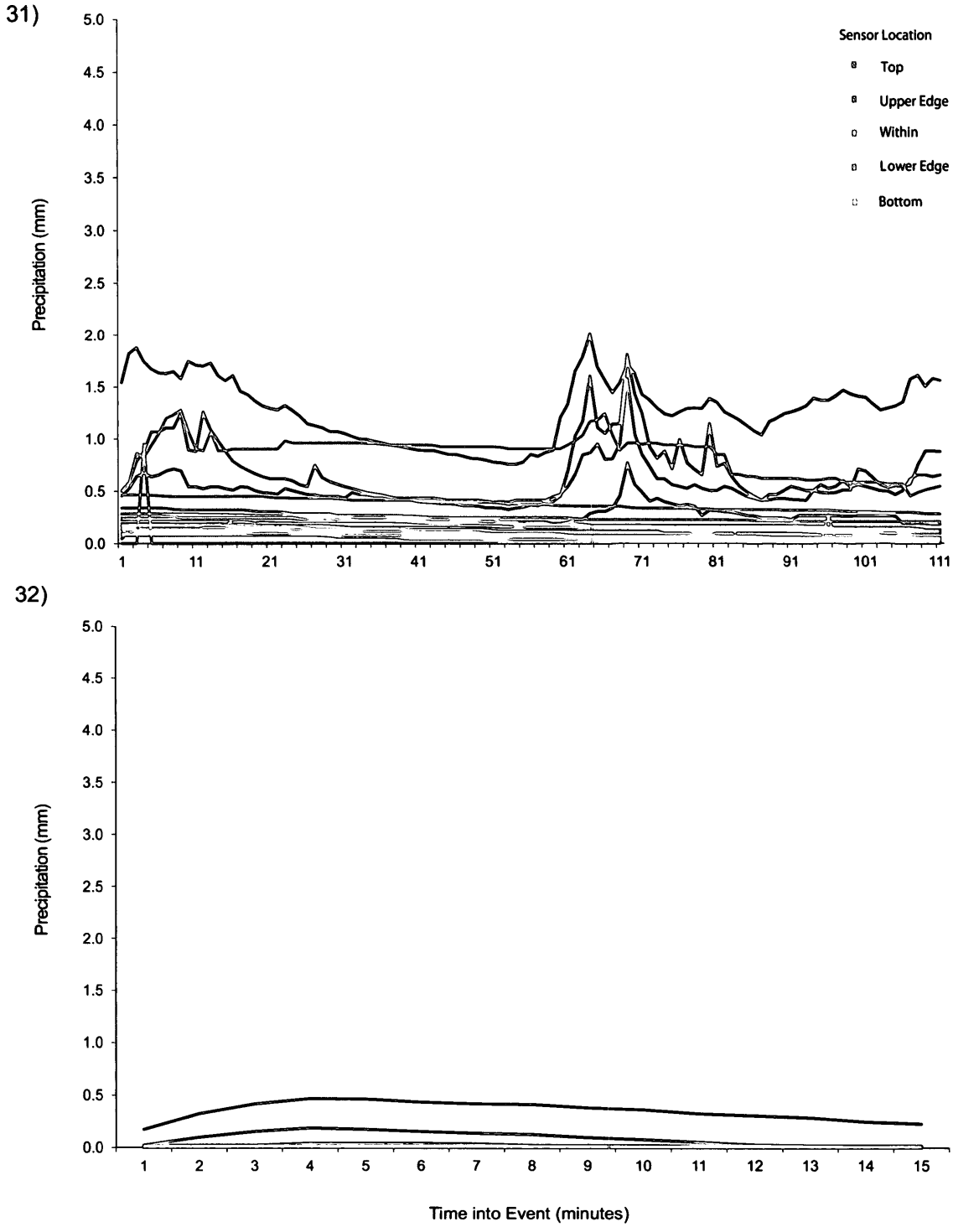

Figure 44. LWS wetness readings recorded for Event 31 (on August 10, 2009 from 03:40 to 05:30) and Event 32 (on August 10, 2009 from 17:04 to 17:18).

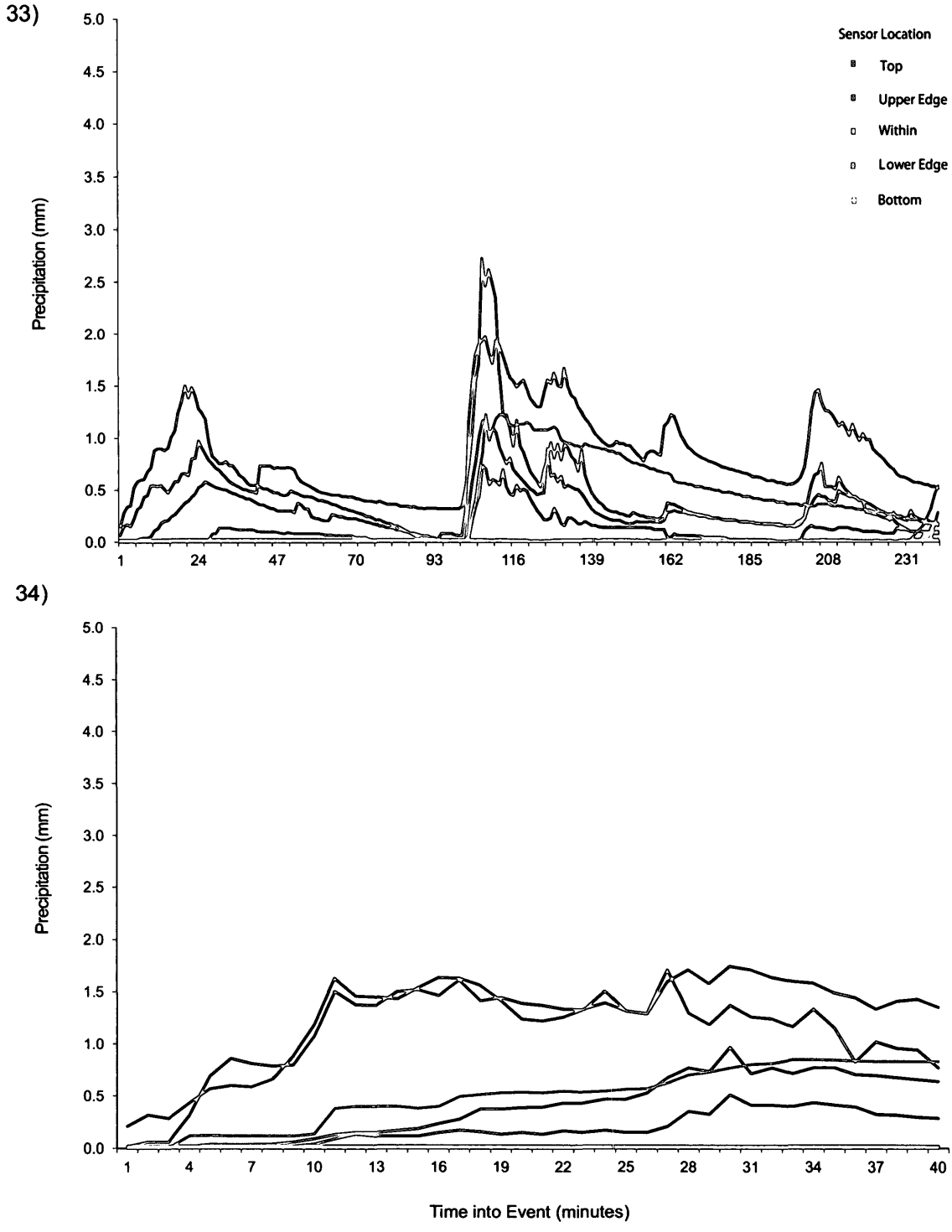

Figure 45. LWS wetness readings recorded for Event 33 (on August 11, 2009 from 13:41 to 17:40) and Event 34 (on August 12, 2009 from 12:51 to 13:30).

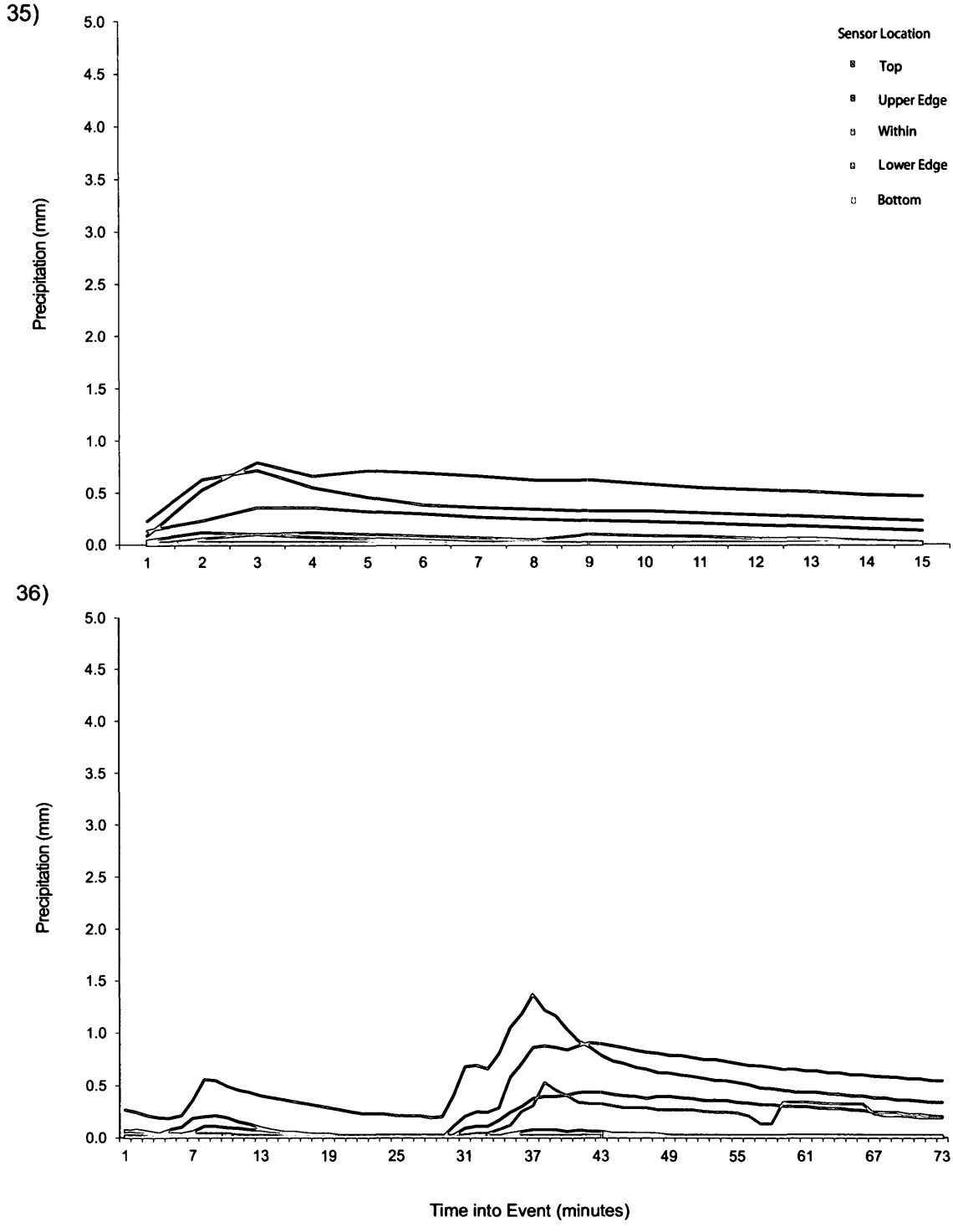

Figure 46. LWS wetness readings recorded for Event 35 (on August 17, 2009 from 15:28 to 15:42) and Event 36 (on August 18, 2009 from 03:53 to 05:05).

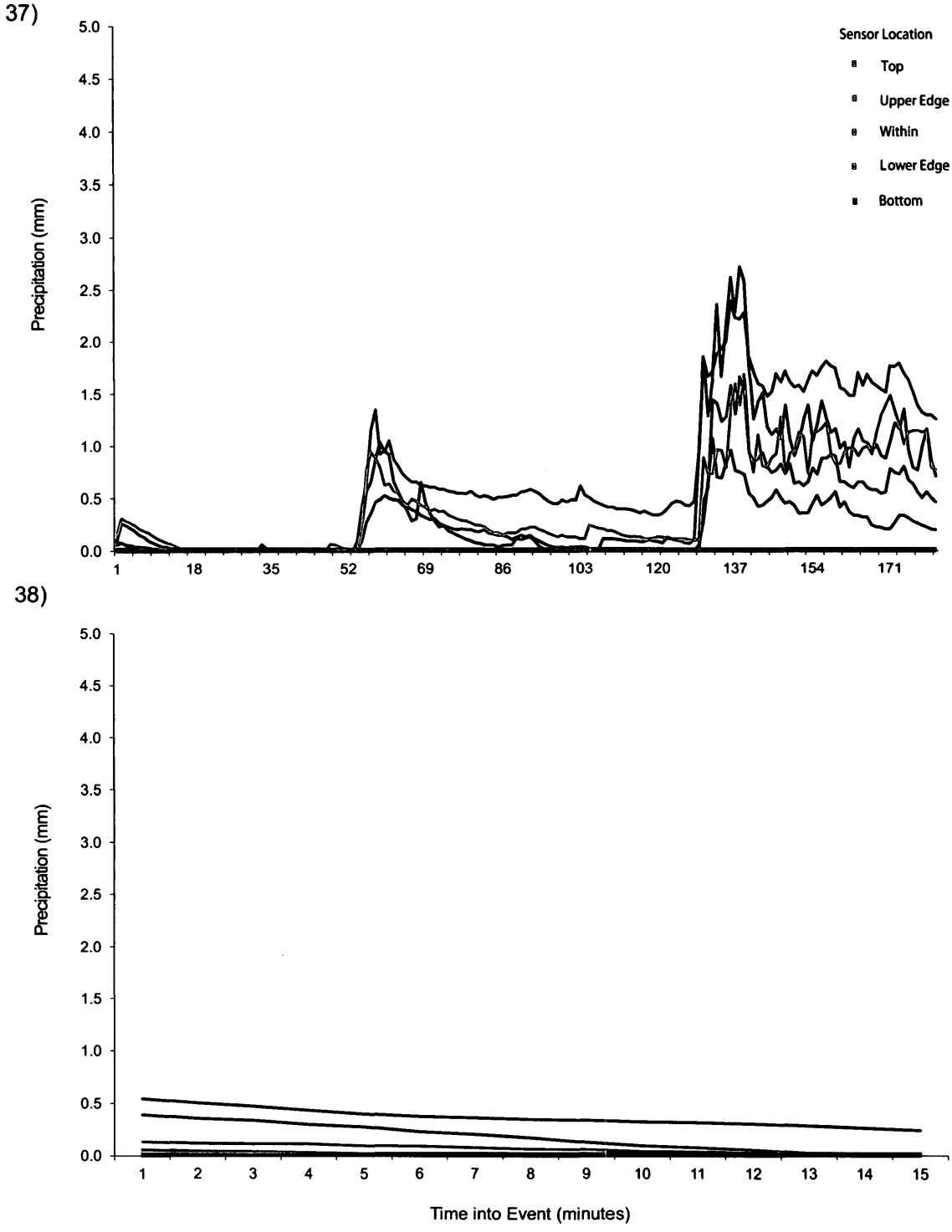

Figure 47. LWS wetness readings recorded for Event 37 (on August 20, 2009 from 16:50 to 19:50) and Event 38 (on August 21, 2009 from 13:10 to 13:24).

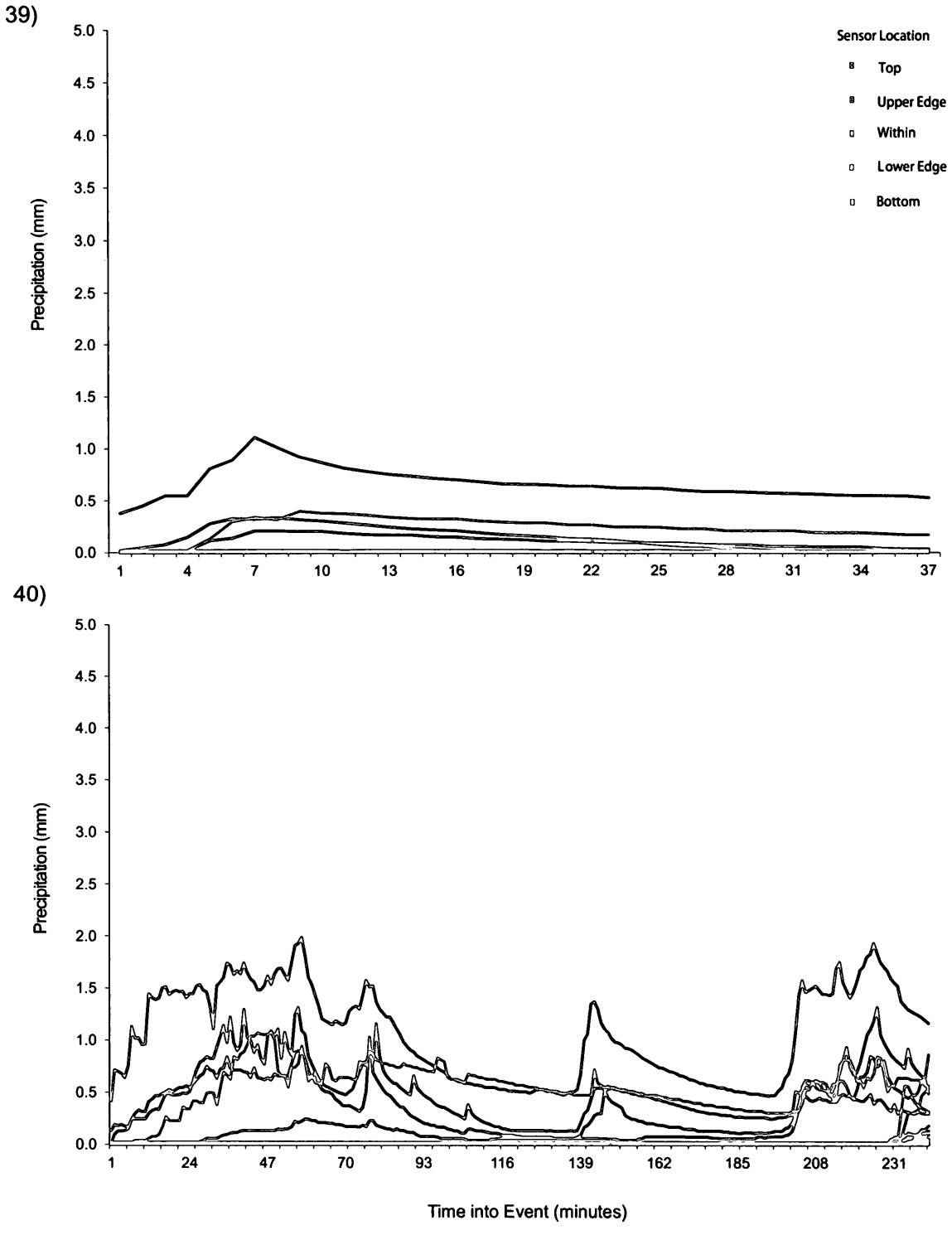

Figure 48. LWS wetness readings recorded for Event 39 (on August 22, 2009 from 13:42 to 14:18) and Event 40 (on August 26, 2009 from 05:20 to 09:20).

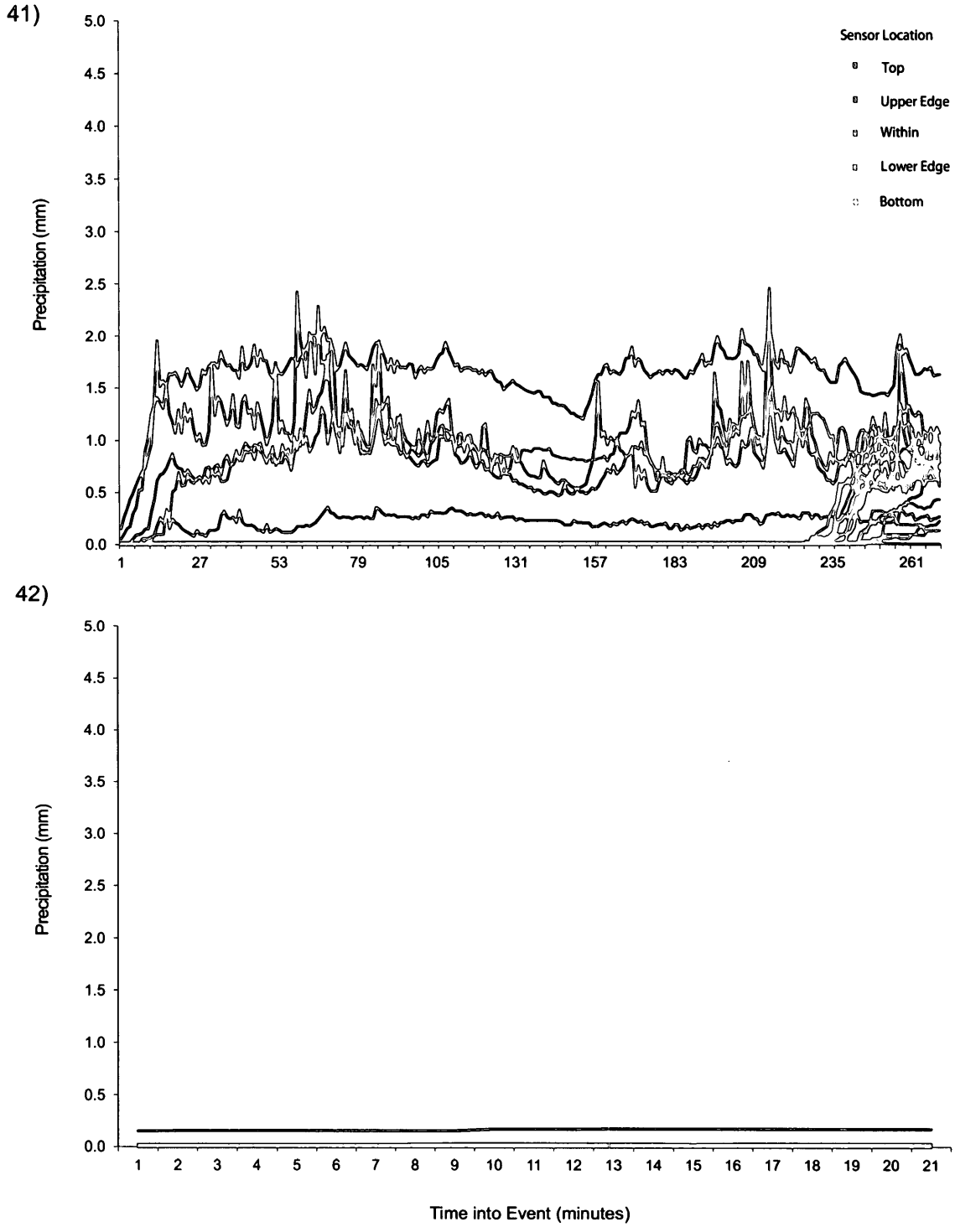

Figure 49. LWS wetness readings recorded for Event 41 (on August 28, 2009 to August 29, 2009 from 23:26 to 03:55) and Event 42 (on September 5, 2009 from 06:55 to 07:15).

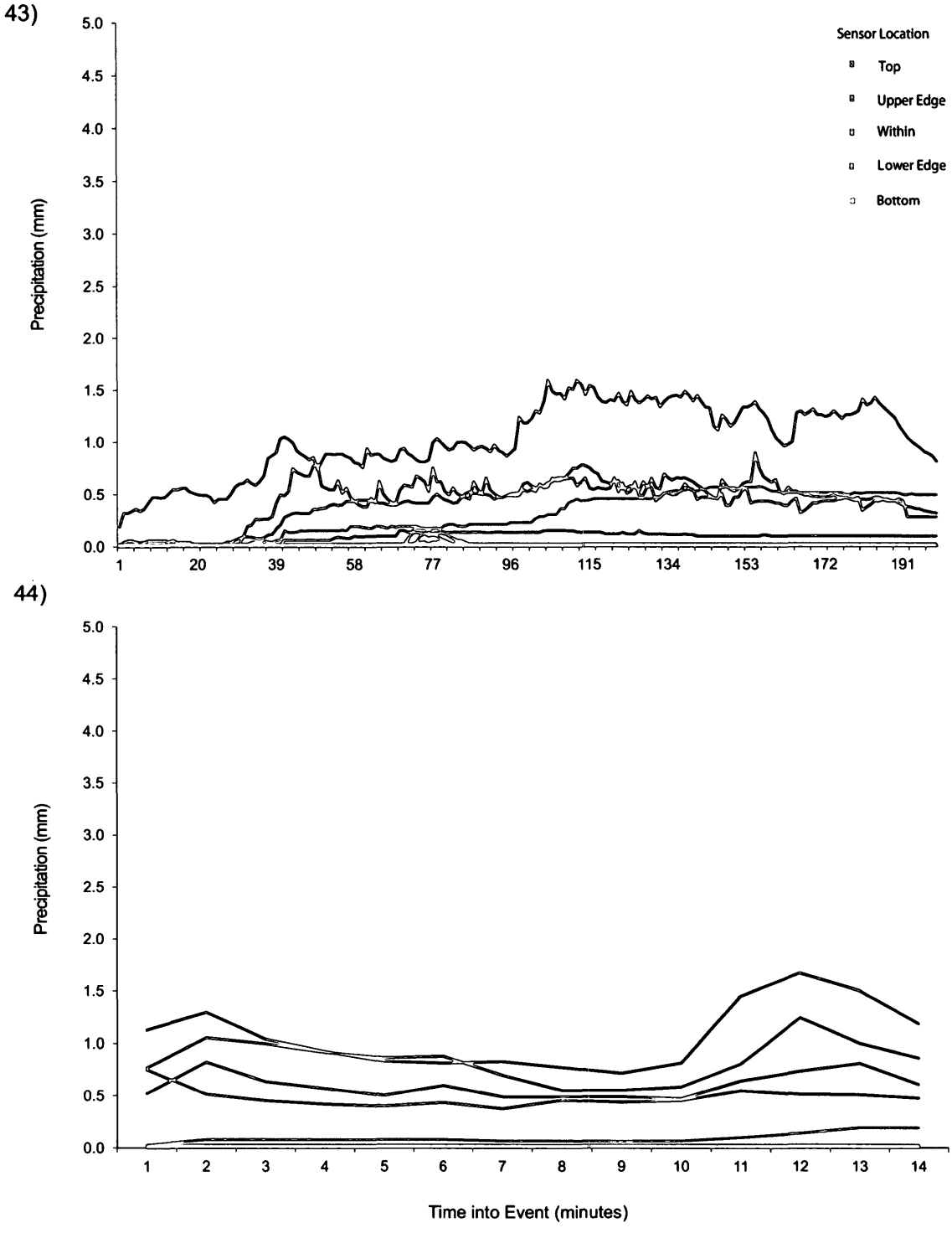

Figure 50. LWS wetness readings recorded for Event 43 (on September 21, 2009 from 15:57 to 19:15) and Event 44 (on September 23, 2009 from 15:27 to 15:40).

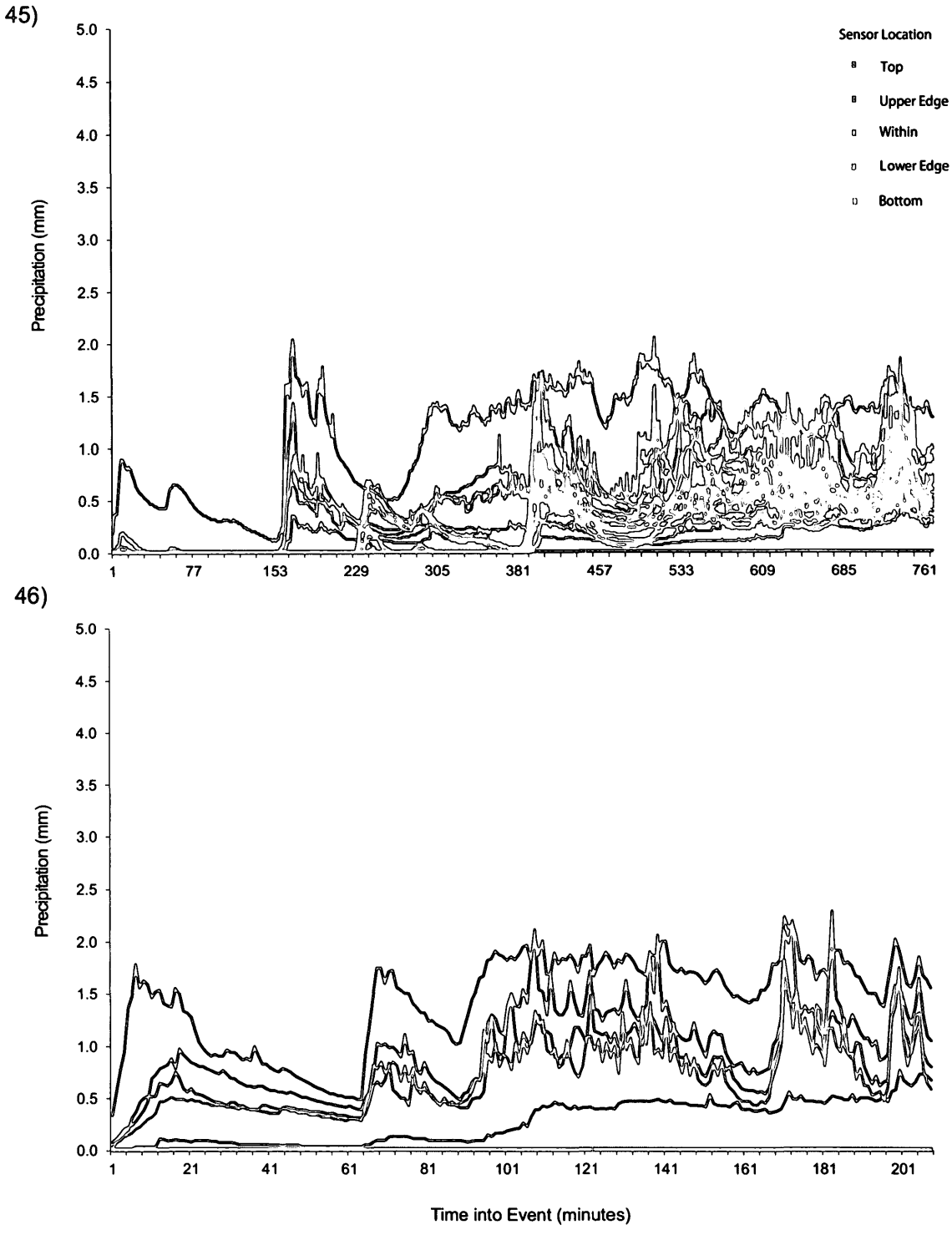

Figure 51. LWS wetness readings recorded for Event 45 (on September 26, 2009 to September 27, 2009 from 15:08 to 03:55) and Event 46 (on September 28, 2009 from 06:38 to 10:05).

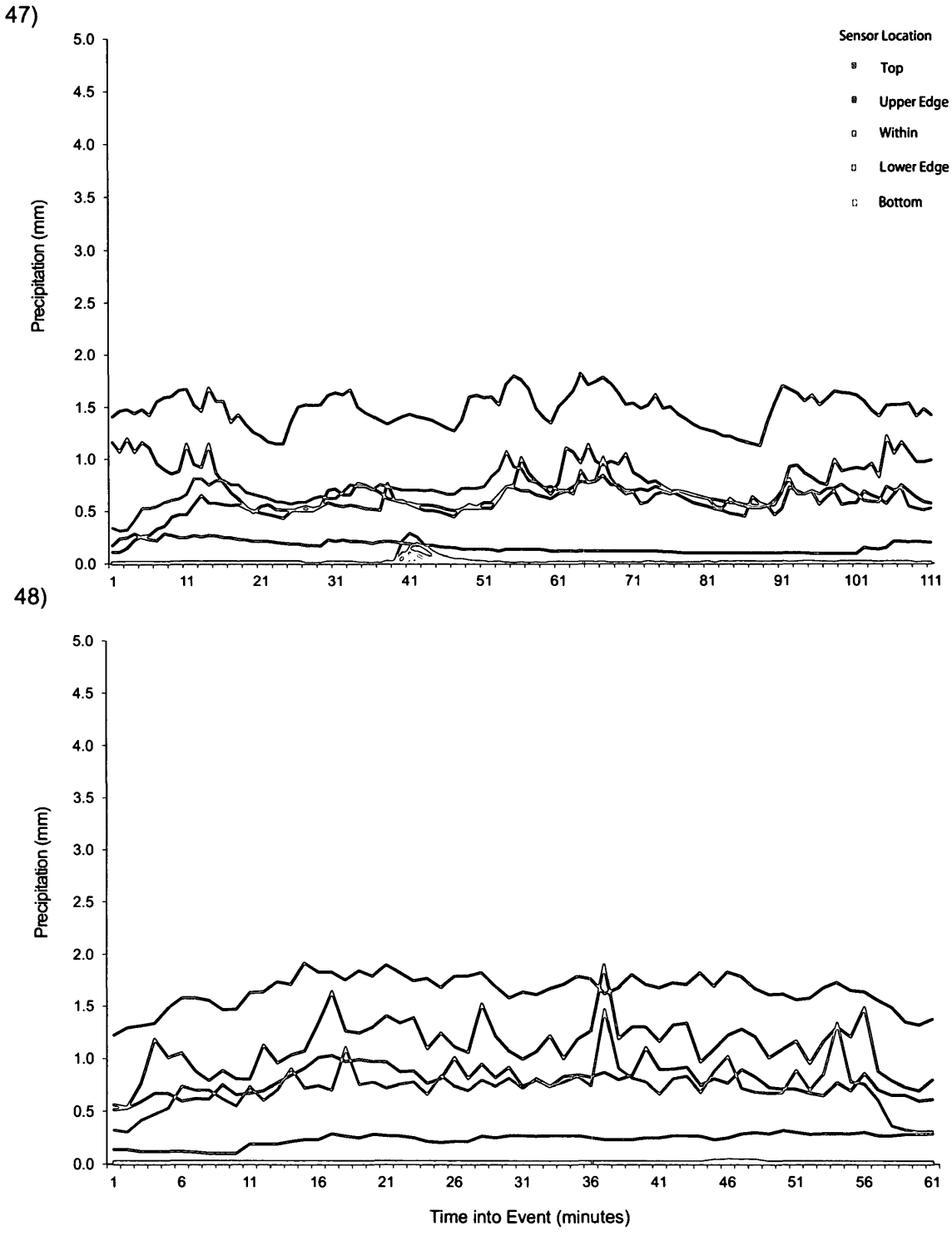

Figure 52. LWS wetness readings recorded for Event 47 (on September 28, 2009 from 17:15 to 19:05) and Event 48 (on September 29, 2009 from 03:25 to 04:25).

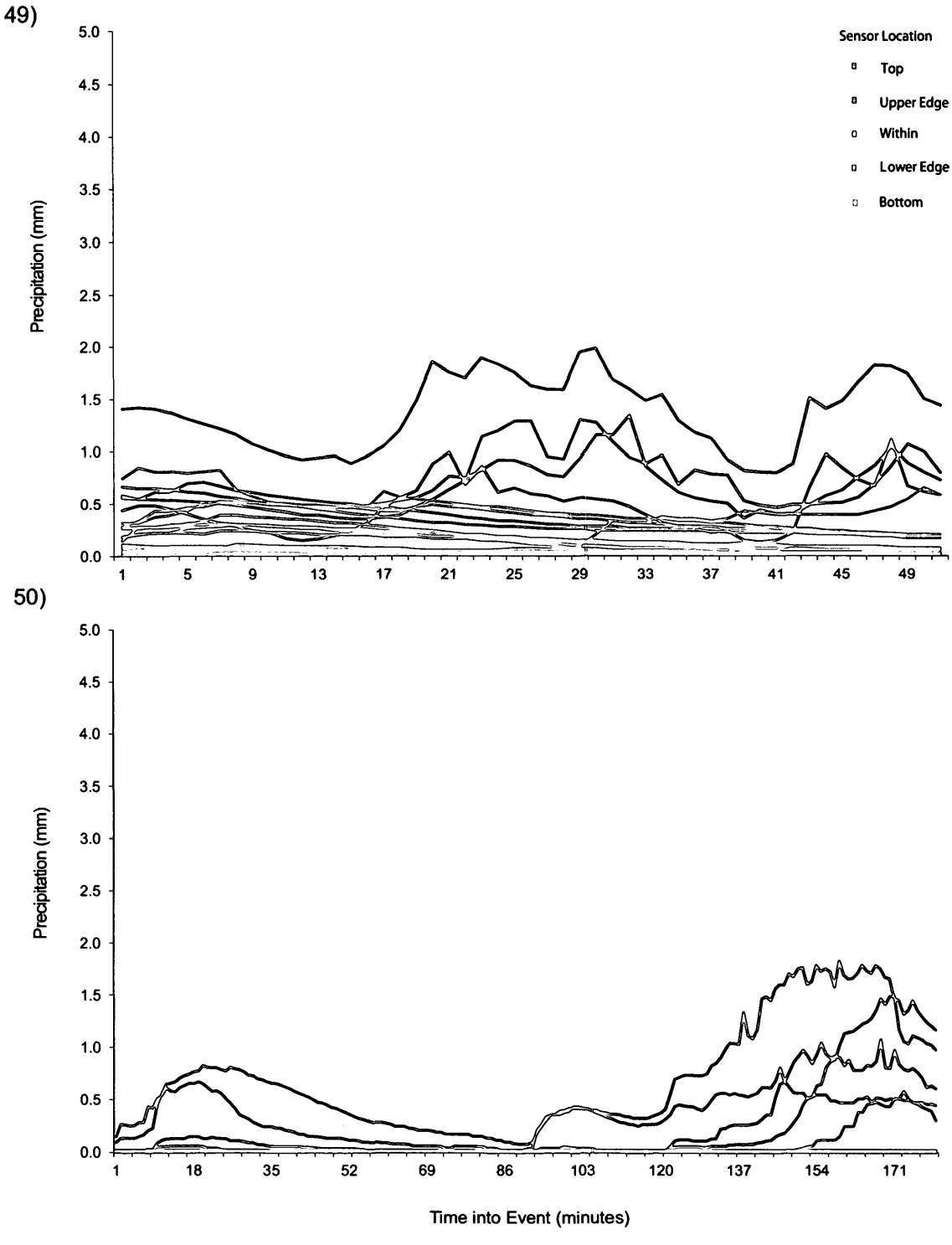

Figure 53. LWS wetness readings recorded for Event 49 (on September 29, 2009 from 11:00 to 11:50) and Event 50 (on September 29, 2009 from 17:41 to 20:40).

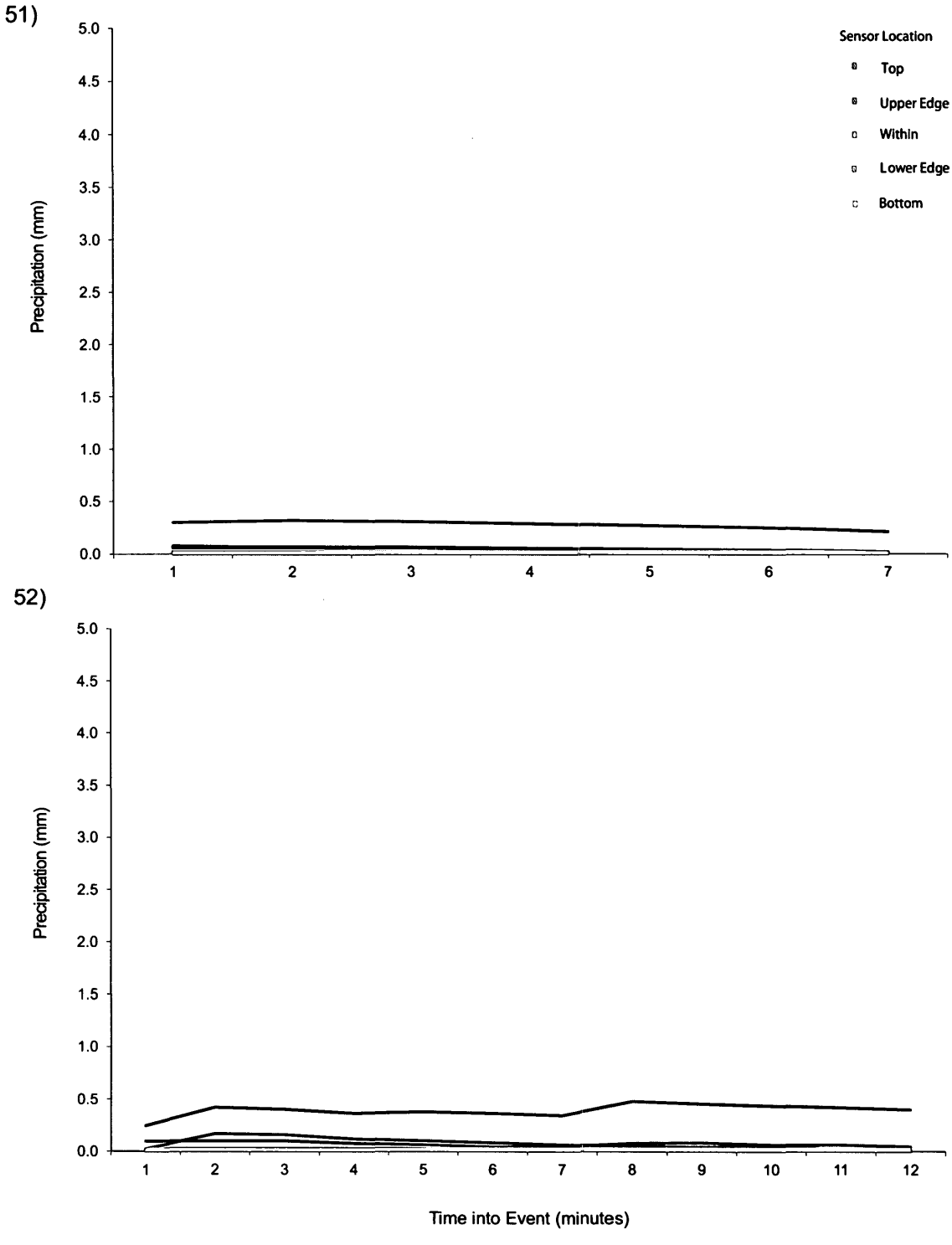

Figure 54. LWS wetness readings recorded for Event 51 (on September 30, 2009 from 14:29 to 14:35) and Event 52 (on October 1, 2009 from 13:57 to 14:08).

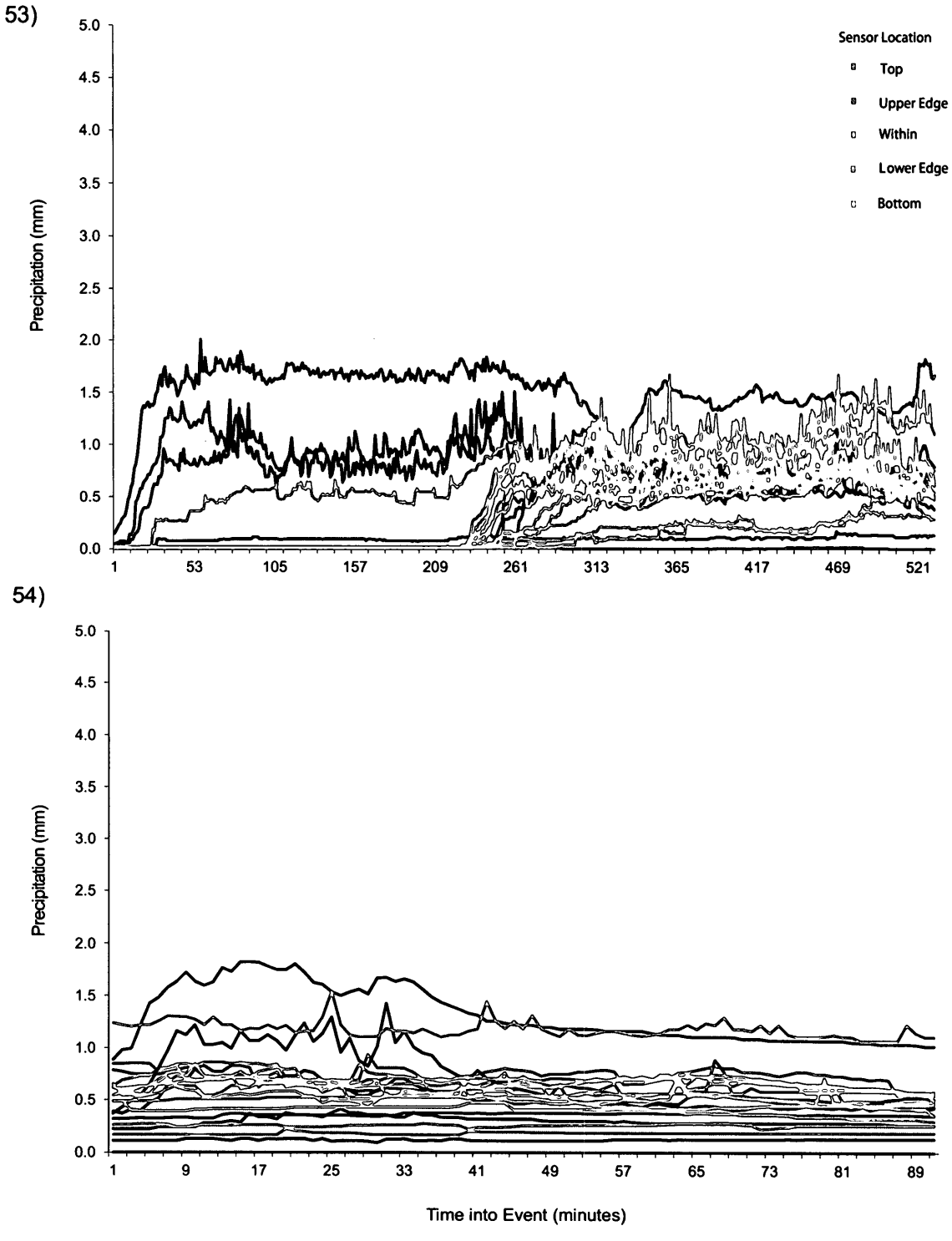

Figure 55. LWS wetness readings recorded for Event 53 (on October 2, 2009 from 11:45 to 20:35) and Event 54 (on October 2, 2009 from 22:25 to 23:55).

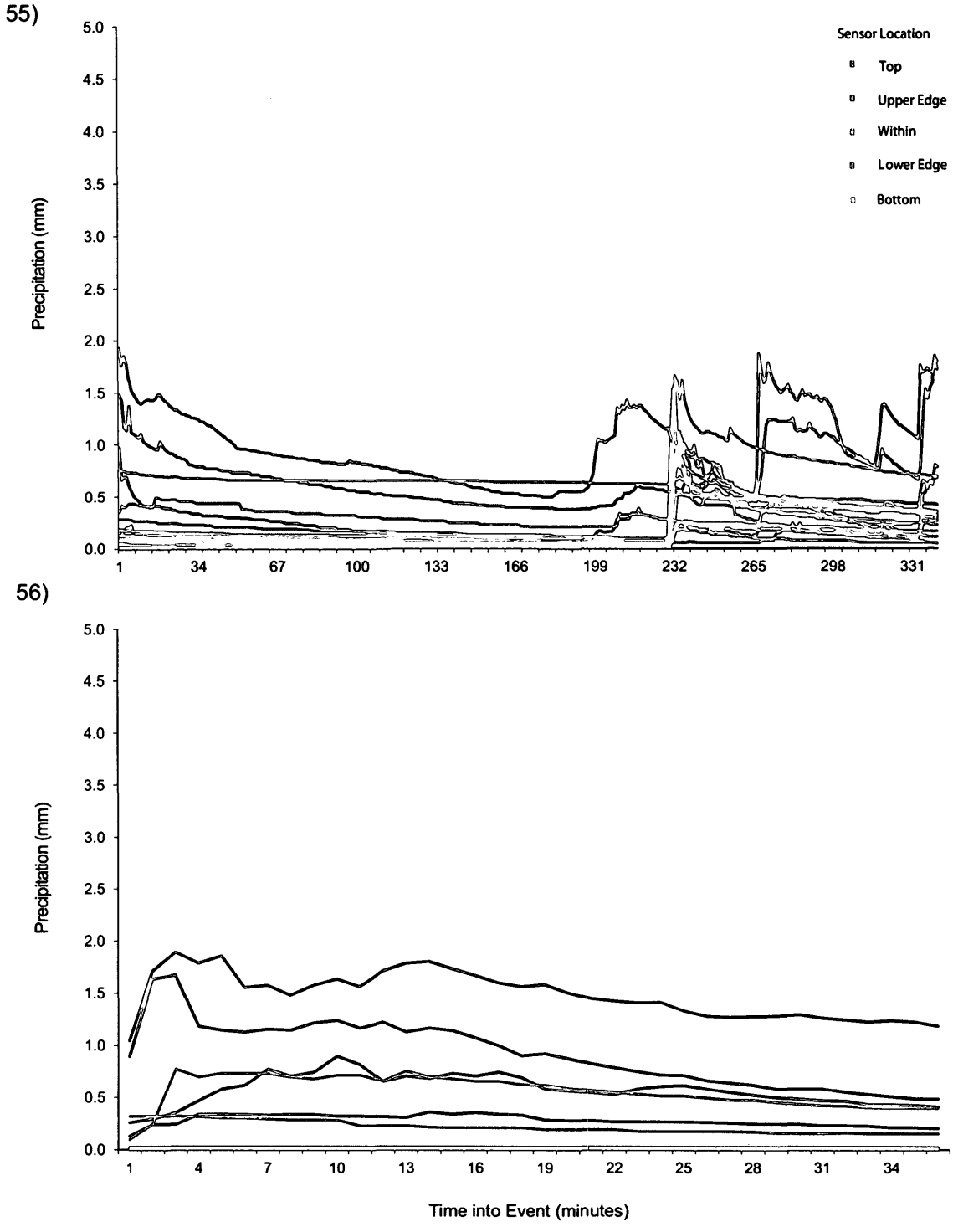

Figure 56. LWS wetness readings recorded for Event 55 (on October 3, 2009 06:45 to 12:25) and Event 56 (on October 3, 2009 fro 17:50 to 18:25).

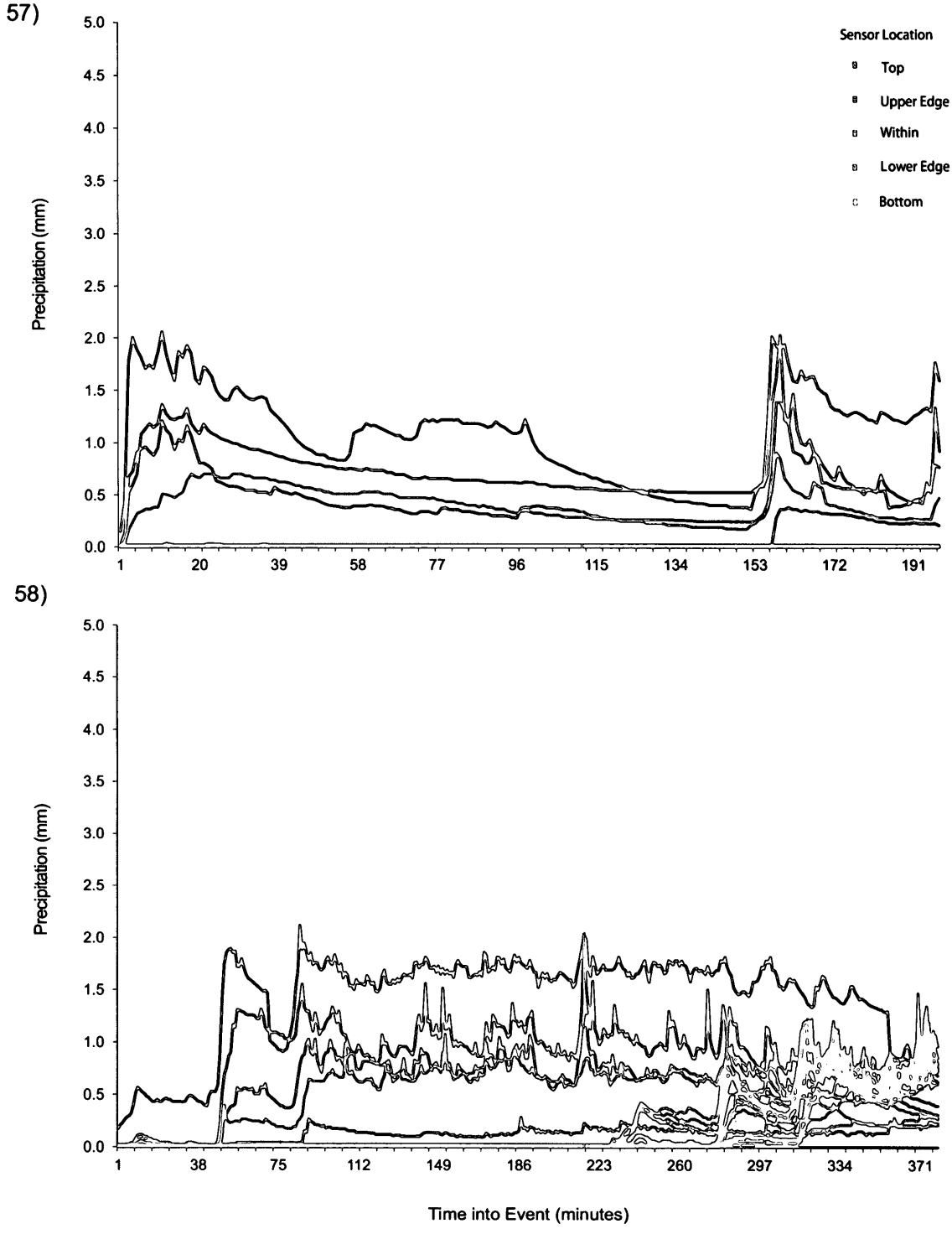

Figure 57. LWS wetness readings recorded for Event 57 (on October 4, 2009 from 12:49 to 16:05) and Event 58 (on October 6, 2009 to October 7, 2009 from 19:02 to 01:20).

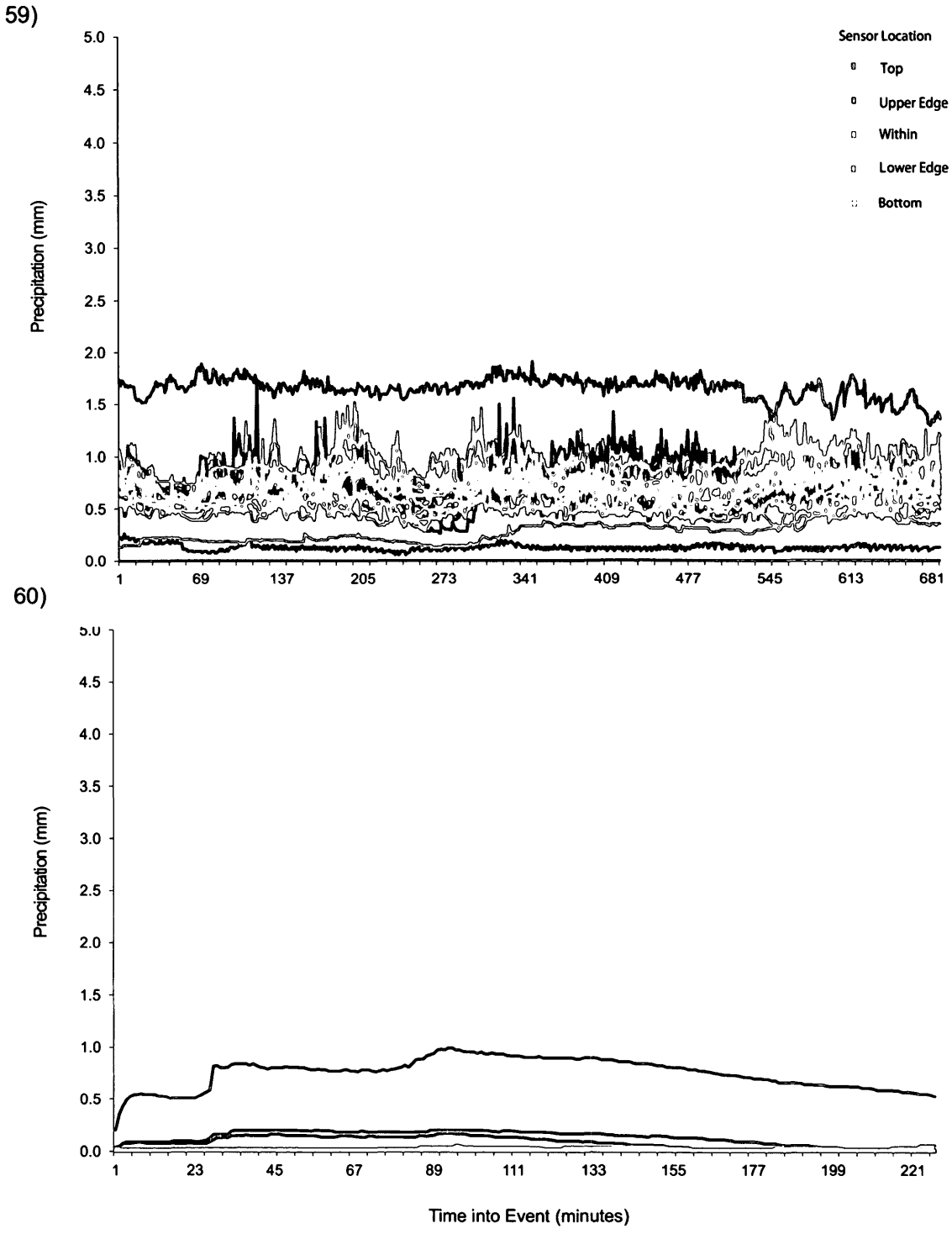

Figure 58. LWS wetness readings recorded for Event 59 (on October 9, 2009 to October 10, 2009 from 12:49 to 00:15) and Event 60 (on October 13, 2009 from 04:35 to 08:21).

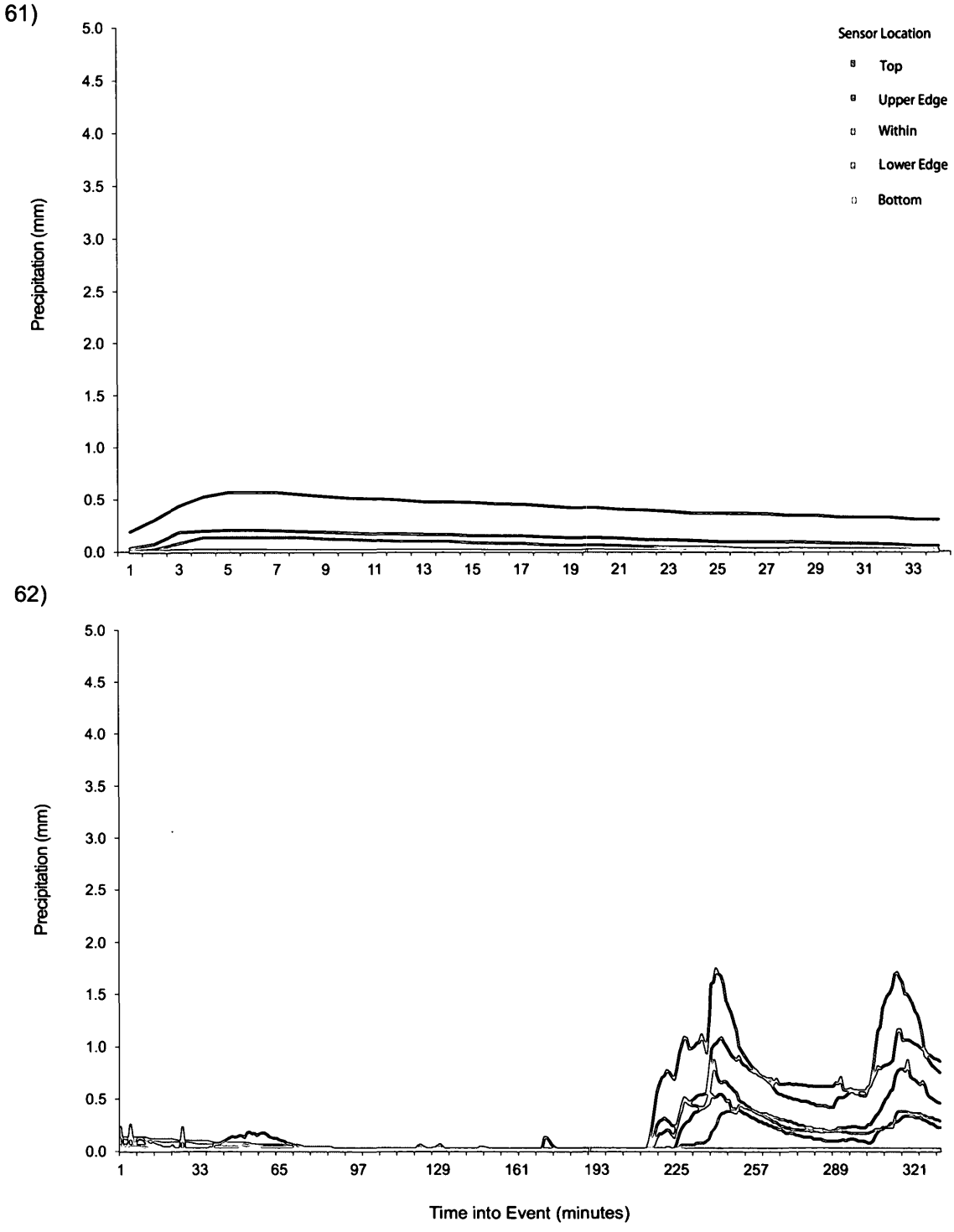

Figure 59. LWS wetness readings recorded for Event 61 (on October 20, 2009 from 21:39 to 22:12) and Event 62 (on October 22, 2009 from 10:25 to 15:55).

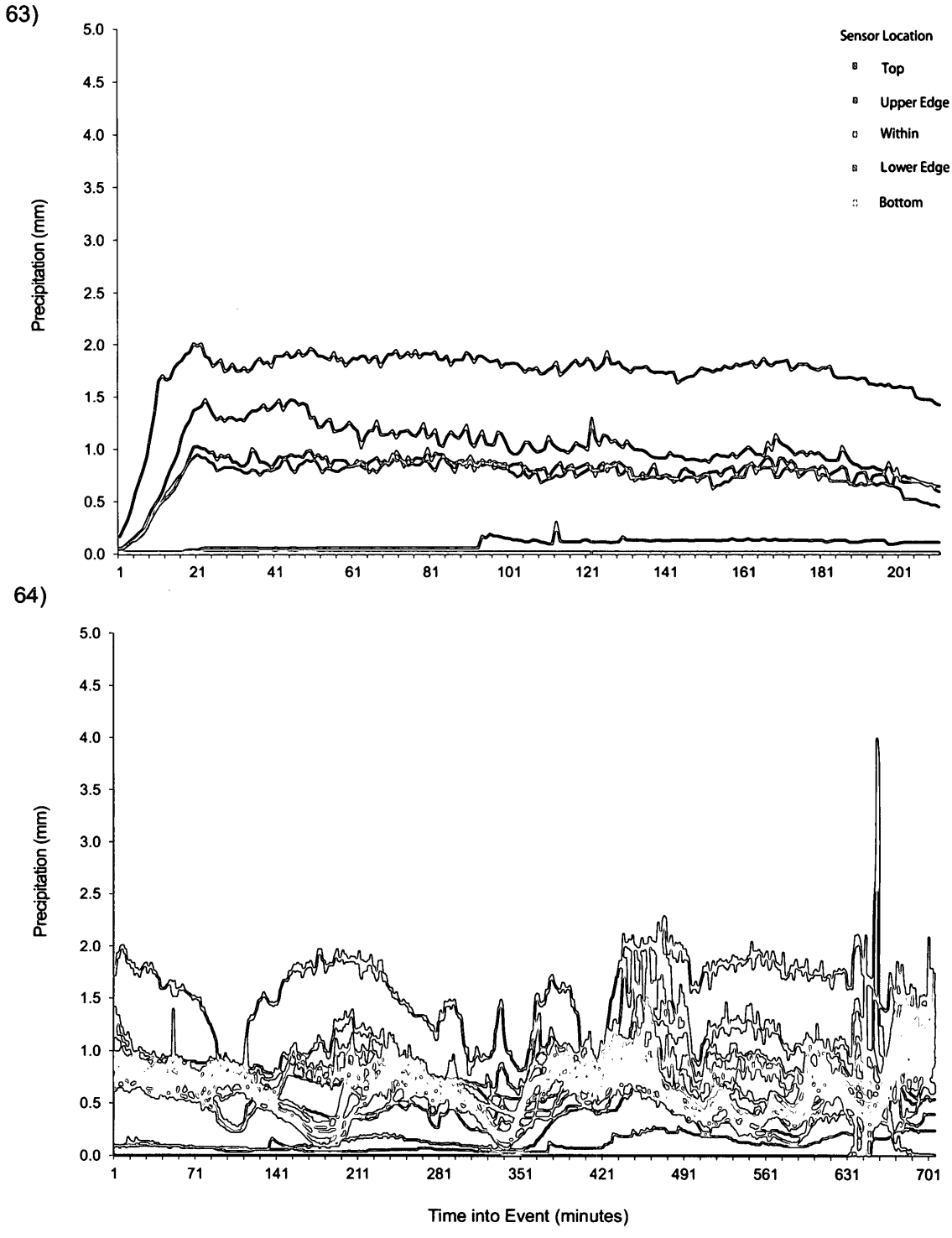

Figure 60. LWS wetness readings recorded for Event 63 (on October 23, 2009 from 06:15 to 09:45) and Event 64 (on October 23, 2009 from 11:20 to 23:05).

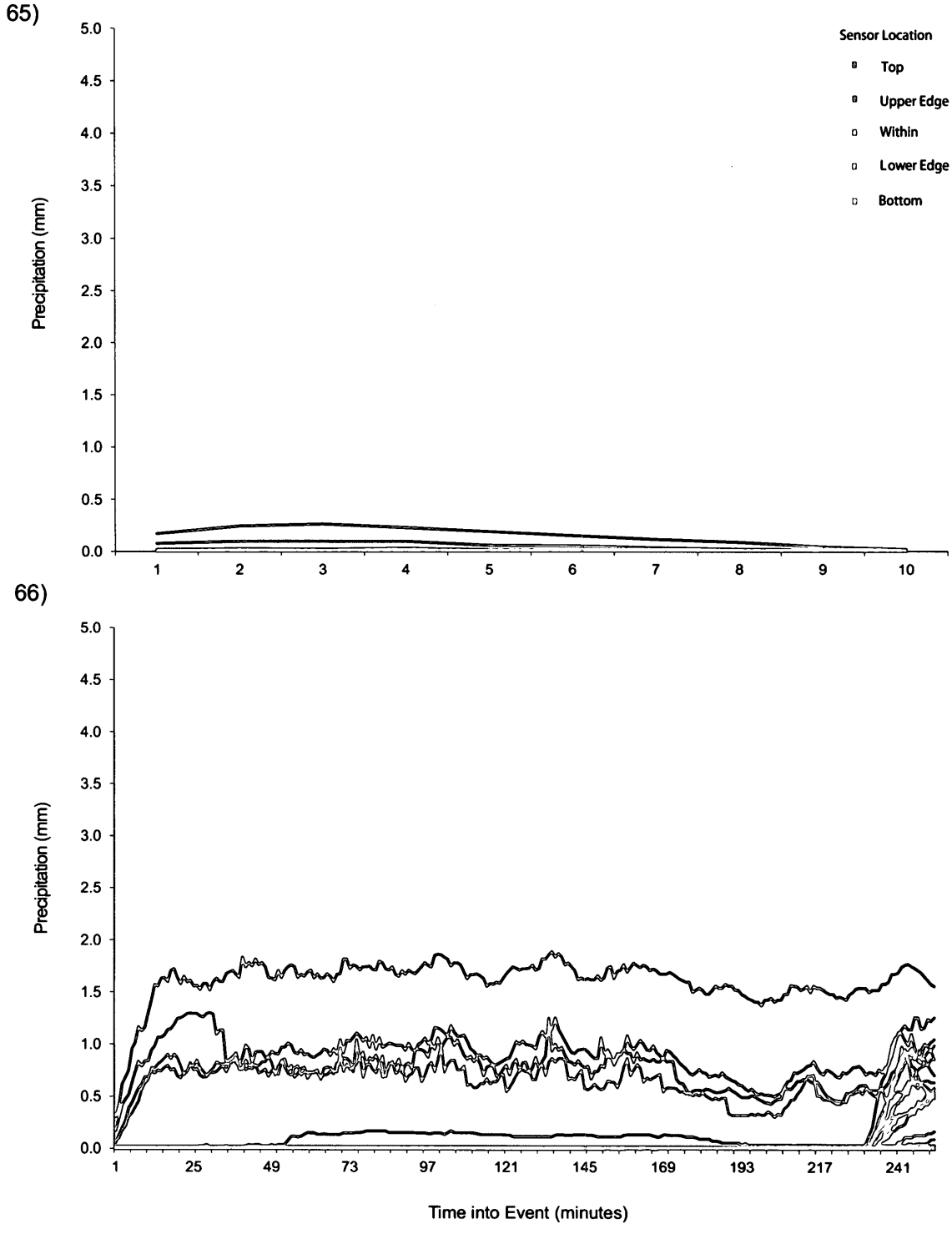

Figure 61. LWS wetness readings recorded for Event 65 (on October 24, 2009 from 15:49 to 15:58) and Event 66 (on October 28, 2009 from 00:39 to 04:50).

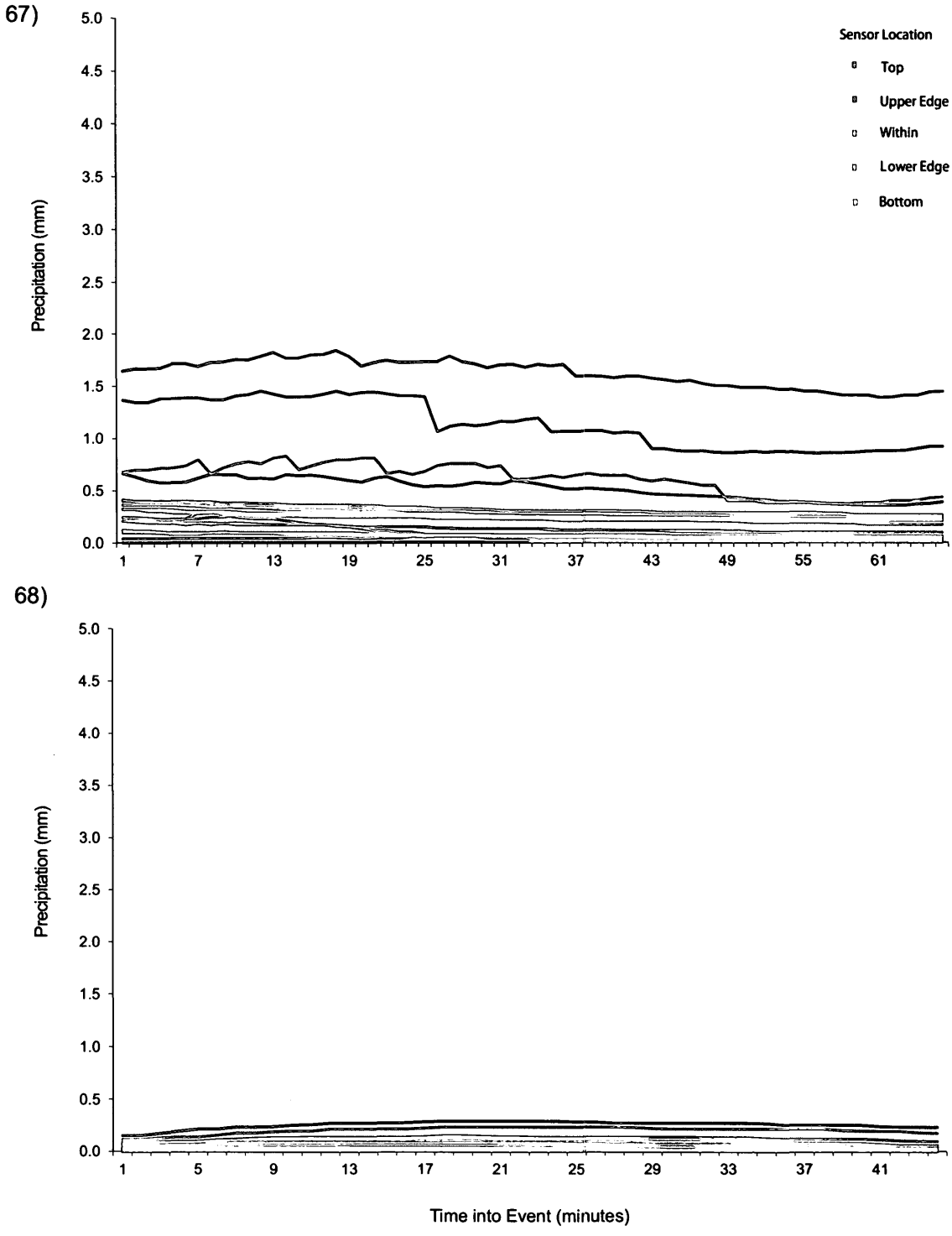

Figure 62. LWS wetness readings recorded for Event 67 (on October 28, 2009 from 09:00 to 10:05) and Event 68 (on October 29, 2009 from 01:31 to 02:14).

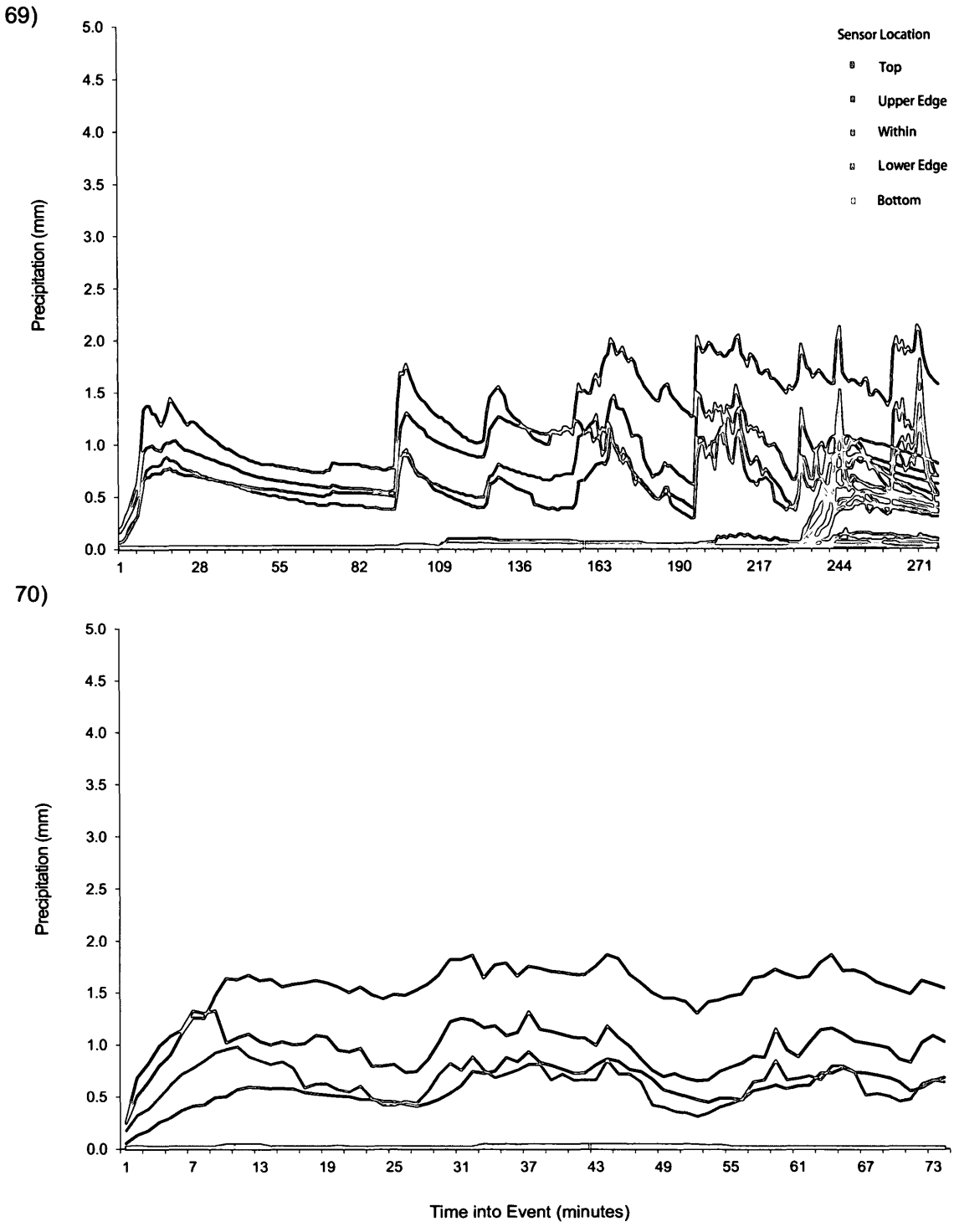

Figure 63. LWS wetness readings recorded for Event 69 (on October 30, 2009 from 08:24 to 13:00) and Event 70 (on October 31, 2009 from 02:25 to 03:38).

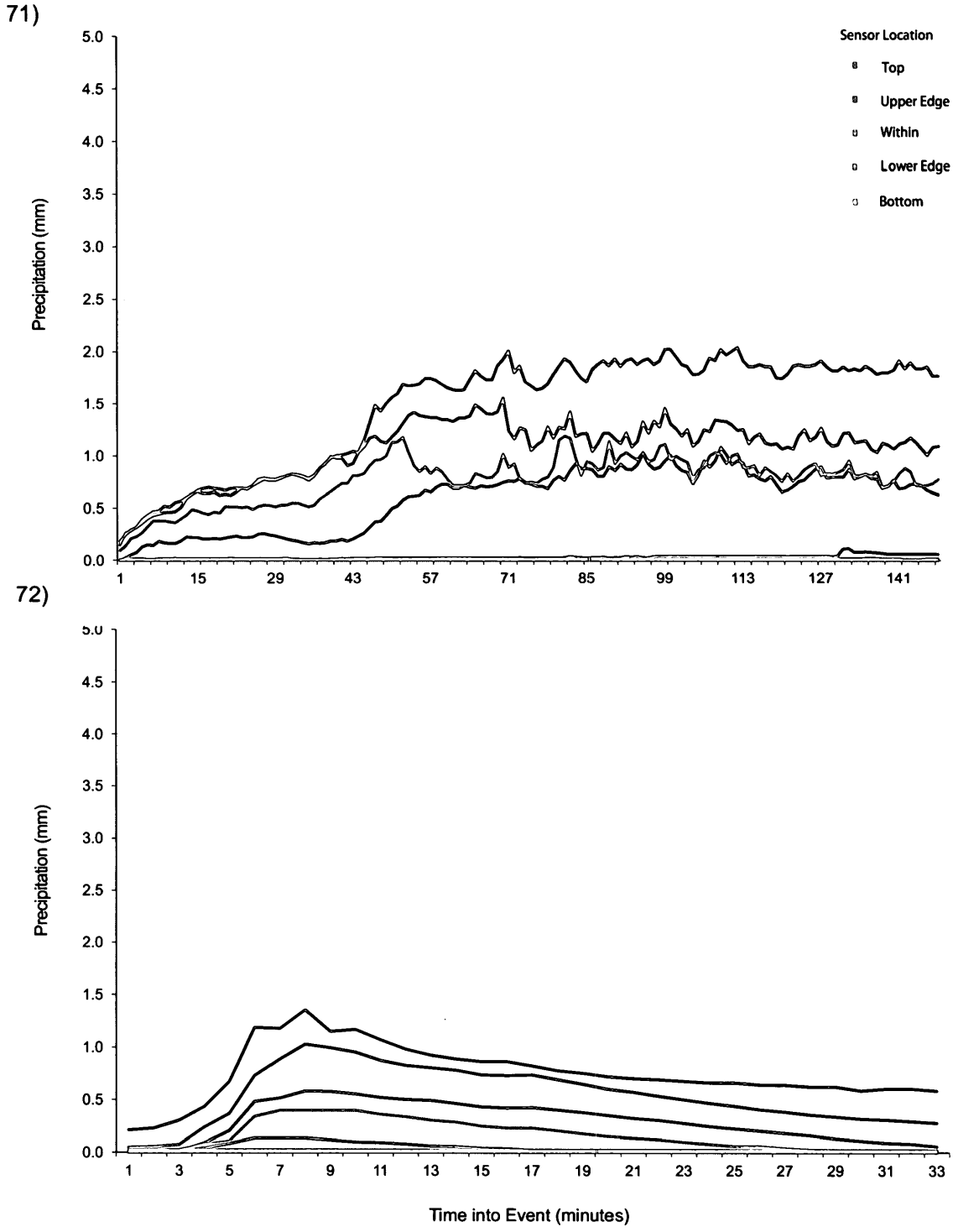

Figure 64. LWS wetness readings recorded for Event 71 (on November 2, 2009 from 17:03 to 19:30) and Event 72 (on November 3, 2009 from 14:46 to 15:18).

73)

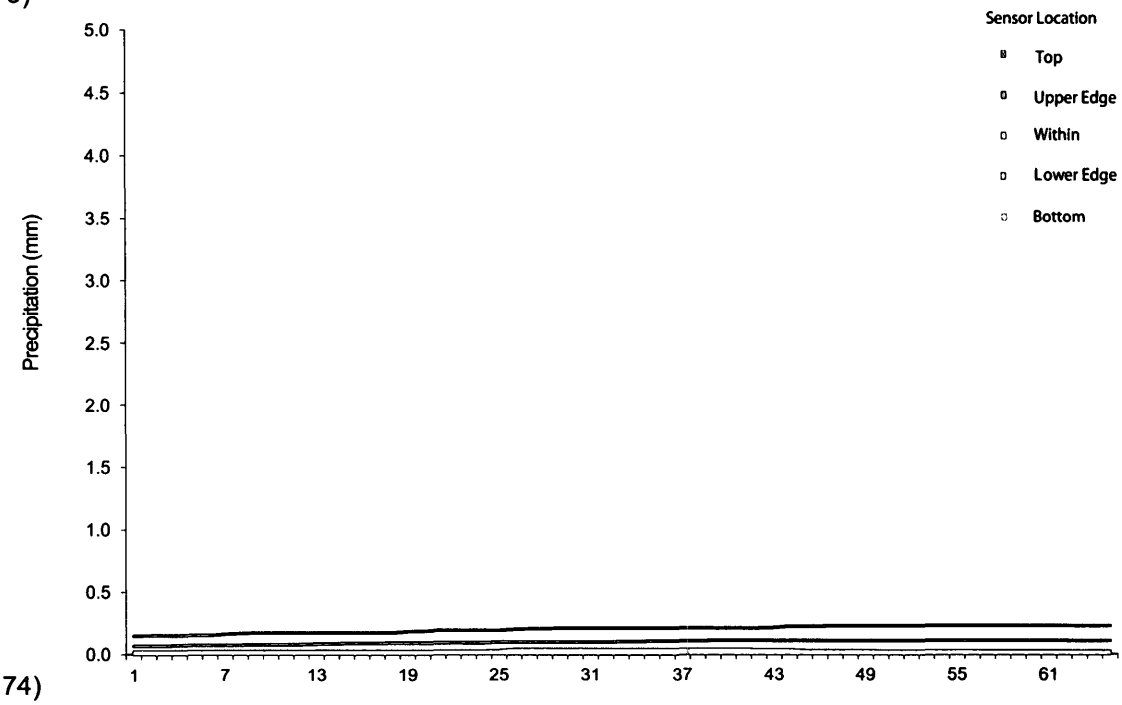

74)

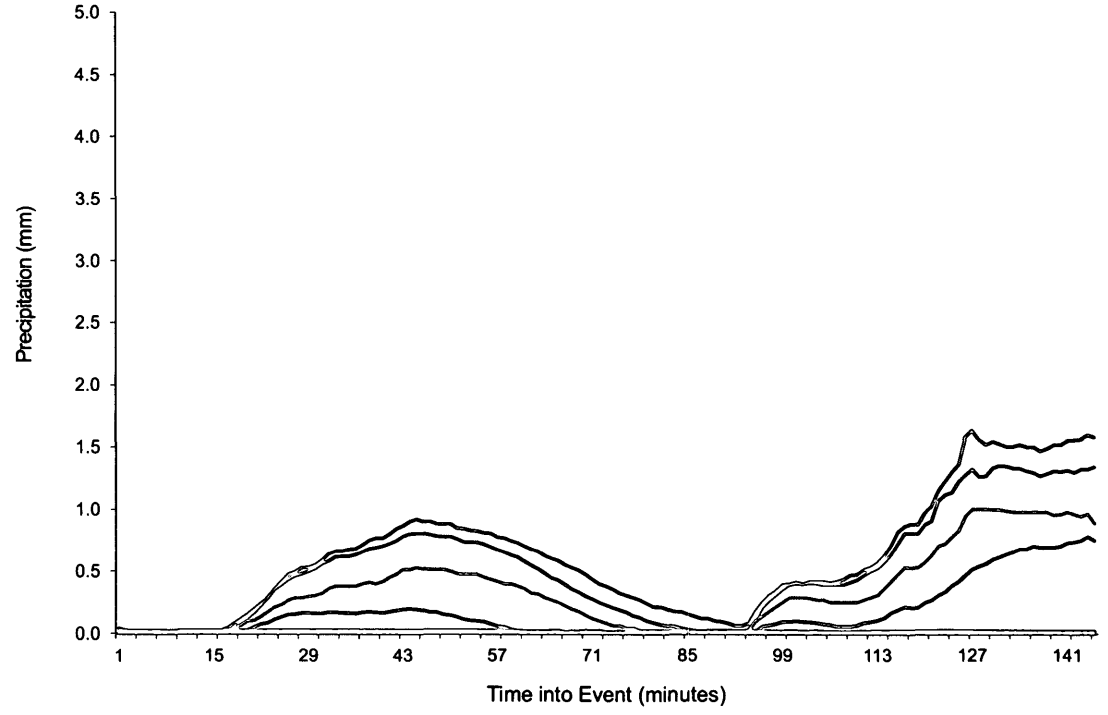

Figure 65. LWS wetness readings recorded for Event 73 (on November 4, 2009 from 07:08 to 08:12) and Event 74 (on November 4, 2009 from 16:46 to 19:10).

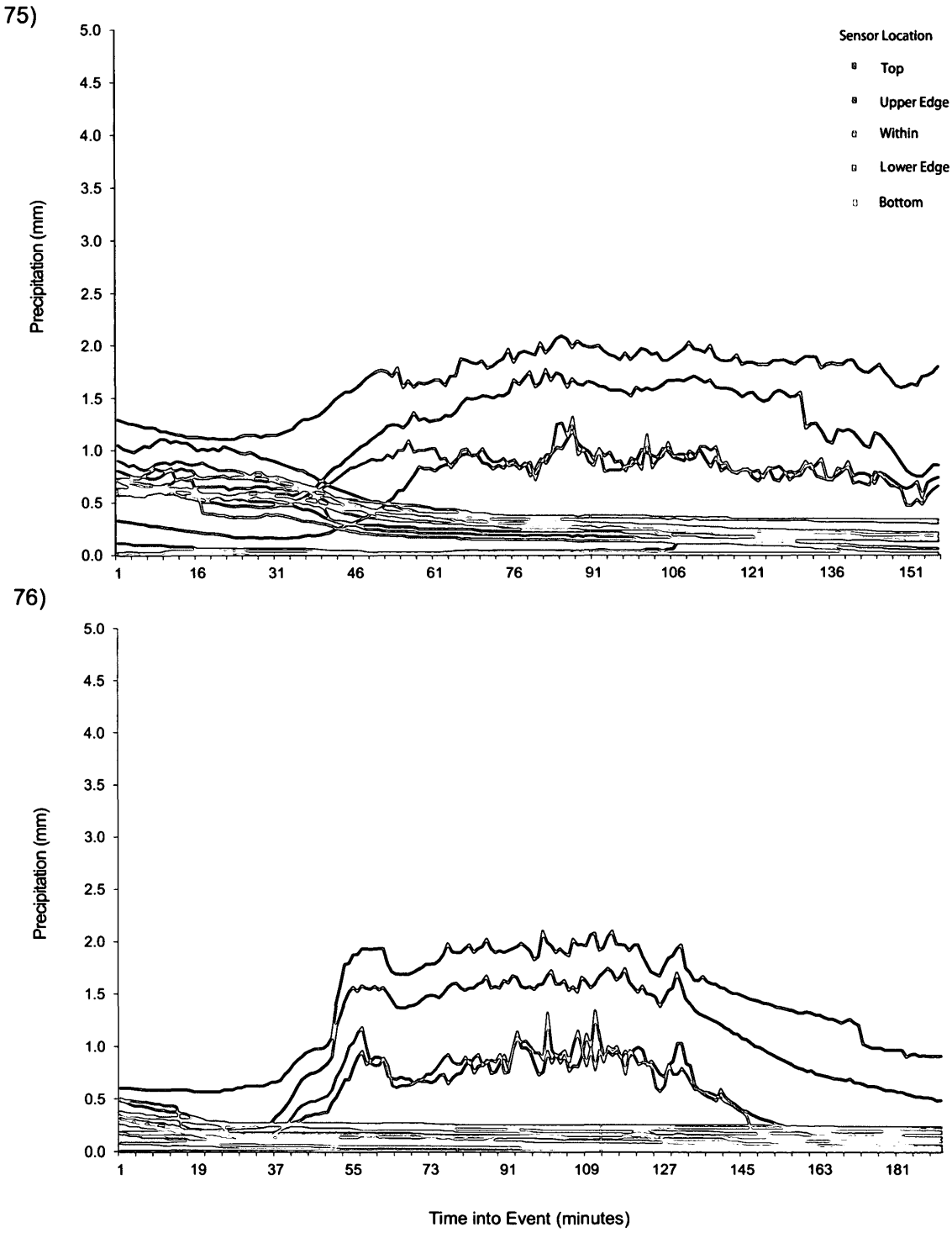

Figure 66. LWS wetness readings recorded for Event 75 (on November 4, 2009 to November 5, 2009 from 23:30 to 02:05) and Event 76 (on November 5, 2009 from 07:20 to 10:30).

77)

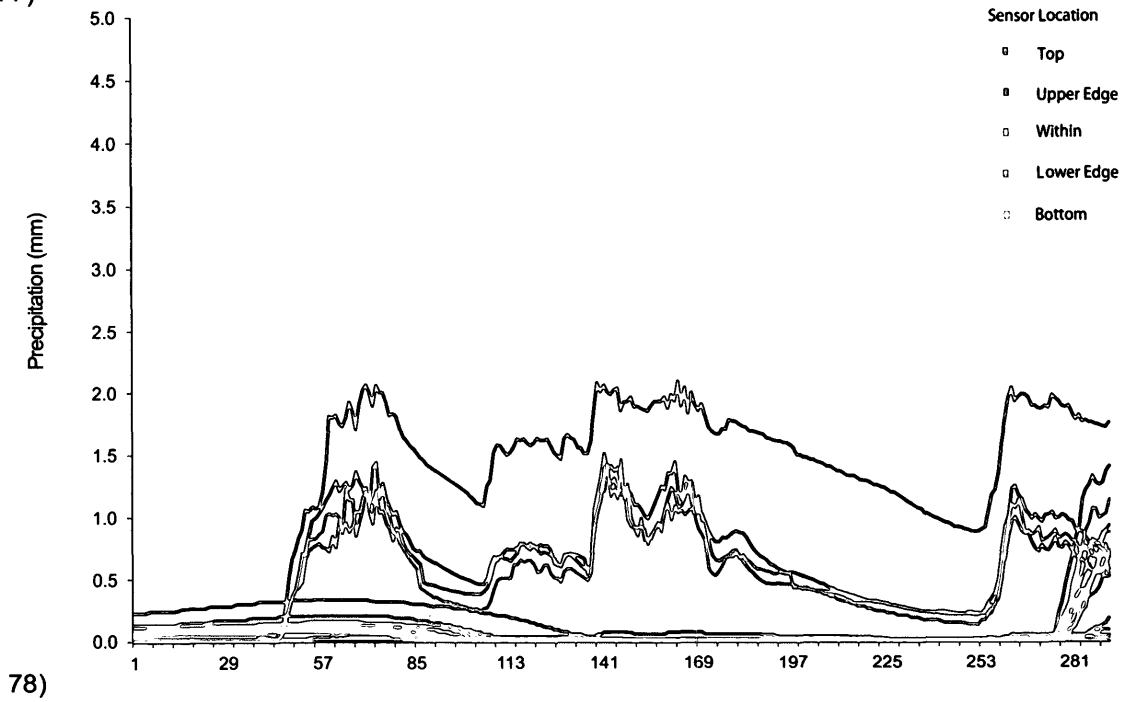

78)

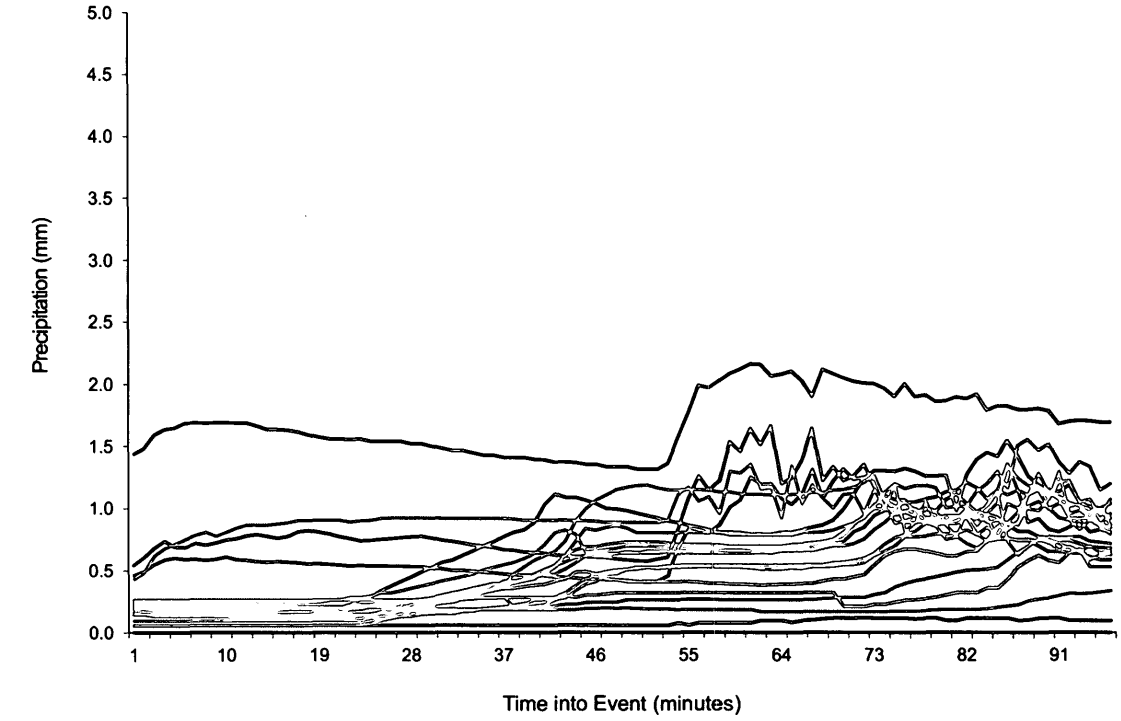

Figure 67. LWS wetness readings recorded for Event 77 (on November 19, 2009 from 05:10 to 10:00) and Event 78 (on November 19, 2009 from 16:05 to 17:40).

79)

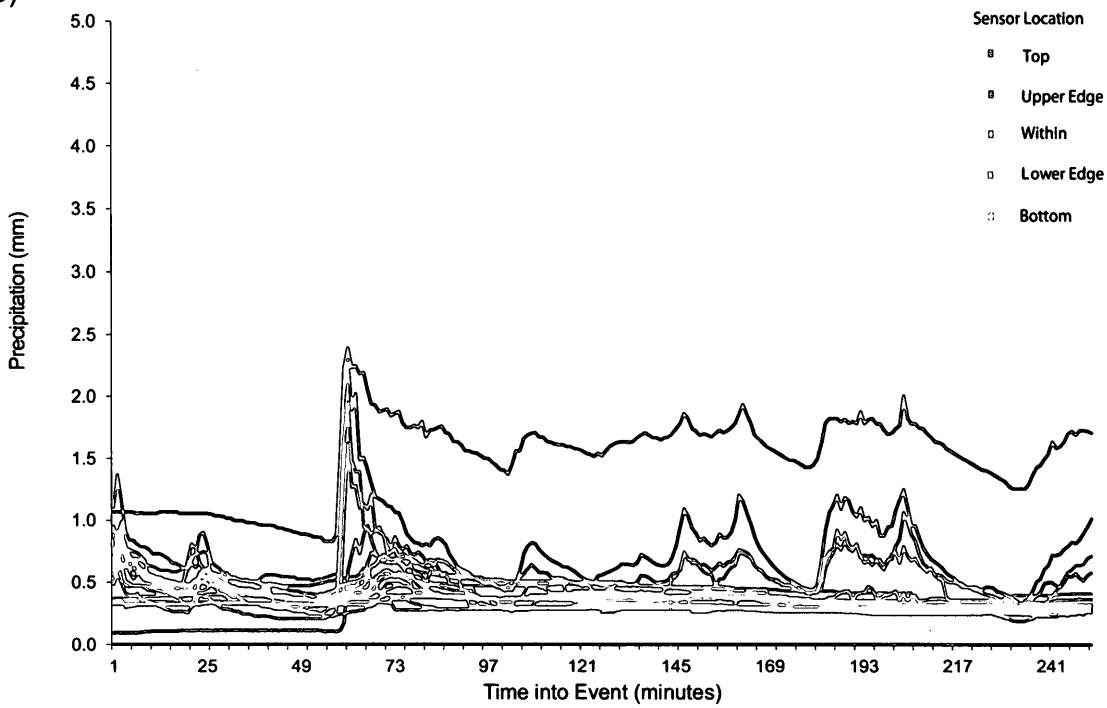

Figure 68. LWS wetness readings recorded for Event 79 (on November 19, 2009 to November 20, 2009 from 22:10 to 02:20).

APPENDIX C

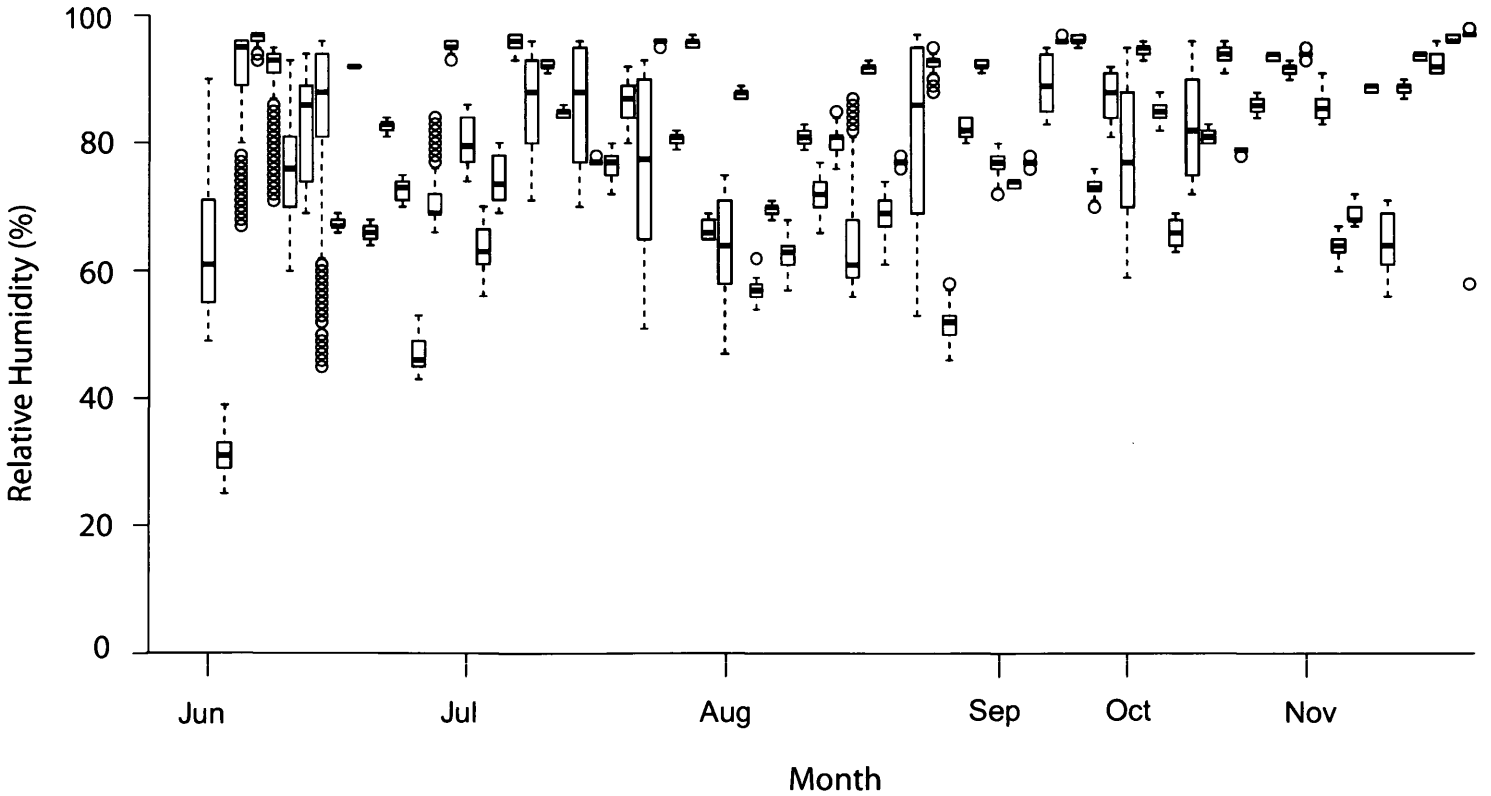

Figure 69. The temporal distribution of relative humidity (%) for each rain event recorded during the study period (June to November 2009) is outlined above in boxplots, where each bar represents a rain event. The thick horizontal line represents the median relative humidity, the lower end of the box presents the lower quartile, and the higher end of the box represents the upper quartile. The whiskers that extend downwards and upwards represent the minimum-recorded relative humidity and the maximum-recorded relative humidity respectively. This uses data recorded by the soil moisture sensors installed at the weather station 3 m from the study site.

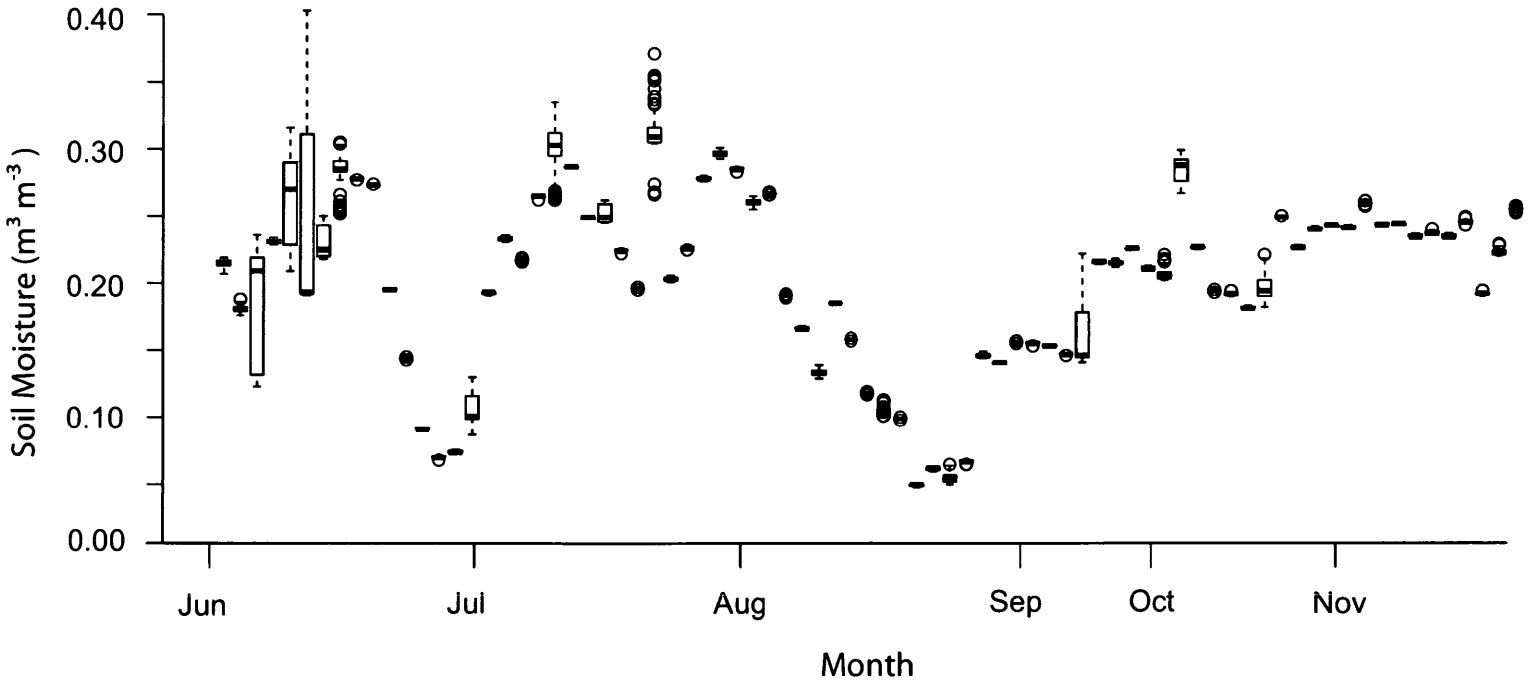

Figure 70. The temporal distribution of soil moisture (m^3 m^{-3}) for each rain event recorded during the study period (June to November 2009) is outlined above in boxplots, where each bar represents a rain event. The thick horizontal line represents the median soil moisture, the lower end of the box presents the lower quartile, and the higher end of the box represents the upper quartile. The whiskers that extend downwards and upwards represent the minimum-recorded soil moisture and the maximum-recorded soil moisture respectively. This uses data recorded by the soil moisture sensors installed at the weather station 3 m from the study site.

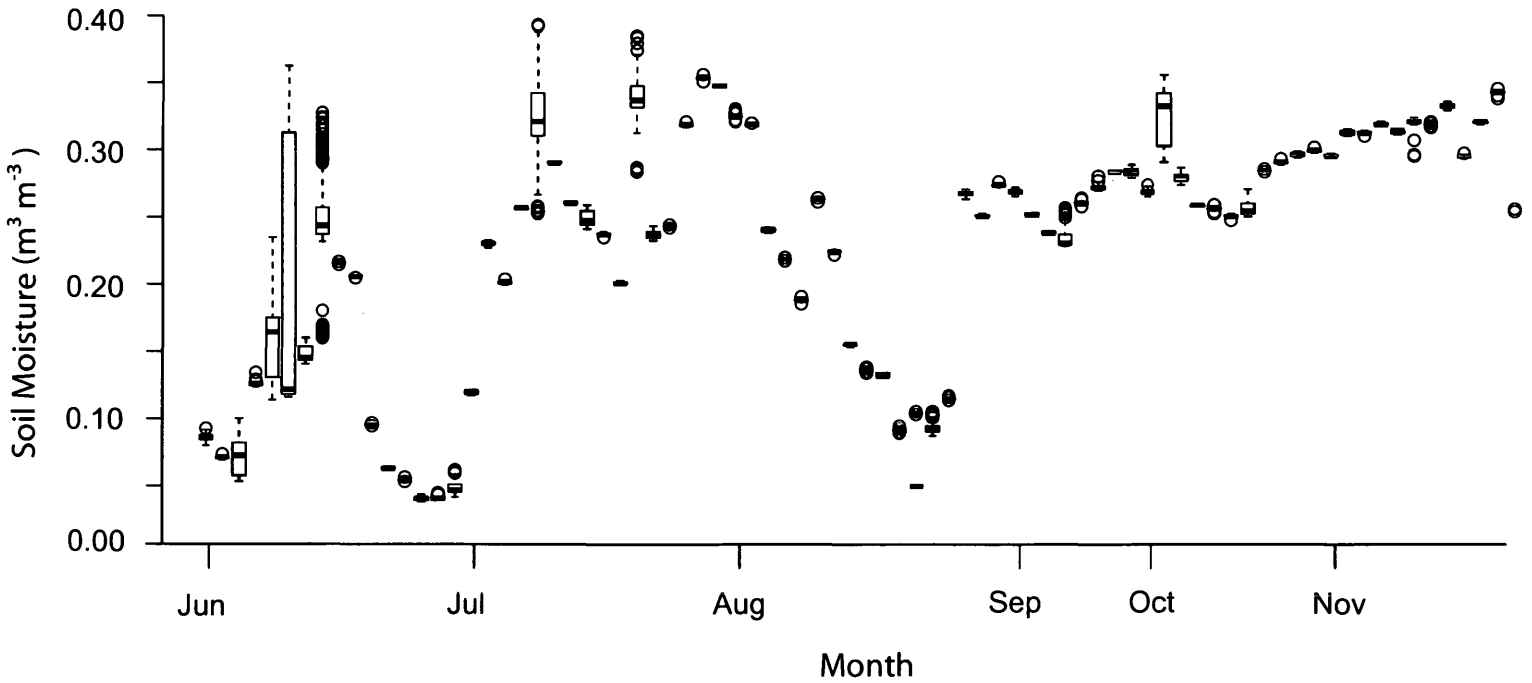

Figure 71. The temporal distribution of soil moisture (m^3 m^{-3}) under the tree canopy for each rain event recorded during the study period (June to November 2009) is outlined above in boxplots, where each bar represents a rain event. The thick horizontal line represents the median soil moisture, the lower end of the box presents the lower quartile, and the higher end of the box represents the upper quartile. The whiskers that extend downwards and upwards represent the minimum-recorded soil moisture and the maximum-recorded soil moisture respectively. This uses data recorded by the soil moisture sensors installed at the weather station 3 m from the study site.

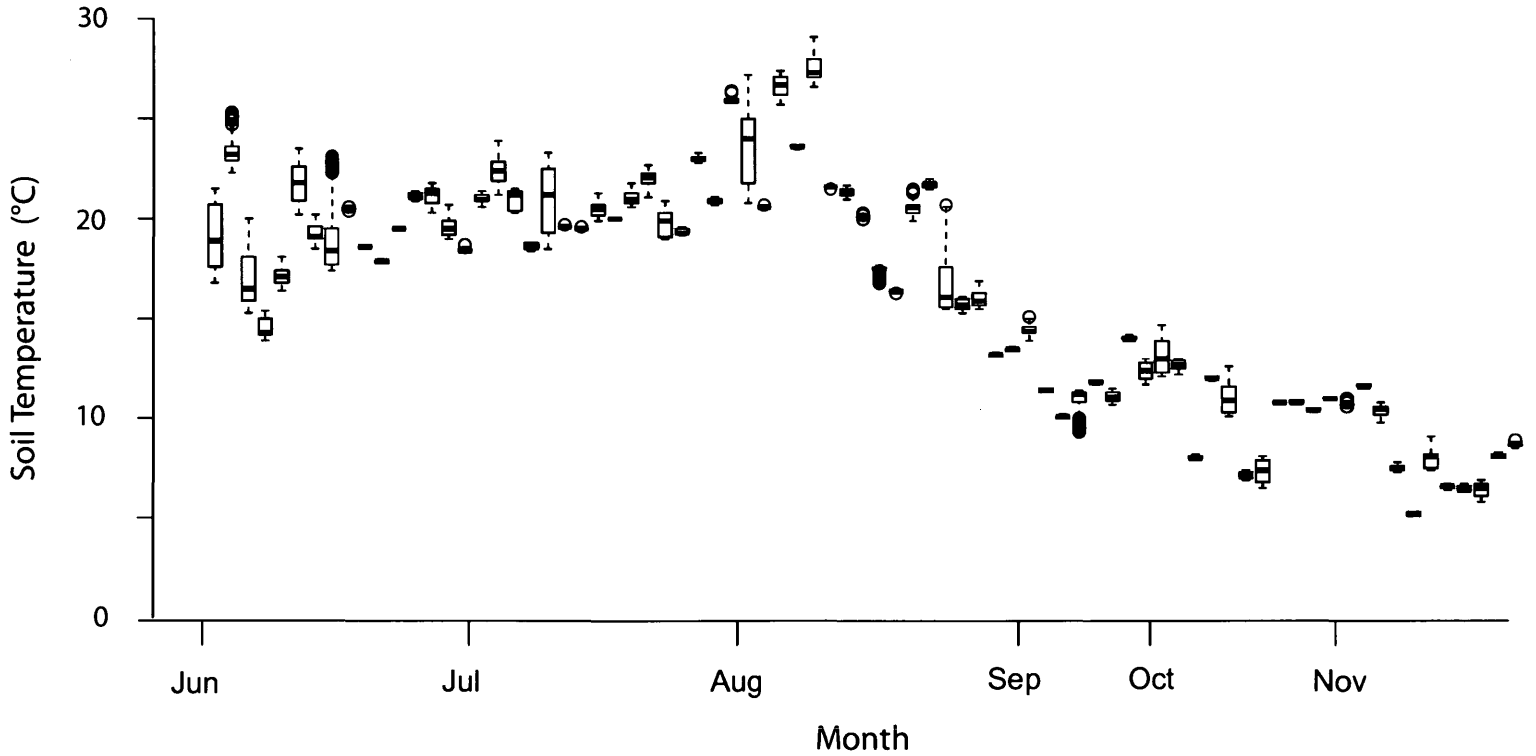

Figure 72. The temporal distribution of soil temperature (°C) for each rain event recorded during the study period (June to November 2009) is outlined above in boxplots, where each bar represents a rain event. The thick horizontal line represents the median soil temperature, the lower end of the box presents the lower quartile, and the higher end of the box represents the upper quartile. The whiskers that extend downwards and upwards represent the minimum-recorded soil temperature and the maximum-recorded soil temperature respectively. This uses data recorded by the soil moisture sensors installed at the weather station 3 m from the study site.

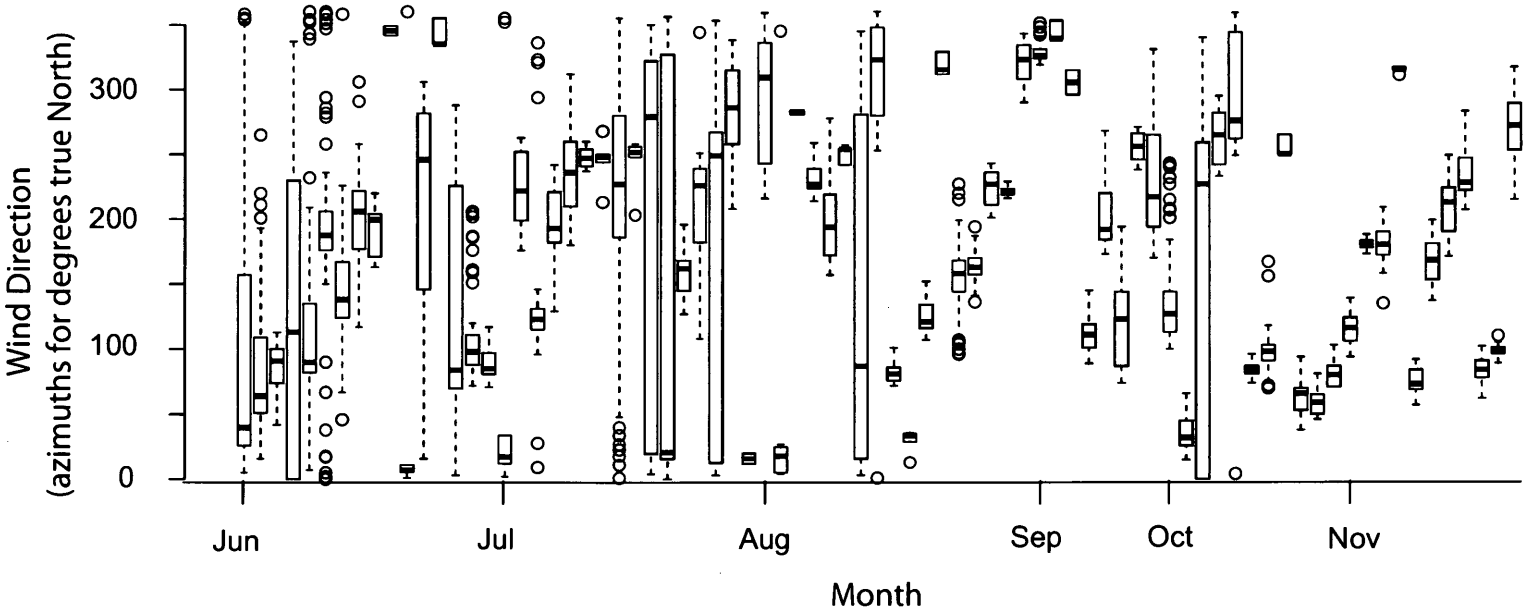

Figure 73. The temporal distribution of wind direction (azimuth degrees true North) for each rain event recorded during the study period (June to November 2009) is outlined above in boxplots, where each bar represents a rain event. The thick horizontal line represents the median wind direction, the lower end of the box presents the lower quartile, and the higher end of the box represents the upper quartile. The whiskers that extend downwards and upwards represent the minimum-recorded wind direction and the maximum-recorded wind direction respectively. This uses data recorded by the anemometer installed at the EMOS weather station.